Royal Netherlands Institute for Sea Research

Utrecht University

High resolution approach to reconstruct Late Pleistocene and Holocene climate of the northern Arabian Sea, with special emphasis on the comparison of biomarker-based sea surface temperature proxies

MSc. thesis - Marit R. van Erk (3816699)

May 2017

Supervisors:
prof. dr. ir. Jaap S. Sinninghe Damsté
Julie Lattaud MSc

Department of Marine Microbiology and Biogeochemistry
Royal Netherlands Institute for Sea Research (NIOZ)

Department of Earth Sciences
Faculty of Geosciences
Utrecht University

ABSTRACT

Multiple organic proxies have the potential to reconstruct sea surface temperature (SST), but their behavior is not completely understood within upwelling areas like the Arabian Sea. Here, we tested the applicability of three organic SST proxies: the $U^{K'}_{37}$ index based on long chain alkenones, the TetraEther indeX (TEX^{H}_{86}) and the Long chain Diol Index (LDI), supported by measures for surface productivity, bottom water oxygenation and upwelling intensity. Sediments from the northern Arabian Sea spanning 76 – 3 ka BP reveal that the three SST records differ in absolute reconstructed SST and furthermore show diverse SST variations. TEX^{H}_{86}-SSTs are highest (28.2 – 31.4 °C) and the record is characterized by a gradual warming between 76 and 3 ka BP, whereas LDI-SSTs are relatively stable around 26 °C with decreases in SST during the periods 22 - 3 ka BP, 45 – 37 ka BP and 57 – 51 ka BP. The $U^{K'}_{37}$-SST record shows a large SST range (17.5 to 26.8 °C). None of the SST proxies follow the stable oxygen isotopic composition ($\delta^{18}O$) of the Northern Hemisphere (NH) GRIP record. Instead, the TEX^{H}_{86} shows a Southern Hemisphere (SH) influence as suggested by synchronous variation with the stable hydrogen isotopic composition (δD) of the EPICA Dome C record. The SH influence within the TEX^{H}_{86} between 29 and 12 ka BP is probably related to increased influence of SH-sourced intermediate waters during periods of low upwelling intensity and sea-level lowstand. The gradual increase of TEX^{H}_{86}-SST from 76 to 3 ka BP might be related to a shift within the production pattern of isoprenoid glycerol dialkyl glycerol tetraethers (GDGTs) or could reflect a gradual warming towards the Holocene. LDI-SST is particularly forced by monsoon dynamics and therefore does not reflect annual mean SST. Changes in southwest monsoon (SWM) intensity have a dampening effect on LDI-SST differences between climatic states by inducing a shift in the blooming season of the biomarker producers. Furthermore, the lower temperature of upwelling waters can be recorded in the LDI during periods characteristic of an intense SWM. During periods of low SWM intensity, preferential degradation might cause an offset towards lower LDI-SST. The $U^{K'}_{37}$ record does not show the variability observed either within reference ice-core records or within the LDI and TEX^{H}_{86} records. This differing behavior may be due to lateral transport of re-suspended alkenones. The results indicate that application of organic SST proxies within upwelling-influenced areas is complex and should be done with caution, since many processes exert an influence on reconstructed temperatures. Clearly, a multi-proxy approach combining SST proxies and information on upwelling-related parameters is required to understand SST dynamics within these regions.

CONTENTS

1 INTRODUCTION

1.1 Sea surface temperature proxies

Reconstruction of past sea surface temperature (SST) is of primary importance in climatic studies, since SST is an important driving force of the thermohaline global circulation and therefore a crucial parameter of global climate. To better understand variations in the thermohaline circulation and resulting phenomena in local climates, strong SST proxies need to be developed. Proxies are based on preserved remains which contain information about the past environment. Several geochemical proxies providing SST estimates exist, with inorganic SST proxies being commonly based on skeletal remains composed of calcium carbonate ($CaCO_3$) or silica (SiO_2). Stable oxygen isotopic compositions ($\delta^{18}O$) and trace elemental ratios (e.g. magnesium (Mg)/ calcium (Ca)) measured on these skeletal remains are well-known SST proxies. However, these proxies have limits, like the preservation of shells and the uncertainties regarding seawater salinity and chemistry of the seawater (Spero et al., 1997; Wefer et al., 1999; Lea, 2003). A second group of SST proxies relies on the distribution of biomarker lipids, also referred to as organic proxies. Biomarkers are compounds that are preserved within sediments and are produced by a select group of organisms, making biomarkers specific for this group. Proxies relying on biomarker lipids can thus provide information on a certain range of environments. To be able to use biomarkers in paleoclimatic studies, they should be relatively resistant to degradation and widely distributed within sedimentary records (Versteegh et al., 1997).

1.2 Biomarker-based sea surface temperature proxies and assessments of terrestrial influence

1.2.1 Long chain alkenones

The alkenone unsaturation index ($U^{K'}_{37}$) is the oldest organic proxy for SST (Prahl and Wakeham, 1987) and has an advantage over inorganic geochemical SST proxies due to its insensibility for seawater chemistry (Herbert, 2003). Development of the $U^{K'}_{37}$ as a proxy for SST started with the index U^{K}_{37} introduced by Brassell et al. (1986) which was based on the relative abundance of di-, tri- and tetra-unsaturated long chain alkenones with a chain length of 37 carbon (C) atoms ($C_{37:2}$, $C_{37:3}$ and $C_{37:4}$ alkenones, respectively; Appendix 1A). It has been shown that the degree of unsaturation of these compounds changes with temperature within culture experiments (Marlowe, 1984; Brassell et al., 1986; Prahl and Wakeham, 1987). Since $C_{37:4}$ alkenones appeared to be not ubiquitously present within particulate matter and sediments (Brassell et al., 1986), Prahl and Wakeham (1987) proposed the use of a simplified version of the index, the $U^{K'}_{37}$:

$$U_{37}^{K'} = \frac{[C_{37:2}]}{[C_{37:2}]+[C_{37:3}]} \quad (1)$$

The production of unsaturated alkenones is specific to unicellular eukaryotic haptophyte marine algae, which live in the photic zone of the ocean (Eglinton and Eglinton, 2008). The widespread and abundant marine coccolithophorids *Emiliana huxleyi* and *Geophyrocapsa oceanica* represent the most important alkenone producers in present-day oceans (De Leeuw et al., 1980; Volkman et al., 1980a; 1995; Marlowe et al., 1984) and are considered as main producers of alkenones found in recent sediments (Volkman et al., 1980a; b). Since these haptophytes are photoautotrophs and therefore restricted to the upper photic zone, $U^{K'}_{37}$-derived temperatures presumably reflect temperatures of this depth interval. Potential alkenone production below the thermocline can be regarded as not important enough to significantly change the SST signal within underlying sediments (Müller et al., 1998).

Attempts to construct a calibration for the $U^{K'}_{37}$ index were based on cultures of *E. huxleyi* and/or *G. oceanica*, water-column particles and recent sediments (Müller et al., 1998 and references therein). The relation found by Prahl and Wakeham (1987) was based on the culture of a northeastern Pacific strain of *E. huxleyi* and became one of the standard calibrations due to its ability to predict the most plausible SST values for the present-day ocean (Müller et al., 1998):

$$SST = \frac{U_{37}^{K'} - 0.043}{0.033} \quad (2)$$

$U^{K'}_{37}$ values can range between 0 and 1, roughly corresponding to temperatures between -1 and 29 ^{0}C. Culture experiments revealed differences in the $U^{K'}_{37}$-SST relationship between different alkenone-producing species (Brassell, 1993; Conte et al., 1994; Prahl et al., 1995; Volkman et al., 1995; Sawada et al., 1996). The global calibration study of Müller et al. (1998) based on oceanic surface sediments revealed that the $U^{K'}_{37}$ signal within sediments is less species-dependent than suggested by the differences between culture experiments and this study furthermore confirms that the calibration of Prahl and Wakeham (1987) is linear despite environmental differences existing between regions. Although the $U^{K'}_{37}$ SST proxy seems robust in terms of inter- and intraspecial differences and regionality, it is limited by the fact that the biosynthetic pathway of formation and function of the alkenones within the producing organism are not known. Furthermore, limited nutrient availability and light-limited conditions induce preferential synthesis of $C_{37:3}$ alkenones and thus a decrease in $U^{K'}_{37}$ (Prahl et al., 2003; Sikes et al., 2005; Prahl et al., 2006). Additionally, an increase in $U^{K'}_{37}$ results when oxic degradation occurs over long time periods, since under these conditions $C_{37:3}$ alkenones are

preferentially degraded (Prahl et al., 1989; Gong and Hollander, 1999; Hoefs et al., 2002; Kim et al., 2009a). Lateral transport by advection of pre-aged alkenones from areas with potentially different temperatures can as well result in a bias in the $U^{K'}_{37}$-SST values (e.g. Sachs and Anderson, 2003; Sicre et al., 2005; Mollenhauer et al., 2006).

1.2.2 Glycerol dialkyl glycerol tetraethers

The TetraEther indeX of tetraethers consisting of 86 carbons (TEX_{86}) was introduced by Schouten et al. (2002) and is based on the distribution of glycerol dialkyl glycerol tetraethers (GDGTs), characteristic membrane lipids of the Archaea. GDGTs consist of isopranyl chains which are linked via ether bonds to a glycerol backbone, which can have a varying number of cyclopentane moieties (De Rosa and Gambacorta, 1988). Since an increasing number of cyclopentane moieties with temperature was observed for hyperthermophilic Archaea within culture experiments (De Rosa et al., 1980; Gliozzi et al., 1983; De Rosa and Gambacorta, 1988; Uda et al., 2001; 2004; Lai et al., 2008; Boyd et al., 2011), it was proposed that temperature has an important influence on GDGT distributions in the environment, including the ocean (Schouten et al., 2013). Members of the Thaumarchaeotal phylum are the most abundant prokaryotes in the present-day ocean and are considered the main producers of GDGTs within the marine environment (e.g. Karner et al., 2001; Herndl et al., 2005). The distribution of their GDGTs indeed strongly correlates with temperature as shown by core-top sediment and mesocosm studies (Schouten et al., 2002; Wuchter et al., 2004). Thaumarchaeota synthesize isoprenoidal GDGTs containing 0 to 4 cyclopentane moieties and additionally produce specific GDGTs, crenarchaeol and the crenarchaeol regio-isomer, where crenarchaeol contains, besides 4 cyclopentane moieties, a cyclohexane moiety (Schouten et al., 2000a; Sinninghe Damsté et al., 2002a). The observed change in distribution of these GDGTs with temperature within Thaumarchaeota forms the basis of the TEX_{86} as a SST proxy, which is defined as follows:

$$TEX_{86} = \frac{[GDGT-2]+[GDGT-3]+[Cren']}{[GDGT-1]+[GDGT-2]+[GDGT-3]+[Cren']} \quad (3)$$

where GDGT-1, GDGT-2 and GDGT-3 are the GDGTs containing 1, 2, and 3 cyclopentane moieties, respectively, and Cren' is the crenarchaeol regio-isomer (Appendix 1B).

TEX_{86} correlated best with annual mean SST for a small set of surface sediments (Schouten et al., 2002). GDGT-0 and crenarchaeol are not included in the TEX_{86}, since their high abundances in marine environments lead to an overpowering influence. A second reason to exclude GDGT-0 is its production by Archaea besides Thaumarchaeota, e.g. methanogenic Euryarchaeota. GDGT-0 within marine sediments is thus not necessarily formed by Thaumarchaeota within the marine water column, potentially leading to a bias in TEX_{86}-SSTs

(Schouten et al. 2002; Schouten et al., 2013). Kim et al. (2010) re-calibrated the initial linear relationship between TEX_{86} and SST as proposed by Schouten et al. (2002) using a global core-top dataset (n = 426). Two different calibration models were proposed: the TEX^{H}_{86} which is better suitable for (sub)tropical (high temperature) oceans and the TEX^{L}_{86} for low temperature polar regions. TEX^{H}_{86} is defined as the logarithmic function of TEX_{86} and is the recommended calibration to use when SSTs above 15 ^{0}C are expected:

$$TEX_{86}^{H} = \log\left(\frac{[GDGT-2]+[GDGT-3]+[Cren']}{[GDGT-1]+[GDGT-2]+[GDGT-3]+[Cren']}\right) \quad (4)$$

$$SST = 68.4 \times TEX_{86}^{H} + 38.6 \quad (5)$$

Kim et al. (2010) found a strong correlation between the TEX^{H}_{86} index and SST (r^2 = 0.87, standard error = 2.5 ^{0}C). Several studies showed that Thaumarchaeota can be heterotrophs and autotrophs, but predominantly appear to be chemolithoautotrophic ammonia-oxidizers (Könneke et al., 2005; Wuchter et al., 2006a; De la Torre et al., 2008; Hatzenpichler et al., 2008). Their chemolithoautotrophic metabolism explains the presence of Thaumarchaeota throughout the water column, without any restriction to the photic zone (e.g. Karner et al., 2001; Herndl et al., 2005). Inhibition for high light levels even results in an inability for Thaumarchaeota to live near the ocean surface (Merbt et al., 2012). It therefore seems peculiar that best correlations for TEX^{H}_{86} were found with SST. Indeed, although global calibration studies showed relations with mixed layer (0 - 30 m) temperature, the TEX^{H}_{86} appeared to be equally significant for water temperatures between 0 and 200 m water depth (Kim et al., 2008; 2012). Furthermore, regional studies have shown that the proxy could reflect a predominant subsurface signal (e.g. Huguet et al., 2007). It can thus be concluded that TEX^{H}_{86} does not necessarily reflects SST. This uncertainty about the production depth of the GDGTs reflected in the TEX^{H}_{86} proxy is one of the main limitations of the proxy. Other limitations include in the first place the uncertainty related to the main season of production and the uncertainties about the degradation of GDGTs (e.g. Schouten et al., 2004; Schouten et al., 2013). Secondly, lateral transport can cause a deviation of the estimated SST from in-situ SST, but this effect is likely much smaller than for $U^{K'}_{37}$-SSTs (Mollenhauer et al., 2007; Shah et al., 2008). Thirdly, production of GDGTs by Thaumarchaeotal and non-Thaumarchaeotal Archaea within either the water column, terrestrial environment or the sediment itself can introduce additional GDGTs to marine sediments (e.g. Pancost et al., 2001; Blumenberg et al., 2004; Weijers et al., 2006; Lipp and Hinrichs, 2009; Sinninghe Damsté et al., 2010; Weijers et al., 2011). In contrast to the $U^{K'}_{37}$, changes in nutrient concentrations do not significantly affect the TEX^{H}_{86} (Wuchter et al., 2004).

The influence of riverine and soil organic matter (OM) in marine sediments can be assessed by the Branched and Isoprenoid Tetraether (BIT) index (Hopmans et al., 2004), which is based on the abundance of branched GDGTs relative to crenarchaeol:

$$BIT = \frac{[GDGT-I]+[GDGT-II]+[GDGT-III]}{[GDGT-I]+[GDGT-II]+[GDGT-III]+[Cren]} \quad (6)$$

where GDGT-I, GDGT-II and GDGT-III refer to the branched GDGTs as indicated in Appendix 1C and Cren to crenarchaeol (Appendix 1B). Branched GDGTs have a different structure than the isoprenoidal GDGT-0 to -4, crenarchaeol and the crenarchaeol regio-isomer. They are the predominant GDGTs in terrestrial environments. Branched GDGTs are synthesized by organisms living in soil and peat, organisms that do not produce isoprenoid GDGTs. Branched GDGTs within the marine environment are suggested to represent riverine transported GDGTs, whereas crenarchaeol is mainly produced in the marine environment itself. These two types of GDGTs thus represent two different environmental sources, i.e. terrestrial and marine. The BIT index can range between 0 and 1, representing open marine environments (no terrestrial input) and purely terrestrial environments (no aquatic input), respectively (Hopmans et al., 2004).

1.2.3 Long chain diols

Long chain diols (LCDs) were discovered in Black Sea sediments (De Leeuw et al., 1981) and have subsequently been identified in a wide variety of environments. They consist of an alkyl chain with lengths equal to or longer than 28 C atoms and alcohol groups at C_1 and a mid-chain position, ranging between C_{11} and C_{19} (Versteegh et al., 1997 and references therein). Dominant LCDs within the marine environment are C_{28} and C_{30} 1,13-diols, C_{28} and C_{30} 1,14-diols and C_{30} and C_{32} 1,15-diols (Appendix 1D; Rampen et al., 2014a). The 1,14-diols are known to be synthesized by species within the *Proboscia* diatom genus and by the marine alga *Apedinella radians* (Sinninghe Damsté et al., 2003; Rampen et al., 2007; Rampen et al., 2011). In contrast to the 1,14-diols, the source of 1,13- and 1,15-diols in the marine environment is still uncertain. Eustigmatophyte algae are until now the only organisms for which 1,13- and 1,15-diol production has been confirmed in culture studies. Volkman et al. (1992; 1999) found 1,13- and 1,15-diols with chain lengths between C_{28} and C_{32} in cultures of both marine and freshwater species belonging to the genus *Nannochloropsis*. Cultures of marine eustigmatophytes (genus *Nannochloropsis*) show a dominance of saturated and mono-unsaturated C_{32} 1,15-diols, in contrast to marine environments in which the mono-unsaturated C_{32} 1,15-diol is not present and saturated C_{32} 1,15-diols only occur in low abundances, suggesting that marine eustigmatophytes are not the major source of marine

LCDs. The uncertainty related to marine eustigmatophytes as producer of marine LCDs is strengthened by their low abundance in the marine environment (Volkman et al., 1992; Versteegh et al., 1997; Rampen et al., 2014b). Nevertheless, Rampen et al. (2012) found a strong relationship between fractional abundances of 1,13- and 1,15-diols and SST within marine sediments. The C_{30} 1,15-diol shows a strong positive correlation ($r^2 = 0.95$) with SST, while the C_{28} and C_{30} 1,13-diols negatively correlate to SST ($r^2 = 0.88$ and $r^2 = 0.30$). This contrasting temperature dependence forms the basis of the Long chain Diol Index (LDI), which contains the fractional abundance of the C_{30} 1,15-diol relative to those of the C_{28} and C_{30} 1,13-diols and the C_{30} 1,15-diol and is defined as follows (Rampen et al., 2012):

$$LDI = \frac{F_{C_{30}1,15-diol}}{F_{C_{28}1,13-diol} + F_{C_{30}1,13-diol} + F_{C_{30}1,15-diol}} \quad (7)$$

SST estimations based on the LDI rely on the global core-top calibration of Rampen et al. (2012):

$$SST = \frac{LDI - 0.095}{0.033} \quad (8)$$

This calibration is based on 209 surface sediments from different oceans (mostly Atlantic Ocean) for which annual mean SSTs varied between -3 and 27 ^{0}C and of which 164 sediments contained quantifiable amounts of the LCDs included in the LDI. The calibration gave the strongest correlation of LDI with mean annual temperatures of the upper 30 m of the water column ($r = 0.984$, $p < 0.001$) and has a calibration error of ± 2 ^{0}C. The fact that a comparison of LDI-SST with $U^{K'}_{37}$-SST revealed general similarities between both records as well as the potential to link variations in LDI to climatic events for a site in the South Atlantic Ocean validates the LDI as a potential proxy for SST, as suggested by Rampen et al., 2012.

Although the strong correlation between the LDI and temperatures of 0 - 30 m water depth suggests that LCDs are likely sourced by photoautotrophic organisms (Rampen et al., 2012), the uncertainty about the source organism and thus mechanism behind the correlation between LDI and SST remains a limitation of the proxy (Smith et al., 2013). Another limitation is related to a potential continental source of some LCDs, particularly the C_{32} 1,15-diol. Several studies showed the relatively high abundance of this LCD in estuarine and river mouth sediments (e.g. Versteegh et al., 2000; Rampen et al., 2014b; De Bar et al., 2016; Lattaud et al., 2017) and De Bar et al. (2016) and Lattaud et al. (2017) suggest an in-situ river source for the C_{32} 1,15-diol. The relative abundance of the C_{32} 1,15-diol (normalized to the 1,13- and 1,15-diols) is therefore proposed by Lattaud et al. (2017) as a measure for the importance of riverine LCDs within the marine environment. Together with the BIT index (soil and riverine

OM) and stable carbon isotopic composition ($\delta^{13}C$; bulk OM), the relative abundance of the C_{32} 1,15-diol can assess potential biases within SST proxies related to terrestrially derived components.

1.3 Biomarkers as indicators for high nutrient or upwelling conditions

As shown by the BIT index and the relative abundance of the C_{32} 1,15-diol, biomarkers have the potential to provide valuable information on environmental conditions other than SST. For example, biomarkers can be used to assess upwelling, an important feature influencing productivity and indirectly preservation in certain areas. Rampen et al. (2008) proposed the use of LCD distributions as an indicator for upwelling conditions, based on the knowledge of the distribution of an important 1,14-diol producer, *Proboscia* diatoms. Cultivated *Proboscia* diatoms biosynthesize both saturated and mono-unsaturated C_{28} and C_{30} 1,14-diols (Sinninghe Damsté et al., 2003; Rampen et al., 2007) and in addition saturated C_{28}, C_{30} and C_{32} 1,14-diols were reported in marine *Apedinella* algae (Rampen et al., 2011). *Apedinella* is proposed as an important source of 1,14-diols within estuarine or brackish environments (Rampen et al., 2011), whereas *Proboscia* diatoms thrive in nutrient-rich upwelling waters and have been shown to be abundant in upwelling-influenced locations (e.g. Hernández-Becerril, 1995; Koning et al., 2001). Together with sediment trap studies in the Arabian Sea (Rampen et al., 2007; 2008), which showed 1,14-diols to be almost exclusively present during upwelling conditions, this knowledge led to the suggestion that the 1,14-diols in upwelling areas are likely sourced by *Proboscia* diatoms hence can serve as a proxy for upwelling intensity. The role of *Apedinella* remains uncertain (Rampen et al., 2011). Since 1,13- and 1,15-diols show a different behavior related to upwelling (Rampen et al., 2007, 2008), Rampen et al. (2008) included the C_{30} 1,15-diol in the proxy and in this way formed an index, the Diol Index 1 (DI 1):

$$DI\ 1 = \frac{[C_{28}+C_{30}\ 1{,}14-diols]}{[C_{28}+C_{30}\ 1{,}14-diols]+[C_{30}\ 1{,}15-diol]} \quad (9)$$

The advantage of DI 1 over absolute concentrations of the 1,14-diols lies in the index of structurally comparable compounds which causes minimization of diagenetic effects. DI 1 is proposed as a measure for upwelling intensity within the Arabian Sea during the southwest monsoon (SWM) and is later used as a proxy for upwelling in other regions. Willmott et al. (2010) introduced Diol Index 2 (DI 2), which is set up as a proxy for upwelling intensity at high latitudes:

$$DI\ 2 = \frac{[C_{28}+C_{30}\ 1{,}14-diols]}{[C_{28}+C_{30}\ 1{,}14-diols]+[C_{28}+C_{30}\ 1{,}13-diols]} \quad (10)$$

Since DI 1 is in addition to upwelling and high nutrients impacted by SST, DI 2 is proposed as a more widely applicable indicator of upwelling or high nutrient conditions (Rampen et al., 2014a).

1.4 Aim of the study

In this study the validity of the $U^{K'}_{37}$, TEX^{H}_{86} and LDI SST proxies within the northern Arabian Sea is assessed for the period between 76 and 3 ka BP. There are still uncertainties related to the applicability of biomarkers and their corresponding proxies. It is thus needed to study the reliability of the different proxies in varying environments. The multi-proxy approach used in this study allows for more precise assessment, since different proxies reflect different SSTs (related to seasonality and depth of production) and have their own limitations. Inorganic geochemical measurements on the bulk sediment, i.e. the strontium(Sr)/Ca ratio, a measure for bottom water oxygenation, and Ba/Al and Ba/Ti ratios, indicating surface productivity, are considered as a support to define whether organic SST proxies have the potential to be used within paleotemperature reconstructions within upwelling areas like the Arabian Sea. The northern Arabian Sea is a highly dynamic environment and the ability to reconstruct its SST is required to be able to understand the coupling of Arabian Sea climate to that on a global scale. The results show that temperatures reconstructed by organic proxies within the northern Arabian Sea can be influenced by a wide range of processes, making interpretation complicated. It is, therefore, suggested that a multi-proxy approach combining these organic SST proxies and proxies reflecting upwelling-related parameters is essential to shed light on temperature variations within this region.

2 ATMOSPHERIC AND OCEANOGRAPHIC SETTING

Seasonal cycles within the Arabian Sea are mainly influenced by monsoonal wind systems, leading to four periods: the moderate and dry northeast monsoon (NEM) from December to March, the spring intermonsoon (SI) from March to June, the strong and humid SWM from June to September and the fall intermonsoon (FI) from September to December (Schulte and Müller, 2001; Wakeham et al., 2002). The monsoonal winds characteristic of the NEM and SWM are driven by a pressure gradient existing between the Tibetan Plateau and the South Indian Ocean (Rixen et al., 2000). High pressures over Central Asia during the NEM are a result of an increased albedo caused by high snow cover over the Himalayas and the Tibetan Plateau. Since a low-pressure zone exists around the Intertropical Convergence Zone (ITCZ), winds are forced over the Arabian Sea. These winds are dry and cold and thereby cool surface waters. As a result, convective mixing occurs (Madhupratap et al., 1996) which brings

nutrients to the surface. The NEM is, therefore, characterized by a weak productivity maximum (Wakeham et al., 2002).

During the SWM a reverse, strong pressure gradient exists between the low-pressure cell that results from maximum heating above the Tibetan Plateau or flow of warm air from the cold extratropics and high pressures in the Southern Ocean (Webster et al., 1998; Boos and Kuang, 2010; Wu et al., 2012). Resulting southwest winds are warm and humid and force Ekman transport and coastal upwelling in the western Arabian Sea off Oman and Somalia (Rixen et al., 2000). This upwelling of nutrient-rich, relatively cold waters leads to a decrease in SST and triggers extremely high surface production during the SWM. High productivity during the SWM is also observed in the northeastern Arabian Sea, most probably caused by northeastward movement of nutrient-rich surface waters from Oman towards Pakistan, related to strong SWM winds (Schulz et al., 1998; Andruliet et al., 2000). Apart from the magnitude of the pressure gradient, the strength of the SWM depends on the release of latent heat during precipitation (Webster, 1987). Although surface production in the Arabian Sea is high year-round, it is concentrated in a maximum during the SWM and a smaller productivity peak during the NEM (Haake et al., 1993; Honjo et al., 1999; Wakeham et al., 2002). Both the SI and FI are characterized by weak winds and are periods of relatively low productivity (Wakeham et al., 2002). With annual primary productivity values of 200 to 400 gC m^{-2} yr^{-1}, the northern Arabian Sea is one of the most productive areas on a global scale (Kabanova, 1968; Qasim, 1982).

The combination of high primary productivity, stratification and advection of water masses with low oxygen (O_2) content results in the existence of a well-developed oxygen minimum zone (OMZ) between about 200 and 1200 m water depth (Von Rad et al., 1999a). The present-day OMZ is characterized by O_2 concentrations below 0.05 mM with seasonal minima between 0.1 and 1.0 µM (Van Bennekom et al., 1995; Paulmier and Ruiz-Pino, 2009). High surface productivity results in a depletion of O_2 at intermediate water depths due to remineralization of sinking OM. Inflow of warm Persian Gulf Water (PGW) and Red Sea Water (RSW) and heating of surface waters leads to relatively high SSTs, preventing overturning of the O_2-rich surface waters. This results in stratification, with warm and O_2-rich surface waters above relatively cold and O_2-poor intermediate waters. In addition, intermediate water flow is strongly influenced by the lack of an opening to the north, resulting in a dominant inflow of Indian Central Water (ICW) from the south. The O_2-poor ICW originates at the Subtropical Front of the Southern Hemisphere (SH; You and Tomczak, 1993; Van Bennekom et al., 1994).

Changes in SWM intensity (e.g. Altabet et al., 1995; Schulz et al., 1996; Reichart et al., 1997), variations in the interplay between SWM intensity and intensity of deep convective mixing during the NEM (e.g. Reichart et al., 1998; Reichart et al., 2004; Klöcker and Henrich, 2006) and/or changes in production of intermediate and deep water masses (e.g. Zahn and

Pederson, 1991; Olson et al., 1993; Rohling and Zachariasse, 1996) are thought to have caused changing OMZ intensities on orbital and suborbital timescales. Northern Hemisphere (NH) climate variability has been observed within Arabian Sea sediments (e.g. Altabet et al., 2002; Clemens and Prell, 2003; Ivanochko et al., 2005), suggesting a teleconnection between both areas. Millennial-scale variability occurs within the North Atlantic region, known as Dansgaard-Oescher (DO) oscillations. Cold conditions (stadials) alternate with warmer conditions (interstadials) and global influences of these cycles have been identified using climate models (Chiang and Bitz, 2005; Zhang and Delworth, 2005) and paleo-proxy data (e.g. Behl and Kennet, 1996; Schulz et al., 1998; Peterson et al., 2000; Wang et al., 2001). Periods of massive iceberg discharge occur during extremely cold stadials which are known as Heinrich events. Freshwater release during these periods is suggested to cause a decrease or shutdown of the Atlantic Meridional Overturning Circulation (AMOC) and thereby a decrease or absence of deep-water formation in the North Atlantic (e.g. McManus et al. 2004), resulting in changes in the Arabian Sea region.

The Indian monsoon system thus responds to changing conditions in the NH climate. O_2-rich conditions in the northern Arabian Sea occur synchronously with cold phases reflected in ice-core records from Greenland, while warm phases are characterized by an intensified Arabian Sea OMZ (Reichart et al., 1998; Schulz et al., 1998; Altabet et al., 2002). The Indian monsoon system mainly responds to changes in NH temperature (Deplazes et al., 2013), but the forcing and response mechanisms are controversial. Independent of the actual mechanism influencing the system, stadials are characterized by colder climates, a decrease in SWM intensity, strong NEM winds and arid conditions in contrast to the warm climate, high SWM intensity, weak NEM winds and wetter conditions observed during interstadials (Deplazes et al., 2014).

3 MATERIALS AND METHODS

3.1 Sampling

The PASOM 3 gravity core was collected along the Murray Ridge in January 2009 during the PASOM research expedition (expedition 64PE301) by the R/V Pelagia. The Murray Ridge is a seamount of which the top reaches into the present-day OMZ. PASOM 3 is located at $22^0$19.9'N; $63^0$36.0'E (Fig. 1). At the same location a multicore has been collected. The multicore allows for retrieval of undisturbed sediments and was used to collect the top, most recent part, of the sediment. Fluffy sediment in the top of the gravity core suggested a minimum loss of sediment (Reichart, 2009). Since water depth at the PASOM 3 station is 1172 m, the

sediment-water interface lies within the present-day OMZ. O_2 concentration of the bottom water was only 5.0 µM at the time of sediment collection, as measured by an O_2 sensor (Fig. 2; SBE43, Sea-Bird, WA USA, accuracy 2% and limit of detection 3.0 µM), which was attached to a CTD frame and calibrated using Winkler titrations. Surface and bottom water temperatures were ± 24 ^{0}C and 7.8 ^{0}C, respectively. Both the multicore and gravity core used in this study were stored at Utrecht University until October 2016. Thereafter, sampling and analyses were performed at the Royal NIOZ. Core sections were stored at the Royal NIOZ at 4 ^{0}C until sampling. The gravity core contained a total of 5.37 m of sediment, divided into 6 sections. Gravity core sediments consisted of homogeneous, dark greenish to light greenish/grey hemipelagic muds. No significant lamination existed. One of the multicores with a diameter of 6.6 cm was selected for further analysis. The sediment consisted of 0.29 m of dark grey hemipelagic muds, again without clear laminations (Fig. 3).

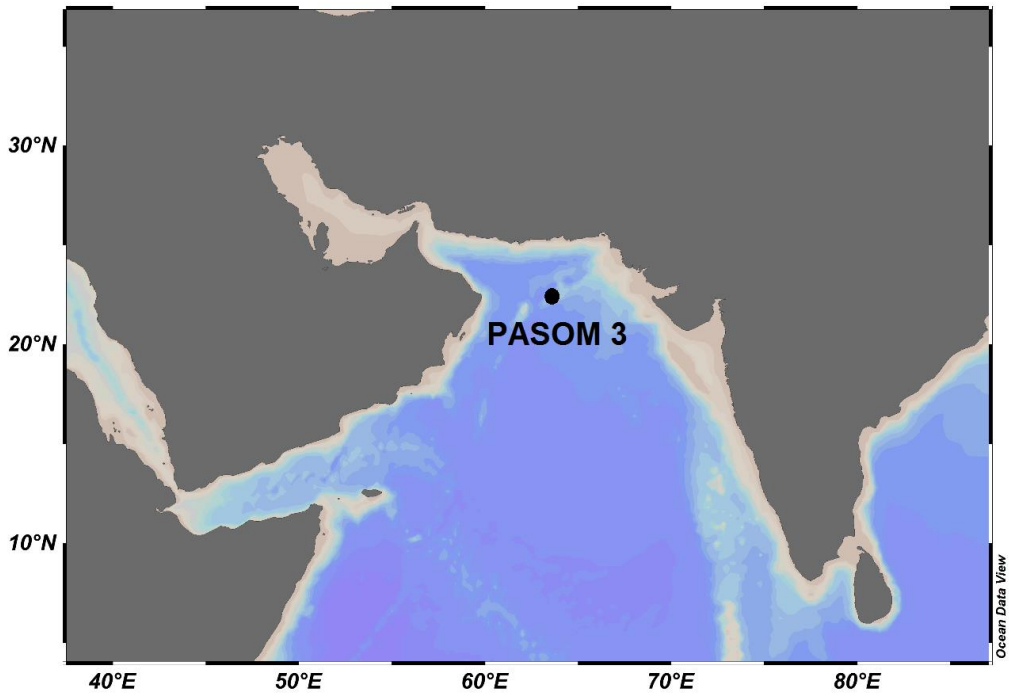

Figure 1: *Map of the Arabian Sea showing the coring location of PASOM 3 (22º19.9'N; 63º36.0'E). The map was made using Ocean Data View software.*

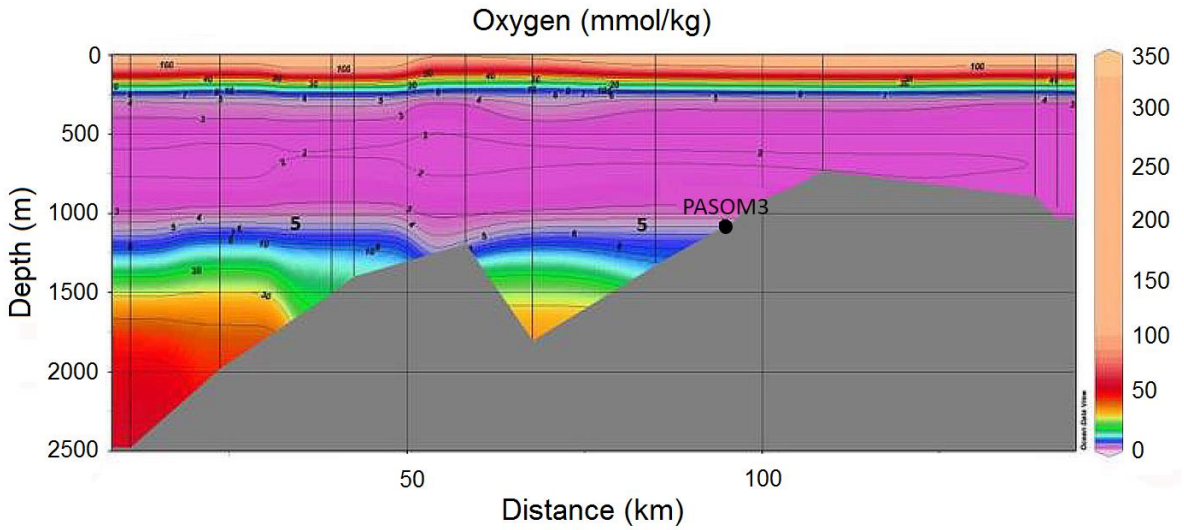

Figure 2: *Dissolved O_2 transect along the Murray Ridge. Measurements were conducted during the PASOM research expedition. Taken from Reichart (2009).*

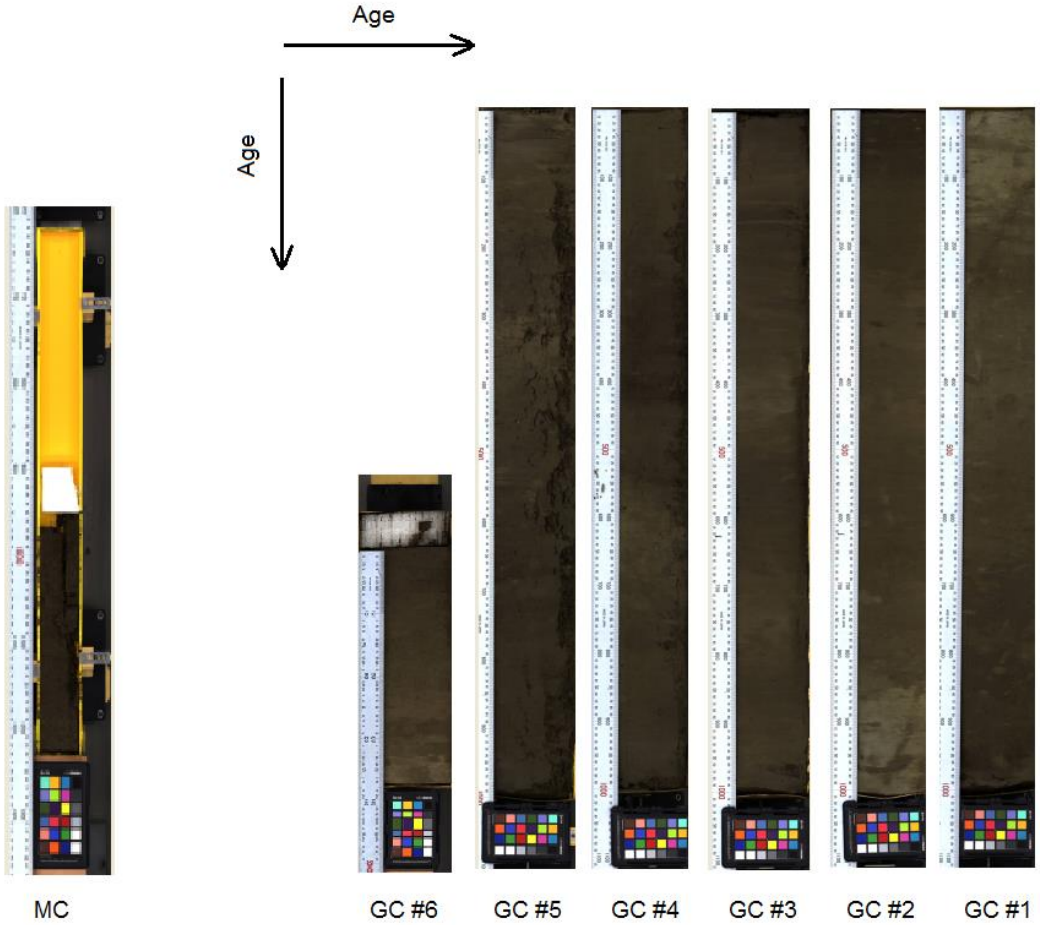

Figure 3: *X-Ray Fluorescence core scanning pictures of the multicore (MC) and the six sections of the gravity core (GC). Oldest sediment from the GC was present within section 1 (#1), while youngest sediment occured in #6. GC #1 to #5 equal 1 m in length, whereas 0.37 m of sediment was present within #6. The MC contained 0.29 m of sediment.*

Gravity core sediments were sampled for foraminifera, organic geochemistry and inorganic geochemistry using 10 mL syringes. Samples for uranium analysis were collected using 5 mL syringes. Syringe diameters were 1.60 cm and 1.25 cm, respectively. Sampling occurred at 5 cm intervals in the upper 470 cm of the core, whereas resolution decreased to 10 cm between 470 and 530 cm, corresponding to a temporal resolution of ~720 and ~1000 years. Syringe diameters led to the collection of sediments within 1.6 cm below the reported depth for foraminifera, organic geochemistry and inorganic geochemistry samples and within 0.63 cm for uranium samples. Between 13.5 mL and 22.5 mL of wet sediment was collected for organic chemistry, with weights ranging between 21.3 g and 36.3 g. Multicore sediments were sampled for foraminifera, organic geochemistry and inorganic geochemistry at 1 cm intervals using sediment slicing. Reported depths of multicore samples represent the upper depth of the slice. Six multicore samples were selected for further analyses and weighted. Water content of both gravity core and multicore sediment was obtained after determination of the weight loss as a result of freeze-drying.

3.2 Methods

3.2.1 X-Ray Fluorescence core scanning

Sediment surfaces were flattened and covered with a thin (4 µm) Ultralene film, which prevents contamination (Richter et al., 2006). Subsequently, bulk elemental composition of the sediment was determined using X-Ray Fluorescence (XRF) core scanning techniques with an irradiation area of 1.2 cm^2 and a sampling interval of 1.0 cm, resulting in an average temporal resolution of ~140 years. To be able to detect both the relatively light and heavy elements, core sections were scanned using an Avaatech XRF Core Scanner with tube voltage set-ups of 10, 30 and 50 kV and count times of 10, 10 and 40 s, respectively. Technical and practical information on the Avaatech XRF Core Scanner can be found in Richter et al. (2006). Among the reported elements were aluminium (Al), Ca, titanium (Ti), bromine (Br), Sr, and barium (Ba). Results were reported for each sample depth as counts of the individual element against the total counts. Since these counts are susceptible to a closed sum effect, it is preferred to report ratios of element intensities instead of intensities of individual elements (Weltje and Tjallingii, 2008). Pictures of the sediment surface were taken using the Avaatech XRF Core Scanner, allowing for a comparison between bulk elemental composition and surface characteristics.

3.2.2 Organic carbon and stable carbon isotope analysis

Freeze-dried and homogenized sediment samples (± 0.5 g) were decalcified by addition of 2.0 M hydrogen chloride (HCl) until the reaction was completed. Dissolved sediments were

shaken overnight and subsequently rinsed with bidistilled water until the pH of the overlying solution decreased to pH ≤ 5. Sediments were again freeze-dried and 1.0 - 1.5 mg of the decalcified sediment was transferred to tin cups. Organic carbon (C_{org}) and $\delta^{13}C_{bulk}$ measurements were conducted using a Flash EA 1112 Series (Thermo Scientific) analyzer coupled to a Finnigan Delta^{plus} mass spectrometer (MS) via a Conflo II interface. Actanilide and benzoic acid standards and blank measurements were added to the measurement series at regular intervals. Reported C_{org} and $\delta^{13}C_{bulk}$ values are averages of duplicate or triplicate measurements, with a mean standard deviation (SD) of 0.11 wt% for C_{org} and 0.05 ‰ for $\delta^{13}C_{bulk}$ values. $\delta^{13}C_{bulk}$ is reported relative to the Vienna Pee Dee Belemnite (VPDB) standard.

3.2.3 Planktonic foraminiferal counts

Specimens of the planktonic foraminiferal species *Globorotalia truncatulinoides* and *Globorotalia crassaformis* were counted within foraminiferal samples from depth intervals that were expected to represent Heinrich event 1 (H1), H6 and an interval after H4. Furthermore, a sample from a depth interval that was thought to represent an interstadial was included. Depth intervals were selected based on the PASOM 3 Br XRF record and the $\delta^{18}O$ record and age scale of the GRIP chronology (Dansgaard et al., 1993), for which Heinrich events are well dated. Selected samples were prepared for counting by freeze-drying and wet sieving to obtain the >150 µm fraction on which counting was conducted. The abundance of *G. truncatulinoides* and *G. crassaformis* was quantified by counting specimens while the sample was mounted on a picking tray, to a maximum number of 30 specimens (Reichart et al., 1998).

3.2.4 Radiocarbon dating

Three accelerator mass spectrometry (AMS) radiocarbon dates based on planktonic foraminifera, mainly *Orbulina* species, were obtained (Beta analytic Inc., Florida, USA). Radiocarbon ages (in BP, with 0 BP equivalent to AD 1950) were calculated using the conventional radiocarbon age, a measure for the regional reservoir age (ΔR; 232 ± 26 yrs) and the Marine13 calibration curve (Reimer et al., 2013) as input for the CALIB software version 7.1 (Stuiver et al., 2017). The regional reservoir age is defined as the deviation from the model ocean with a reservoir age of 400 yrs and was obtained by a weighted mean ∆R for two available data points located closest to the PASOM 3 location (Von Rad et al., 1999b) with the Intcal13 software (Stuiver et al., 2017).

3.2.5 Biomarker analysis

3.2.5.1 Lipid extraction

Sediments were freeze-dried and subsequently homogenized using an agate mortar. Depending on sediment availability, 9.0 to 18.0 g of sediment was extracted after addition of diatomaceous earth using a solvent mixture of 9:1 (v:v) dichloromethane (DCM):methanol (MeOH). Extraction was conducted using an Accelerated Solvent Extractor 350 (ASE 350, DIONEX) at 100 ^{0}C and 7.6 × 10^6 Pa. Extracted solvents were subsequently reduced using a TurboVap LV Caliper, dried over a Pasteur pipette containing sodium sulfate ($NaSO_4$) and concentrated under a stream of nitrogen (N_2). The used total lipid extract (TLE) was a fraction containing 4.5 mg TLE, unless this amount was not available. Several internal standards were added to the TLE prior to column chromatographic separation, i.e. 3 µg 10-nonadecanone, 4 µg C_{22} 7,16-diol and 1 µg C_{46} GDGT per 4.5 mg TLE. These internal standards allowed for quantitation of alkenones, LCDs and GDGTs, respectively. Internal standards were added to TLE dissolved in DCM:MeOH 1:1 (v:v) and the solvent was subsequently dried under a stream of N_2. Apolar, ketone and polar fractions were obtained by column chromatographic separation of the TLE over a column formed by a Pasteur pipette filled with activated aluminimum oxide (Al_2O_3; activated at 150^{0}C for 3 h and cooled for 1 h before use). The solvents hexane:DCM 9:1 (v:v), hexane:DCM 1:1 (v:v) and DCM:MeOH 1:1 (v:v) were used as eluents to elute the apolar, ketone and polar fractions. Obtained fractions were dried under a N_2-stream and stored cooled in pre-weighted vials until further preparation.

3.2.5.2 Alkenone analysis and $U^{K'}_{37}$ sea surface temperature

Ketone fractions were analysed after re-dissolution in 100-800 µL ethyl acetate. Analysis was conducted on a Hewlett Packard 6890 gas chromatograph (GC) equipped with a flame ionization detector (FID) and helium as the carrier gas. After an autosampler injected 1 µL of the sample, the initial oven temperature of 70 ^{0}C increased with 20 ^{0}C per min to 200 ^{0}C and subsequently with 3 ^{0}C per min to 320 ^{0}C, a temperature which was held for 25 min. Peak areas of $C_{37:2}$ and $C_{37:3}$ alkenones (Fig. 4) were determined by integration and quantified using the 10-nonadecanone as internal standard. The $U^{K'}_{37}$ was calculated and the standard calibration of Prahl and Wakeham (1987) based on laboratory cultures of *E. huxleyi* was used to obtain the SST as follows:

$$U_{37}^{K'} = \frac{[C_{37:2}]}{[C_{37:2}]+[C_{37:3}]} \quad (1)$$

$$SST = \frac{U_{37}^{K'} - 0.043}{0.033} \quad (2)$$

Several samples were analysed in duplicate, with a mean SD of 0.009, corresponding to a mean SD of 0.27 ^{0}C following the Prahl and Wakeham (1987) calibration.

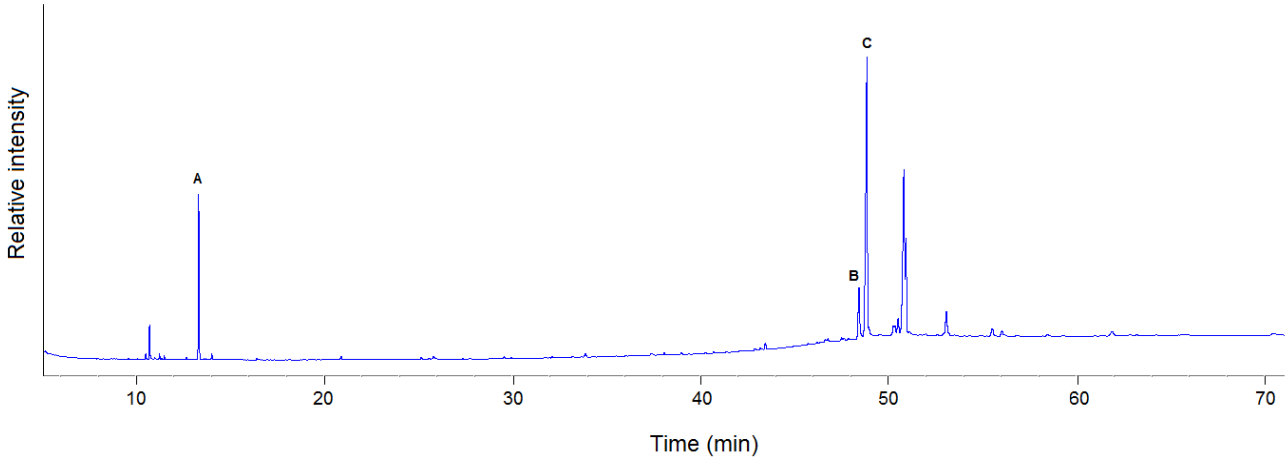

Figure 4: *Example GC chromatogram of a ketone fraction. Letters refer to: A = internal standard (10-nonadecanone), B = $C_{37:3}$ alkenone and C = $C_{37:2}$ alkenone.*

3.2.5.3 GDGT analysis, TEX^{H}_{86} sea surface temperature and BIT index

Polar fractions were divided into two aliquots with equal weights by addition of DCM:MeOH 1:1 (v:v) and subsequent transfer of half of the volume to a second vial. One aliquot of the polar fraction was analysed for GDGTs. Samples were redissolved in a mixture of hexane:isopropanol 99:1 (v:v), filtered through 0.45 µm polytetrafluoroethylene (PTFE) filters attached to 1 mL syringes and dried under a N_2-stream. Analysis was conducted using Ultra High Pressure Liquid Chromatography (UHPLC)-MS after dissolution of the sample in 100 µL hexane:isopropanol 99:1 (v:v). Sample injection volume was 5 µL. The UHPLC-MS method used is that discussed by Hopmans et al. (2016). An Agilent 1100 series LC/MSD SL performed the analysis. Two UHPLC SiO_2 columns in series (BEH HILIC columns, 2.1 by 150 mm, 1.7 µm; Waters), with a 2.1 by 5 mm SiO_2 pre-column (Waters) induced separation, and were held at a constant temperature of 30 ^{0}C. Elution was performed isocratically for 25 min with 18% hexane: isopropanol 9:1 (v:v) and 82% hexane, followed by a linear gradient to 35% hexane:isopropanol 9:1 (v:v) in 5 min and a linear gradient to 100% hexane:isopropanol 9:1 (v:v). Solvent flow rate was 0.2 mL/min. The total run time was 90 min per sample including 20 min of re-equilibration. The source settings were equal to Schouten et al. (2007). GDGT detection occurred via Selected Ion Monitoring (SIM; Schouten et al., 2007). Relevant peak areas of the $[M+H]^+$ ions were obtained using Agilent Chemstation software (Fig. 5). The response factor was calculated as the ratio between the area of the internal standard C_{46} GDGT divided by the area of crenarchaeol, and was used to correct the areas of the internal

standard before quantification. Response factors were 0.462 for the first measurement series (35 – 3 ka BP) and 0.249 for the second measurement series (76 – 35 ka BP), respectively.

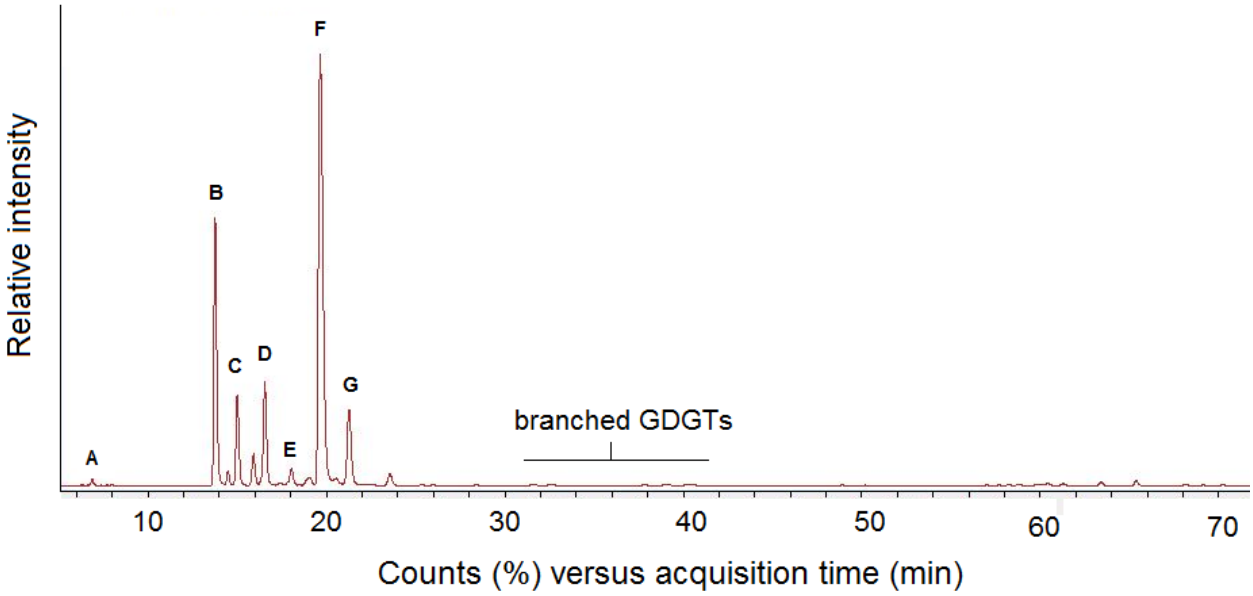

Figure 5: *Example UHPLC-MS chromatogram of a polar fraction (GDGT aliquot). Letters refer to: A = internal standard (C_{46} GDGT), B = GDGT-0, C = GDGT-1, D = GDGT-2, E = GDGT-3, F = crenarchaeol and G = crenarchaeol regio-isomer.*

Peak areas of isoprenoid GDGT abundances were used to calculate TEX^{H}_{86}, as defined by Kim et al. (2010). TEX^{H}_{86} was converted to SST based on the global core-top calibration of Kim et al. (2010), which covers a temperature range between -3 and 30 ^{0}C and has a calibration error of 2.5 ^{0}C:

$$TEX_{86}^{H} = \log\left(\frac{[GDGT-2]+[GDGT-3]+[Cren']}{[GDGT-1]+[GDGT-2]+[GDGT-3]+[Cren']}\right) \quad (4)$$

$$SST = 68.4 \times TEX_{86}^{H} + 38.6 \quad (5)$$

Duplicate measurements were conducted at identical intervals within the core. The resulting mean SD was 0.002, corresponding to a mean SD of 0.14 ^{0}C based on the calibration of Kim et al. (2010).

The BIT index was calculated as follows, using the equation of Hopmans et al. (2004):

$$BIT = \frac{[GDGT-I]+[GDGT-II]+[GDGT-III]}{[GDGT-I]+[GDGT-II]+[GDGT-III]+[Cren]} \quad (6)$$

Mean SD of the BIT index was 3.3×10^{-3} and after removal of an outlier, the mean SD was 7.96×10^{-4}.

3.2.5.4 LCD analysis, LDI sea surface temperature and diol indices

The second aliquot of the polar fraction was analysed for LCDs after silylation by the addition of 15 µL pyridine and 15 µL BSTFA (N,O-bis(trimethylsilyl)trifluoroacetamide), followed by heating at 60 ºC for 30 min. Samples were subsequently dissolved in 300 - 600 µL ethyl acetate. LCD analysis was conducted using an Agilent 7990B GC coupled to an Agilent 5977A MS. The GC was equipped with a fused SiO2 column (25 m; 0.32 mm) coated with CP Sil-5 (film thickness 0.12 Im). The method used was that described by Lattaud et al. (2017). Oven temperature during injection was 70 ºC and increased thereafter to 130 ºC at 20 ºC/min and to 320 ºC at 20 ºC/min, which was held for 25 min. The GC operated with helium as carrier gas set on a constant flow of 2 mL/min. Temperature of the MS source was held constant at 250 ºC and the MS source electron ionization energy was 70 eV with a cycle time of 1.9 s. Sample injection volume was 1 µL. Peak areas were defined using SIM (Fig. 6) of characteristic m/z ratios of LCD ions: 299.3 (C28 1,14-diol), 313.3 (C28 1,13-diol and C30 1,15-diol), 327.3 (C30 1,14-diol) and 341.3 (C30 1,13-diol and C32 1,15-diol) (Versteegh et al., 1997; Rampen et al., 2012), the quantification has been done relatively to the internal standard (C22 7,16-diol; m/z = 187). Full scan mode allowed for identity confirmation, since the different LCDs show characteristic spectra of fragmentation (Versteegh et al., 1997). Peak areas of several compounds different from LCDs (lolliolide, isololiolide and dinosterol; Appendix 1E) were obtained using the full scan mode (Fig. 6). Peak areas were corrected using a response factor of 0.22 for the internal standard and 0.129 for the other LCDs.

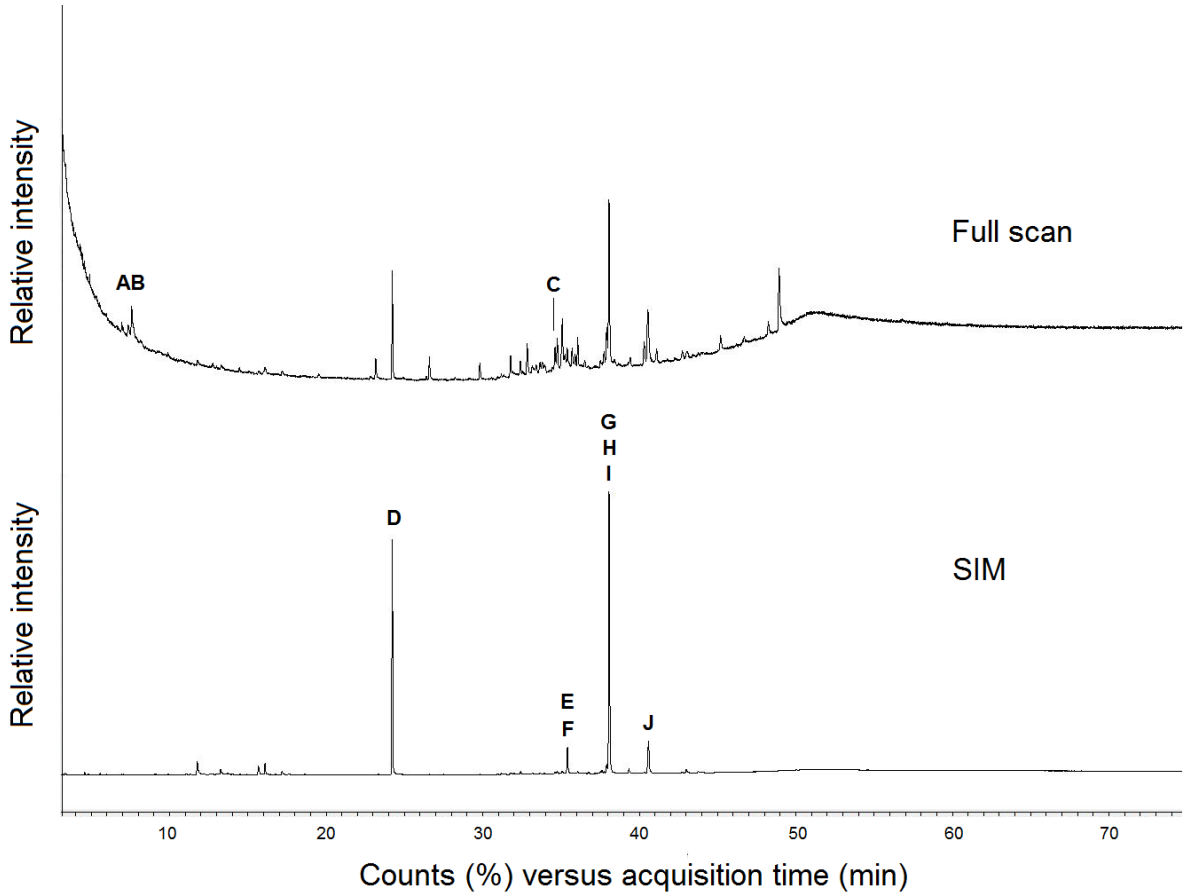

Figure 6: *Example GC-MS chromatogram of a polar fraction (LCD aliquot), both full scan and SIM mode are shown. Letters refer to: A = isololiolide, B = loliolide, C = dinosterol, D = internal standard (C_{22} 7,16-diol), E = C_{28} 1,13-diol, F = C_{28} 1,14-diol, G = C_{30} 1,13-diol, H = C_{30} 1,14-diol, I = C_{30} 1,15-diol and J = C_{32} 1,15-diol.*

Fractional abundances of the C_{30} 1,15-diol, C_{30} 1,13-diol and C_{28} 1,13-diol were calculated and used to obtain the LDI as described by Rampen et al. (2012). The LDI was subsequently converted to SST following the calibration of Rampen et al. (2012), which is based on more than 200 globally distributed marine surface sediments, covers a temperature range from -3 to 27 ºC and has a calibration error of 2 ºC:

$$LDI = \frac{F_{C_{30}1,15-diol}}{F_{C_{28}1,13-diol} + F_{C_{30}1,13-diol} + F_{C_{30}1,15-diol}} \quad (7)$$

$$SST = \frac{LDI - 0.095}{0.033} \quad (8)$$

Diol indices 1 and 2 were obtained following equations proposed by Rampen et al. (2008) and Willmott et al. (2010) after calculation of the fractional abundances of the C_{28} and C_{30} 1,14-diols, C_{30} 1,15-diol and C_{28} and C_{30} 1,13-diols (normalized to the total abundance of LCDs):

$$DI\ 1 = \frac{[C_{28}+C_{30}\ 1{,}14-diols]}{[C_{28}+C_{30}\ 1{,}14-diols]+[C_{30}\ 1{,}15-diol]}$$ (Rampen et al., 2008) (9)

$$DI\ 2 = \frac{[C_{28}+C_{30}\ 1{,}14-diols]}{[C_{28}+C_{30}\ 1{,}14-diols]+[C_{28}+C_{30}\ 1{,}13-diols]}$$ (Wilmott et al., 2010) (10)

3.2.6 Biomarker concentrations and mass accumulation rates

Mass accumulation rates (MARs) of biomarkers were calculated to gain insight into the temporal changes in productivity, preservation and species composition. Parameters required for this calculation were the concentration of the individual biomarker (in µg/g dry sediment), dry bulk density and the sedimentation rate. First, concentrations of $C_{37:2}$ and $C_{37:3}$ alkenones, isoprenoid GDGTs (GDGT-0, GDGT-1, GDGT-2, GDGT-3, crenarchaeol, crenarchaeol regio-isomer), branched GDGTs (m/z 1018, 1020, 1022, 1034, 1036 and 1050), loliolide, isololiolide and dinosterol were calculated as follows:

$$[C] = \frac{\frac{A_x * m_{IS}}{A_{IS}}}{m_{sed}}$$ (11)

where [C] is the concentration of the individual biomarker, A_x is the biomarker area, m_{IS} the amount of internal standard added (in µg), A_{IS} the area of the internal standard and m_{sed} the amount of sediment extracted (in g dry sediment). Secondly, sedimentation rates were calculated as the ratio of the difference in sample depth over the difference in sample age, calculated for two adjoining samples. Dry bulk densities were obtained as the ratio of the weight of freeze-dried sediment over the total volume before freeze-drying. Finally, MARs were calculated for individual biomarkers as follows:

$$MAR = [C] \times sedimentation\ rate \times dry\ bulk\ density$$ (12)

Sedimentary concentrations of individual biomarkers were reported in µg/gC_{org} in order to shed light on changes in biomarker concentrations that are not governed directly by production or preservation of C_{org}. Relative concentrations would allow for analysis on possible changes in species composition through time. Therefore, the sum of the sedimentary concentrations (in µg/gC_{org}) of individual biomarkers ($C_{37:2}$ alkenone, LCDs, dinosterol and the sum of loliolide and isololiolide) was calculated per time interval. Relative concentrations of individual biomarkers were subsequently obtained using the total concentration of biomarkers. LCDs were grouped based on the position of the mid-chain alcohol group, i.e. 1,13-diols, 1,14-diols and 1,15-diols.

3.2.7 Statistical analyses

The variability in the biomarker distribution was analysed by performing a Principal Component Analysis (PCA) on the sedimentary concentrations of LCDs, $C_{37:2}$ alkenones, crenarchaeol, dinosterol and the sum of loliolide and isololiolide using XLStat 2016. Isoprenoid GDGTs, represented by crenarchaeol, were not always included in the PCA, since the behavior of these GDGTs is expected to be significantly different due to the non-photosynthetic character of the source organism and the different seasonality of production within the Arabian Sea (Prahl and Dymond, 1996; Prahl et al., 2000; Wuchter et al., 2006b; Rampen et al., 2007; 2008). Including GDGTs would lead to a decrease in separation of the other biomarkers, thereby complicating the PCA results. A second PCA was performed on the sedimentary concentrations of the $C_{37:2}$ alkenone and the individual LCDs. Data points representing marine isotope stage (MIS) 1 to 5a as defined by the age model based on the LR04 stack of benthic foraminiferal $\delta^{18}O$ records (Lisiecki and Raymo, 2005) were included, thereby enabling analysis of the behavior of the biomarkers relative to MIS 1 to 5a. Heinrich events were taken as a separate group of data points. Pearson r values were used to evaluate potential correlations which were considered significant for p values below 0.05.

4 RESULTS

4.1 Age model

Since the PASOM 3 gravity core was partly stored frozen, it must first be examined whether the freezing caused any disturbance of the sedimentary stratigraphy. Disturbances and related movement of sedimentary layers would result in errors within the age model. Ziegler et al. (2008) reported a correlation between Br XRF scanning counts and marine C_{org} records within the Arabian Sea NIOP 463 core (22^{0}32.9 N; 64^{0}02.8' E; 920 m water depth), thereby introducing the potential of Br XRF records as a proxy for C_{org} content. Furthermore, Reichart et al. (1998) found co-varying C_{org} records for several stations which are in close proximity and in the same area as the PASOM 3 station. Comparison between the PASOM 3 Br XRF record and the Br XRF record of a core from the same area (NIOP 463) could therefore be used as a way to determine whether C_{org} profiles are correlated and thus whether any disturbance occurred within the PASOM 3 core. The close resemblance between the PASOM 3 Br XRF record and the NIOP 463 Br XRF record, of which the last is not normalized to total counts, provided evidence for the undisturbed character of the sedimentary record provided by the PASOM 3 gravity core (Fig. 7). No errors associated with storage circumstances are thus expected. As a first step in constructing the age model, PASOM 3 Br XRF counts were correlated to that of NIOP 463 using Analyseries 2.0.8 software (Paillard et al., 1996). Control

points were created by connecting minima or maxima that occur in both records, while keeping in mind that correlation values given by the software should not decrease after addition of a control point. The final correlation was based on a total of 17 control points (Fig. 7). Linear interpolation between control points was used to calculate ages of individual depths (at 1 cm intervals, equal to the resolution of the XRF Br record) within the PASOM 3 core.

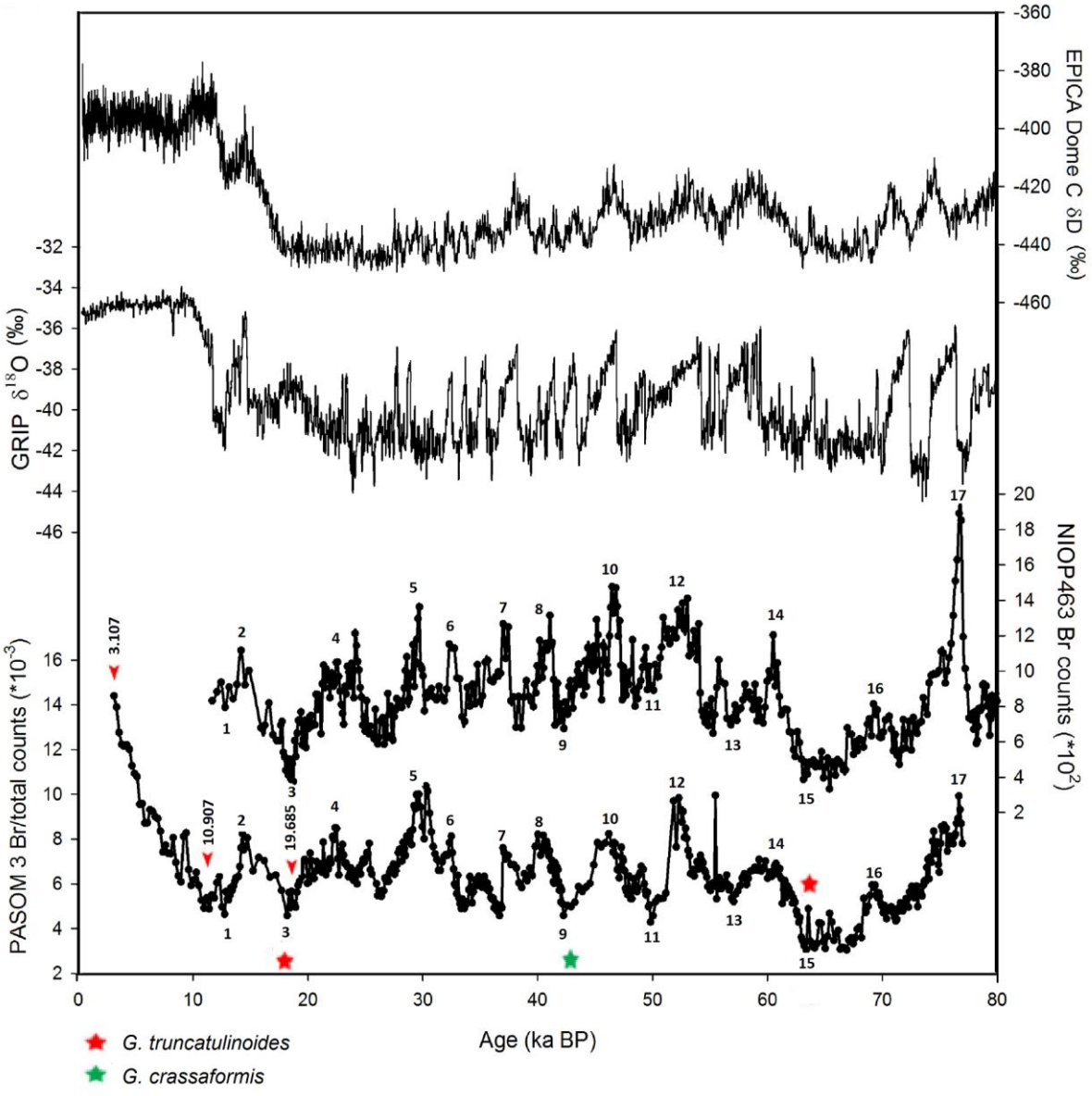

Figure 7: *Comparison of the PASOM 3 Br/total counts record with the NIOP 463 Br record (not normalized; Ziegler et al., 2010), $\delta^{18}O$ of GRIP from Greenland (Dansgaard et al., 1993) and δD of EPICA Dome C from Antarctica (Jouzel et al., 2003). Numbers refer to control points on which the age model was based. Radiocarbon ages and presence of G. truncatulinoides and G. crassaformis within samples selected for foraminiferal counting are shown.*

An age model based on correlation of the PASOM 3 Br XRF record with the NIOP 463 Br XRF record was the preferred approach, since the identification of control points is most reliable between two records of the same proxy. No $\delta^{18}O$ or stable hydrogen isotopic composition (δD) records were available for the PASOM 3 core and correlation of these records to the same records of chronologies based on $\delta^{18}O$ of GRIP and δD of EPICA Dome C (Jouzel et al., 2003) was thus not possible. By comparison to NIOP 463, PASOM 3 is correlated to a core with a well-established age model (Ziegler et al., 2010), which is indirectly tuned to the global SPECMAP chronology (Imbrie et al., 1984). The NIOP 463 age model is in first instance based on identification of the last five glacial terminations using the $\delta^{18}O$ record *of Neogloboquadrina dutertrei*. Since planktonic isotopic signals are sensitive to temperature variations and freshwater fluxes, an alternative age model was constructed to avoid these problems, based on peak occurrences of *G. truncatulinoides* and *G. crassaformis* (*Globorotalia* events; Reichart et al., 1998). *Globorotalia* events were correlated to the North Atlantic ice rafted debris record of ODP site 980, which was in turn tuned to SPECMAP (McManus et al. 1999). A detailed description of the NIOP 463 age model can be found in Ziegler et al. (2010).

Radioisotopically dated high abundances of *G. truncatulinoides* and *G. crassaformis* have been shown to be coeval with major climatic cooling in the North Atlantic Ocean (Reichart et al., 1998; 2004). These cold events, also called Heinrich events, are coupled to a strongly diminished intensity or complete absence of the OMZ within the Arabian Sea (Reichart et al., 1998; 2004). As an independent test of the constructed PASOM 3 age model, abundances of these deep-dwelling planktonic foraminifera were counted within intervals that were expected to represent *Globorotalia* events, i.e. H1, H6 and an interval after H4 (Reichart et al., 1998). To confirm the validity of the method, a sample from a depth interval that was thought to represent an interstadial was included, for which thus no *Globorotalia* event was expected. PASOM 3 foraminiferal counts were in accordance with counts conducted on sediments from the NIOP 464 core from the Murray Ridge and the NIOP 478 core from the Pakistan Margin (Reichart et al., 1998; 2004), with the presence of *G. truncatulinoides* at the depth interval selected as H1, *G. crassaformis* within the interval after H4 and high abundances of *G. truncatulinoides* during H6 (Fig. 7). On the contrary, neither *G. truncatulinoides* nor *G. crassaformis* were found in sediments of the interstadial. The age model of PASOM 3 is thus able to identify Heinrich events and *Globorotalia* events. Reichart et al. (1998) found neither *G. truncatulinoides* nor *G. crassaformis* during the Younger Dryas (YD; 12.9 - 11.6 ka BP; Alley et al., 1993), H2, H3 and both *G. truncatulinoides* and *G. crassaformis* during H5 within the NIOP 464 core. It can thus be excluded that the Heinrich events in PASOM 3 are numbered incorrectly.

The age model was further refined by three AMS radiocarbon dates (Fig. 7). Two of the resulting corrected radiocarbon ages were compared with the ages assigned to the same depth

by linear interpolation. Age differences were 50 and 1227 years, thereby indicating that the approach that relies on control points and linear interpolation is robust enough for our purposes. The third radiocarbon age corresponded to the core-top and therefore served as an 18th control point (Fig. 7). Linear interpolation then allowed for the assignment of ages to the upper part of the sedimentary succession. The subsequently calculated linear sedimentation rates varied between 2.0 and 15.1 cm/ka, with a mean sedimentation rate of 8.5 cm/ka (Fig. 8). This agrees well with sedimentation rates found by other studies in the same area (Van der Weijden et al., 1999; Lengger et al., 2012).

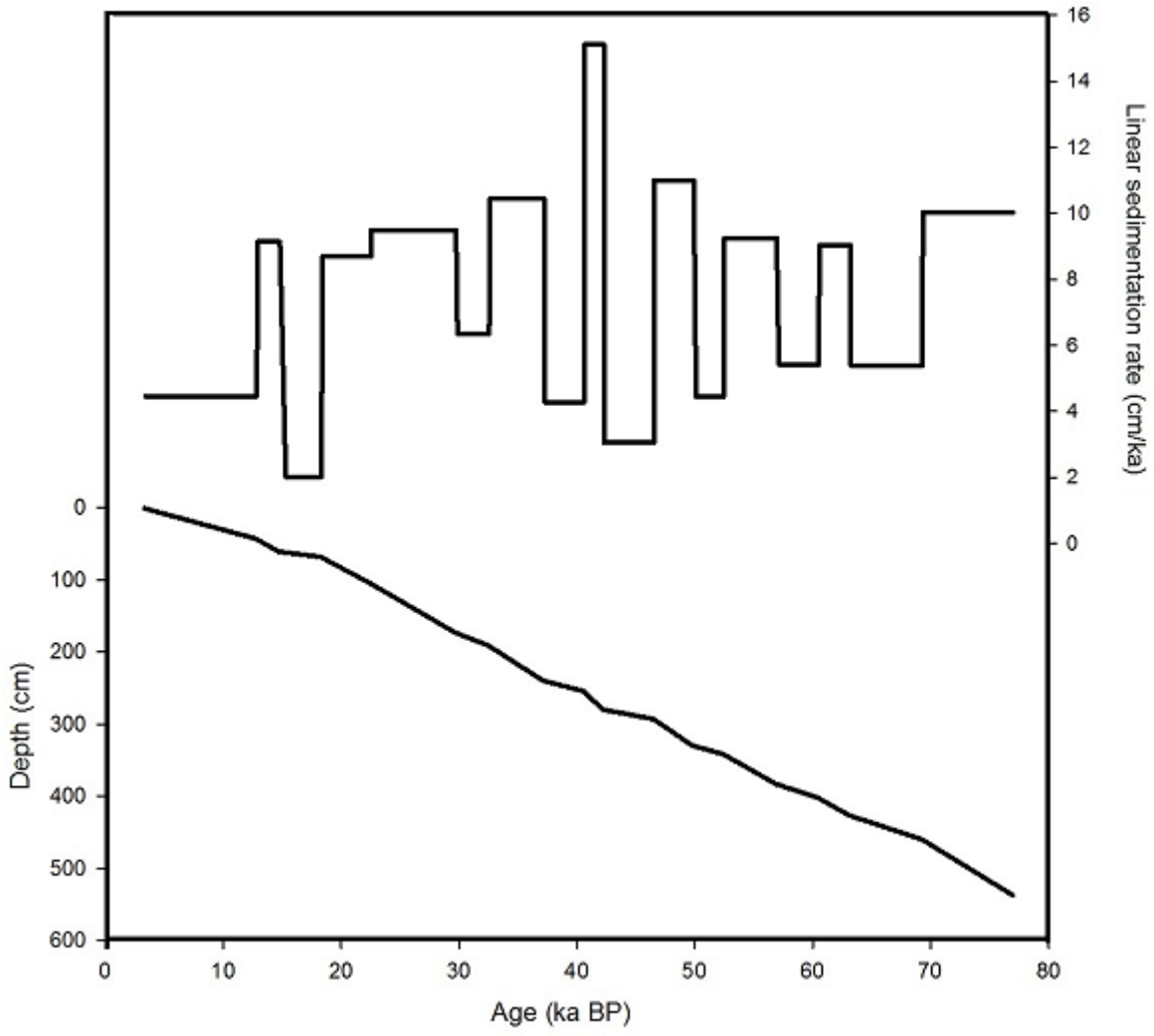

Figure 8: *Age versus depth relationship as calculated from the PASOM 3 age model and the corresponding linear sedimentation rates.*

The uppermost part (< 3 ka BP) of the succession is missing, as is evidenced by the radiocarbon age of planktonic foraminifera within the core-top sediments (3.107 ka BP). This is probably related to a loss of sediment during gravity core deployment rather than absence of more recent sediments at the PASOM 3 station. An attempt was made to couple the

multicore to the core-top of the gravity core, thereby extending the record provided by the gravity core into more recent times. The occurrence of equal water contents at the top of the gravity core and an interval within the multicore could suggest that they were located at equal depth within the sediment. AMS radiocarbon ages of planktonic foraminiferal tests from the multicore (Koho et al., 2013) led to a rejection of this hypothesis. Since the multicore could not be tied to the gravity core, sediment within the multicore could not be dated and therefore, although analysis on the samples was conducted, the multicore was not further included in this study.

Ages of MIS boundaries as defined by the age model based on the LR04 benthic $\delta^{18}O$ stack are used to assign MIS 1 to 5a to sediments of the PASOM 3 gravity core. The basis of the MIS timescale is the alternation of periods with high $\delta^{18}O$ values, the even-numbered warmer stages, and periods with low $\delta^{18}O$ values, the odd-numbered colder stages. The present-day interglacial, the Holocene, is defined as MIS 1. The last glacial (occurring during the Late Pleistocene) extents from MIS 2 to the boundary between two sub-stages of MIS 5 (5d and 5e), at 123 ka BP. Since PASOM 3 sediments cover ages until 76 ka BP, only sub-stage 5a can be defined, which is a warmer sub-stage of MIS 5. Shorter term DO millennial-scale variabilities are also recorded. Coldest DO stadials correspond to North Atlantic Heinrich events. H1 to H6 are identified based on ages proposed by Hemming (2004) and references therein. The age of H6 is poorly constrained and defined by Hemming (2004) at 60 ka BP, although this could be different by at least ± 5 ka. Based on the PASOM 3 Br XRF record and foraminiferal counts, H6 is set at 63 ka BP, but this age might thus be slightly off.

4.2 X-Ray Fluorescence records and organic carbon

The C_{org} record shows considerable variation through time, with contents ranging between 0.40 and 3.02 wt% (Fig. 9F). A mean C_{org} content of 1.52 ± 0.51 wt% illustrates that sediments are OM-rich. Climatic variability is reflected in the record, since the Heinrich events are generally lower in C_{org} content compared to adjacent sedimentary layers, although this is not as pronounced for H4 and especially H3. The decreases in C_{org} content associated with Heinrich events are significantly larger in magnitude than the analytical error of 0.11 wt% and are, furthermore, also clearly visible in the higher-resolution Br XRF record, with H3 and H4 as exceptions (Fig. 9G). Apart from these millennial-scale variabilities larger-scale variations can be distinguished. Highest C_{org} values occur during MIS 1 and MIS 5a, while MIS 4 is characterized by C_{org} values as low as 0.40 wt%. C_{org} contents decrease sharply from 2.91 wt% at 75 ka BP towards 0.84 wt% at the start of MIS 4. During most of MIS 4, C_{org} values remain low and only start to increase after H6 towards a maximum of 1.80 wt%. During MIS 2 and MIS 3, the record is characterized by several oscillations. Maxima within these oscillations

range between 2.00 wt% and 2.35 wt%, while minima show variations between 0.94 and 1.11 wt%. During the Last Glacial Maximum (LGM; ± 23 - 19 ka BP; based on Lisiecki and Raymo, 2005) C_{org} values decrease from 2.00 towards 0.84 wt% and remain low during H1. After a rise in C_{org} content during the Bølling-Allerød interstadial (BA; 14.7 - 12.9 ka BP; Alley et al., 1993) and low values characterizing the YD, C_{org} content rises steadily through MIS 1 from YD values of 1.02 wt% to the core-top value of 3.02 wt%. Values of $\delta^{13}C_{bulk}$ show only minor variations, ranging between -20.5 and -19.2 ‰ with a mean of -19.8 ± 0.3 ‰ (Appendix 2).

The significant correlation ($r^2 = 0.63$, $p < 0.001$) between the Br XRF and C_{org} records validates the use of Br XRF scanning counts as a measure for C_{org} content during age model construction. Furthermore, the similarity between both records (Fig. 9F and 9G) indicates that significant bias in the Br XRF record related to formation of a water film during XRF core scanning (Tjallingii et al., 2007) can be ruled out, although small differences might be related to a variation in the water film thickness. Br is an element particularly susceptible to this bias, since it is predominantly present in pore water.

Although there exists no significant correlation between the records of C_{org} content and Sr/Ca, certain periods of C_{org} depletion coincide with an enrichment of Sr compared to Ca and thereby with higher Sr/Ca ratios, i.e. H1, H4, H6 and, to a lesser extent, H2 and H5 (Fig. 9E and 9F). These periods are not necessarily recognized as periods with extremely low C_{org} or high Sr/Ca values, but do show significant depletions or enrichments in comparison to surrounding sedimentary layers. Besides these millennial-scale periods of low C_{org} content and high Sr/Ca values, MIS 5a is characterized by a significant increase in Sr/Ca, while a decrease is visible for MIS 1. Deviations from the synchronous opposing trends of C_{org} and Sr/Ca values occur throughout the records, with the BA being the most pronounced. Both C_{org} and Sr/Ca values are relatively high during this period. The Sr/Ca record shows clear differences within MIS 1 to 5a, with consistently higher absolute Sr/Ca values during MIS 2 and MIS 4. In contrast to Sr/Ca, Ba/Al and Ba/Ti in general increase or decrease together with the C_{org} record, despite the absence of a significant correlation (Fig. 9C, 9D and 9F). Ba/Al and Ba/Ti vary synchronously, but magnitudes of change differ significantly during certain periods. The magnitude of increase is higher for Ba/Al between 6 and 3 ka BP while it shows a lower magnitude of decrease between 75 and 63 ka BP (Fig. 9B). These two periods are coeval with periods of highest and lowest water content, respectively (Fig. 9A). No distinction between MIS 1, MIS 3 and MIS 5a and MIS 2 and MIS 4 exists for the Ba/Al and Ba/Ti records, a distinction which was observed within the Sr/Ca record. Ba/Al and Ba/Ti in general vary synchronously with C_{org} content. MIS 5a shows a different behavior, and is associated with decreasing Corg

values towards the MIS 4, while both Ba/Ti and Ba/Al remain relatively constant (Fig. 9C, 9D and 9F).

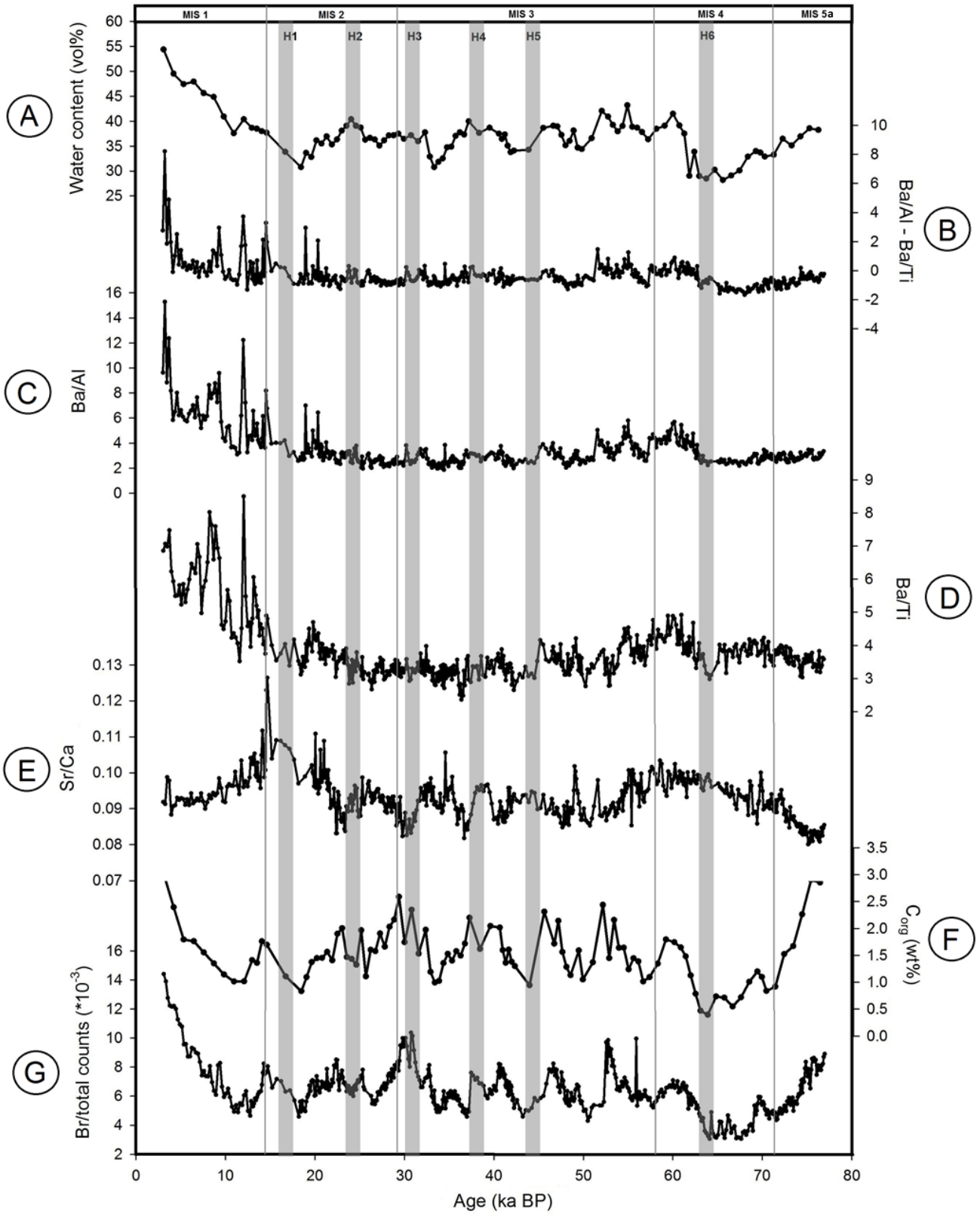

Figure 9: *Comparison of PASOM 3 C_{org} content (F) with PASOM 3 XRF core scanning records of Ba/Al (C), Ba/Ti (D), Sr/Ca (E), Br/total counts (G). Also shown are the sedimentary water content (A) and the difference between Ba/Al and Ba/Ti (B) versus age.*

4.3 Biomarker concentrations and mass accumulation rates

All samples contain detectable amounts of the LCDs of interest. By far the dominant LCD is the C_{30} 1,15-diol, with a mean fractional abundance of 0.55 ± 0.11 (normalized to the total pool of LCDs; Appendix 2). The second most abundant LCD is the C_{30} 1,14-diol (0.23 ± 0.09), followed by the C_{32} 1,15-diol (0.10 ± 0.02). High variabilities are observed for the 1,14-diols and especially the C_{28} 1,14-diol, for which fractional abundances range between 0.02 and 0.31 with a mean of 0.10 ± 0.05. Both the C_{28} and C_{30} 1,13-diol show a low fractional abundance with a low variability (0.008 ± 0.002 and 0.022 ± 0.005). The mean fractional abundance of the C_{32} 1,15-diol (normalized to 1,13- and 1,15-diols) equals 0.16 ± 0.04 and ranges between 0.07 and 0.23 (Appendix 2). LCD concentrations are highly variable, with a mean concentration of 34 µg/gC_{org} for the 1,14-diols and a range between 2 µg/gC_{org} occuring at 61 ka BP and 108 µg/gC_{org} at 70 ka BP (Fig. 10C). Highest 1,14-diol concentrations occur between 76 and 68 ka BP and between 12 and 3 ka BP. Concentrations of the sum of 1,13- and 1,15-diols vary between 6 and 250 µg/gC_{org}, observed at 61 ka BP and 22 ka BP (Fig. 10C). The mean concentration of the sum of 1,13- and 1,15-diols equals 70 ± 41 µg/gC_{org}, which is higher than the mean concentration of the 1,14-diols. Relative changes in concentrations of 1,14-diols and 1,13- and 1,15-diols do not vary accordingly, indicating a different behavior with respect to environmental factors, although both profiles show comparable variation as the biomarker sum (Fig. 10A; sum of $C_{37:2}$ alkenone, 1,13-, 1,14- and 1,15-diols, dinosterol, loliolide and isololiolide concentrations). $C_{37:2}$ alkenone concentrations range between 2 and 191 µg/gC_{org}, with a mean of 47 ± 39 µg/gC_{org} (Fig. 10B). Concentrations of dinosterol are relatively low, with mean values of 15 ± 9 µg/gC_{org} (Fig. 10D). Dinosterol is absent between 18.5 and 14.5 ka BP. The sum of loliolide and isololiolide showed the lowest concentration of all biomarkers, ranging between 0 and 19 µg/gC_{org} with a mean value of 6 µg/gC_{org} (Fig. 10D).

Summed isoprenoid and branched GDGTs show synchronous variations (Fig. 11), but their behavior differs significantly from that of the other biomarkers and was furthermore not correlated with the Sr/Ca, Ba/Ti and C_{org} records and diol indices. Branched GDGTs constitute only a minor fraction of the total pool of GDGTs, as shown by their low concentrations. Crenarchaeol and GDGT-0 are the dominant GDGTs through the whole record, which is in line with the suggestion that the isoprenoid GDGTs predominantly derive from marine Thaumarchaeota (Schouten et al., 2013 and references therein).

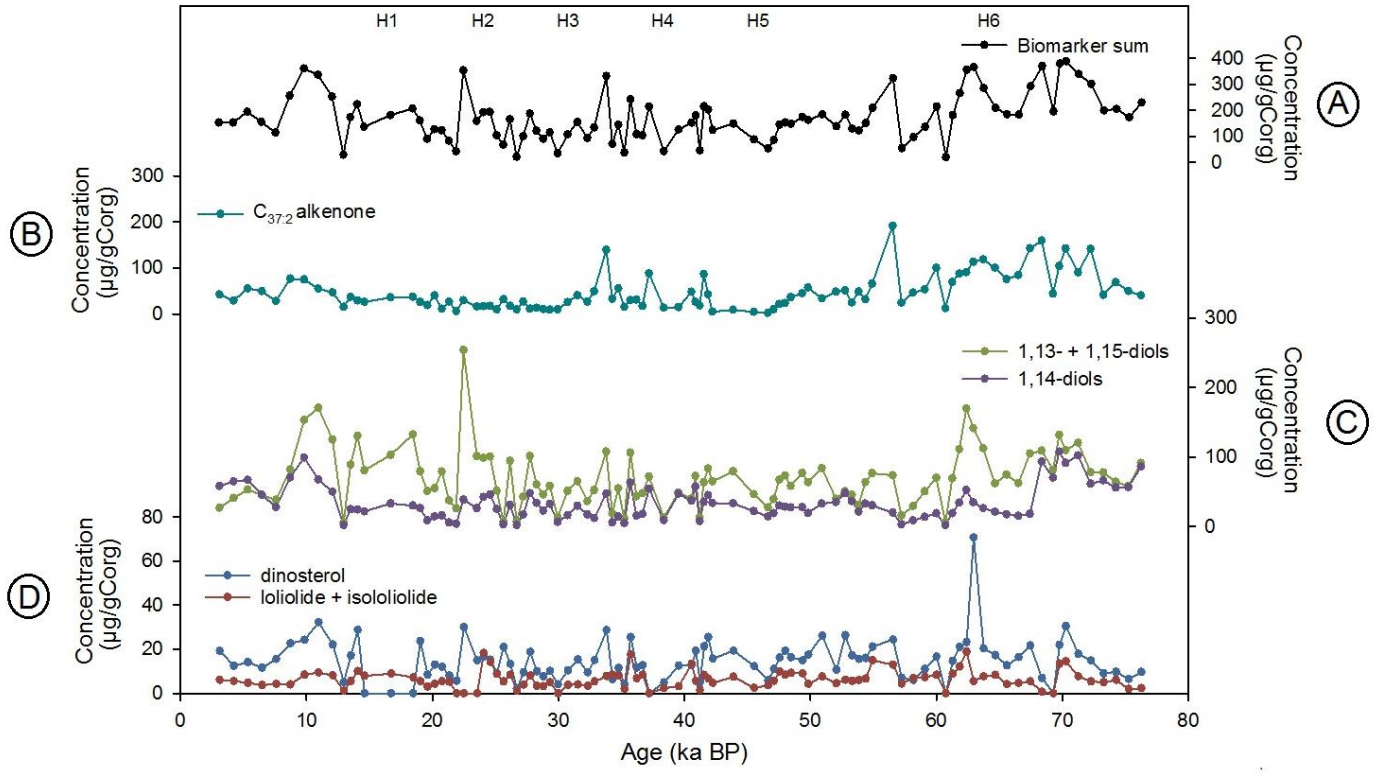

Figure 10: *Abundance of the biomarkers $C_{37:2}$ alkenone (B), 1,13- + 1,15-diols (C) and 1,14-diols (C), loliolide+isololiolide (D), dinosterol (D), and the sum of these abundances (A; biomarker sum) against age for the PASOM 3 core.*

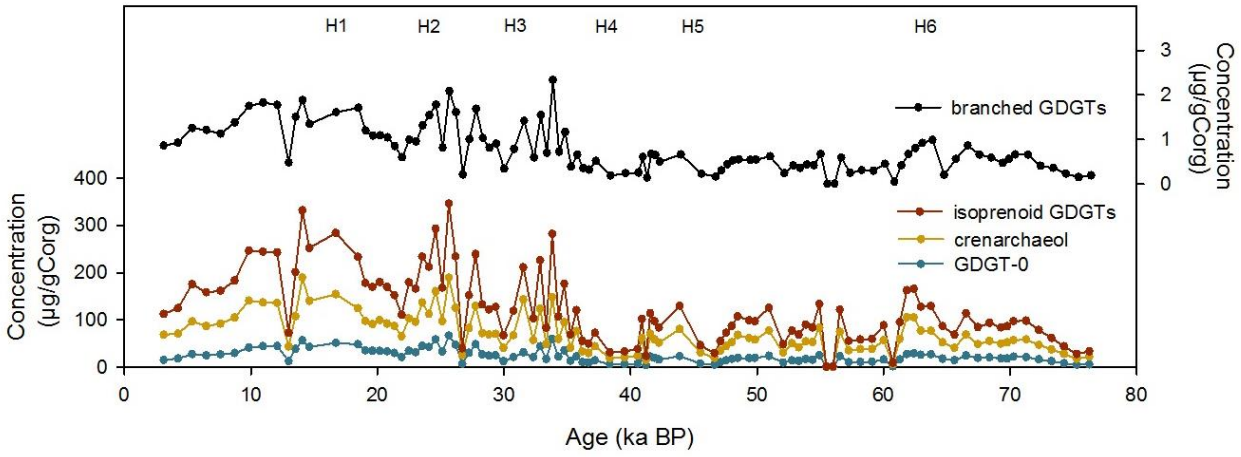

Figure 11: *Abundance of PASOM 3 isoprenoid GDGTs, branched GDGTs and the abundant isoprenoid GDGTs GDGT-0 and crenarchaeol against age.*

Relative abundances of the 1,14-diols, i.e. concentrations normalized to the summed concentrations of 1,13-, 1,14- and 1,15-diols, dinosterol, loliolide, isololiolide and the $C_{37:2}$ alkenone show a relation with the periods MIS 1 to 5a, with relative abundances of the 1.14-diols being higher during MIS 1 and MIS 5a (Fig. 12). Also, H6 is characterized by low relative 1,14-diol abundances, low diol indices, low Ba/Ti, low Ba/Al and high Sr/Ca. Over longer periods of time, 1,14-diols have consistently lower relative abundances during MIS 2 and MIS 4 compared to MIS 1, MIS 3 and MIS 5a, a pattern which is also observed for the diol indices. The relative abundance of 1,13- and 1,15-diols shows a different behavior, with high relative abundances occurring synchronously with several periods of high Sr/Ca, e.g. BA.

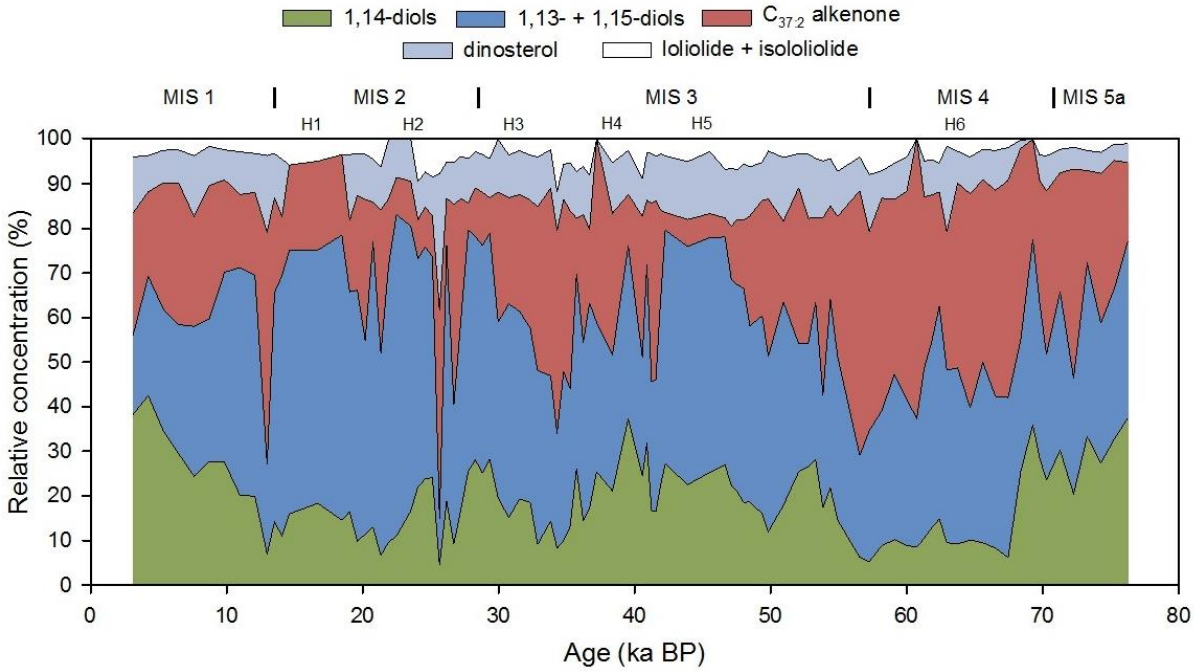

Figure 12: *Relative abundance of the biomarkers loliolide+isololiolide, $C_{37:2}$ alkenone, 1,13- + 1,15-diols and 1,14-diols against age. The sum of abundances of these biomarkers within PASOM 3 was set to 100%.*

To gain more insight into the delivery of biomarkers to the sediment and its relation to production and preservation within the area MARs of individual biomarkers are calculated and plotted for summed isoprenoid GDGTs, summed alkenones, 1,14-diols and summed 1,13- and 1,15-diols (Fig. 13). Heinrich events are in general associated with low biomarker MARs and this is especially pronounced during H4 and H5 when MARs nearly reach zero (Fig. 13A). H2 stands out, as being the only Heinrich event associated with high biomarker MARs of isoprenoid GDGTs and LCDs. Highest biomarker MARs occur during MIS 5a and the BA interstadial. Low biomarker MARs characterize the Holocene between 6 and 3 ka BP. Although MARs of the 1,14-diols and MARs of the 1,13- and 1,15-diols in general vary synchronously, their magnitude of change is different (Fig. 13C). Throughout the largest part of the records,

1,13- and 1,15-diols show higher MARs compared to 1,14-diols. During part of MIS 1, MIS 5a and the two periods characterized by a decrease in LDI-SST associated with an increase in diol indices (57-51 ka BP and 45-37 ka BP), MARs of the 1,14-diols are equal or even dominate over MARs of 1,13- and 1,15-diols. High diol indices during these periods are thus associated with high concentrations and MARs of the 1,14-diols, a feature which can also be observed for LCD concentrations within the sediment (Fig. 10C). The MARs of the $C_{37:2}$ + $C_{37:3}$ alkenones show a different variation than that of isoprenoid GDGTs and LCDs, with as most pronounced example the low MARs during the period 33 – 3 ka BP, while peaks occur during this period for the isoprenoid GDGTs and LCDs (Fig. 13A, 13B and 13C).

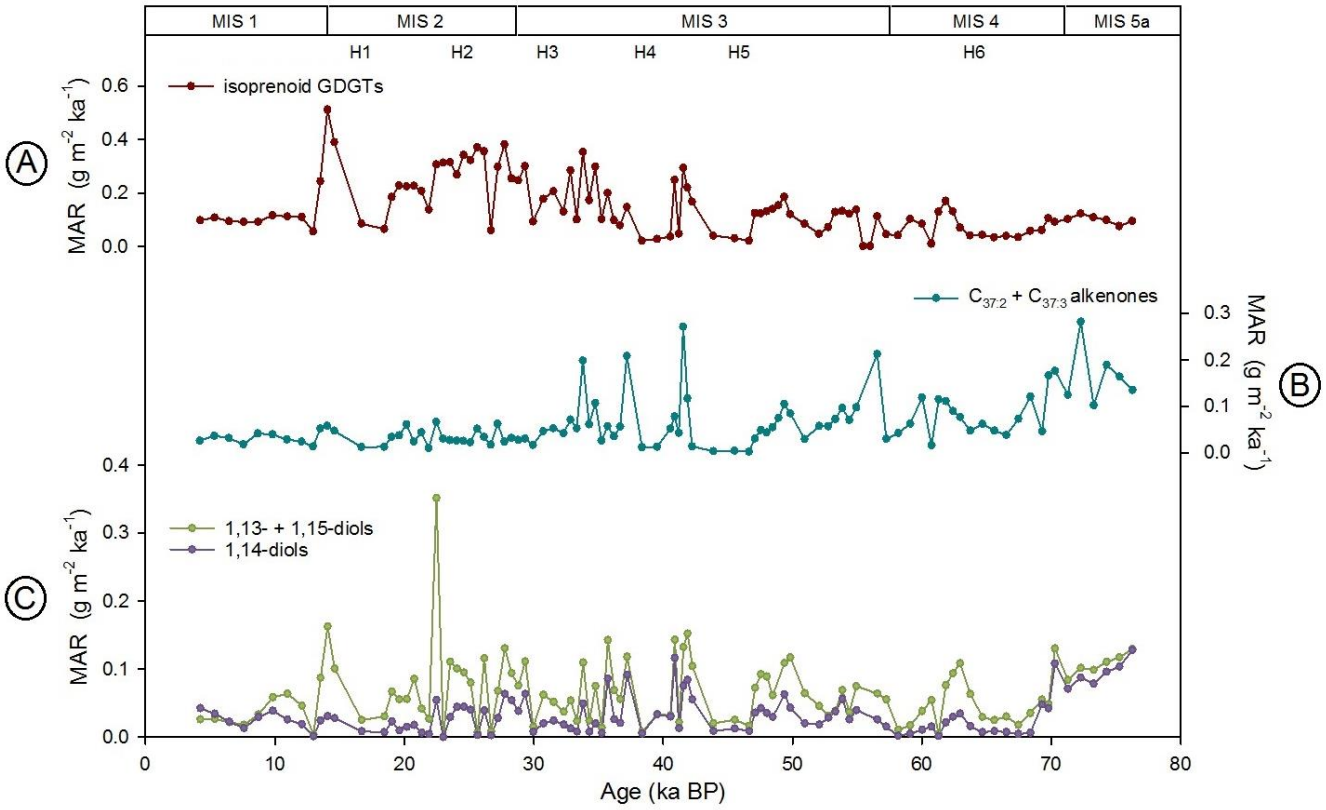

Figure 13: *PASOM 3 MARs of different groups of biomarkers, plotted against age. Shown are the total MARs of isoprenoid GDGTs (A; sum of GDGT-0, GDGT-1, GDGT-2, GDGT-3, crenarchaeol and the crenarchaeol regio-isomer), alkenones (B; sum of $C_{37:2}$ and $C_{37:3}$ alkenones) and of the LCDs, separated in two groups (1,13+ 1,15-diols and 1,14-diols) based on the position of the mid-chain alcohol group* (C).

4.4 Biomarker proxies

LDI values range between 0.90 and 0.97, corresponding to temperatures of 24.4 and 26.5 ^{0}C (Fig. 14B). Temperature variations are low and fluctuate around a mean of 25.8 ± 0.5 ^{0}C throughout most of the record. No SST changes related to transitions between MIS stages are visible. Three periods are characterized by relatively larger changes in SST. SST decreases from 26.2 ^{0}C at 22 ka BP towards a core-top value of 24.8 ^{0}C. The other two

significant deviations occur between 57 and 51 ka BP and 45 and 37 ka BP, during which cooling towards 24.9 ^{0}C and 24.6 ^{0}C and a subsequent return to the mean SST is observed. Further indications of changing environmental conditions during these three intervals comes from accompanying increases in the diol indices. DI 1 ranges between 0.14 at 21 ka BP and 0.74 at the core-top. DI 2 shows lower changes in magnitude and ranges between 0.80 at 21 ka BP and 0.97 during both 76 and 3 ka BP (Fig. 10C). The LDI-inferred cooling between 22 and 3 ka BP is associated with an increase in DI 1 from 0.14 to 0.74 (Fig. 14C). DI 2 increases accordingly from 0.80 to 0.97 (Fig. 14C). Diol indices 1 and 2 increase and decrease synchronously, with MIS 2 and MIS 4 being associated with relatively low values while both diol indices are on average high during MIS 1, MIS 3 and MIS 5a, a pattern which was also observed for the relative abundance of 1,14-diols (Fig. 12). Especially MIS 1 and MIS 5a show high values for the diol indices, although the variability within these periods differs greatly. MIS 5a is characterized by a plateau of high diol indices, whereas a gradual increase of the indices towards high core-top values occurs during MIS 1.

TEX^{H}_{86} values range from -0.17 to -0.11. The TEX^{H}_{86} record is quite different from the LDI record, with TEX^{H}_{86}-SSTs being consistently higher. Absolute SST differences between the two proxies vary between 1.0 and 6.5 ^{0}C (Fig. 14B). A significant gradual warming within the TEX^{H}_{86} record occurs from 28.2 ^{0}C to 31.4 ^{0}C between 76 and 3 ka BP. TEX^{H}_{86}-SSTs increase synchronously with the δD EPICA DOME C record between 18.5 and 14.6 ka BP after a relatively stable period between 29 ka BP and 18.5 ka BP (Fig. 14A and 14B). This increase in δD is associated with a warming of 1.3 ^{0}C within the TEX^{H}_{86} -SST record. Both records show a decrease until 13.5 ka BP, when SST is as low as 29.5 ^{0}C. The two records start to deviate after 12 ka BP and TEX^{H}_{86}-SST increases towards the core-top value of 31.4 ^{0}C. The BIT index is consistently low and varies between 0.002 and 0.010, with a mean of 0.006 ± 0.001 (Appendix 2).

Alkenone-derived $U^{K'}_{37}$ values show a wide range (0.62 - 0.93) which corresponds to SSTs between 17.5 ^{0}C and 26.8 ^{0}C (Fig. 14B). No relation to climatic events or the TEX^{H}_{86} or LDI SST proxies can be observed. Millenial-scale SST fluctuations as large as 6.0 ^{0}C occur. Trends extending over longer periods are not distinguishable.

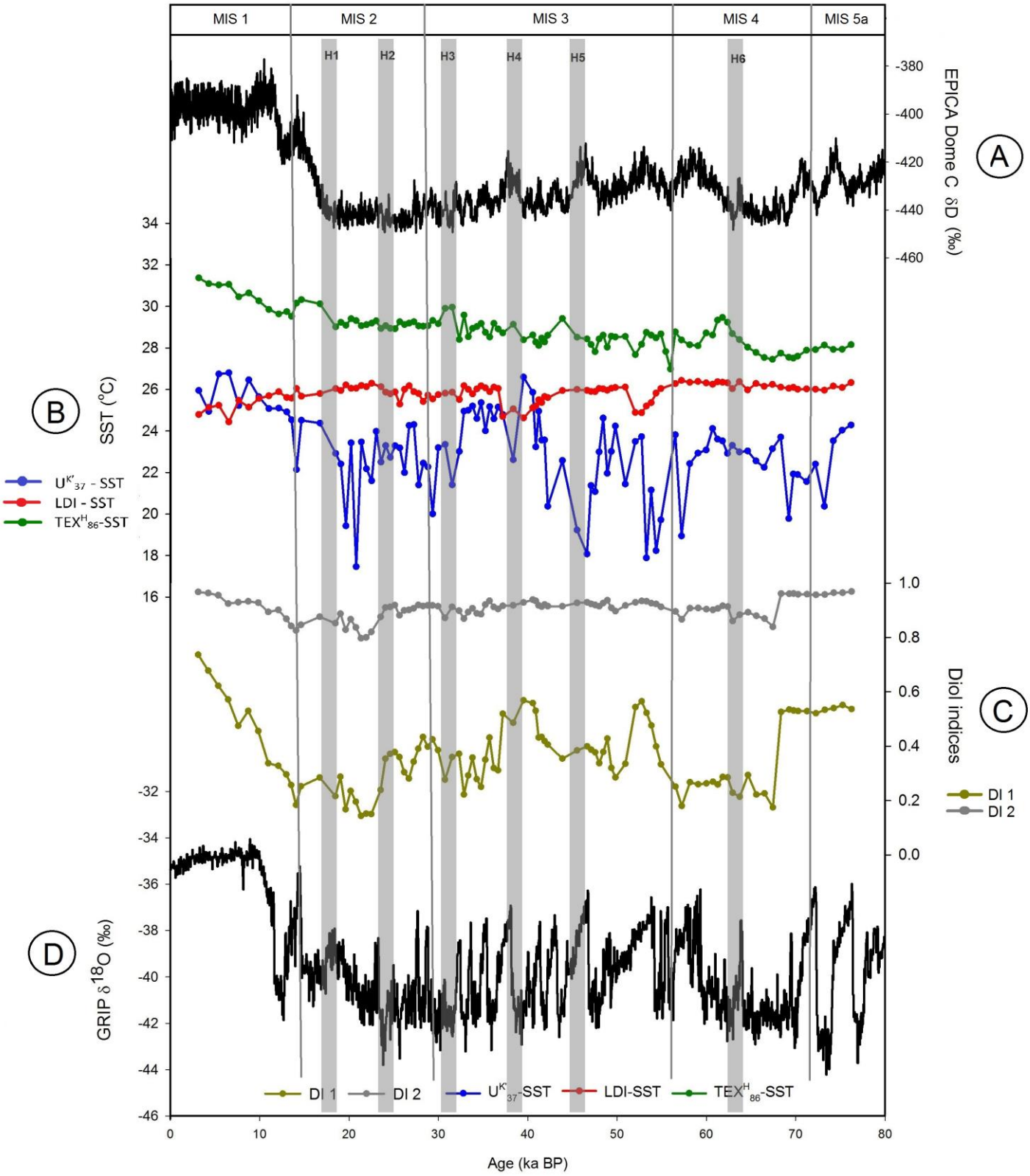

Figure 14: *PASOM3 records of the three organic SST proxies ($U^{K'}_{37}$, LDI and TEX^{H}_{86}) plotted against age (B), compared with PASOM3 DI 1 and DI 2 records (C). For reference, the δD of EPICA Dome C from Antarctica (A; Jouzel et al., 2003) and the $\delta^{18}O$ of GRIP from Greenland (D; Dansgaard et al., 1993) and are shown.*

4.5 Principal Component Analysis

The input for the PCA analyses were biomarker concentrations in µg/gC_{org}. Several combinations of biomarkers were included in different PCAs, in order to detect all variations in biomarker distributions. Inclusion of a biomarker with a largely different behavior could overwhelm differences between other biomarkers. Figure 15 shows a PCA only considering the six LCDs included in this study, combined with data points reflecting MIS 1 to 5a and Heinrich events. The first two principal components explain 79.57% and 18.30% of the total variance in LCD distribution, respectively. The 1,14-diols load separately from the 1,13- and 1,15-diols. MIS 1, MIS 3 and MIS 5a load closer to 1,14-diols, whereas MIS 2, MIS 4 and Heinrich events generally load negatively on PC2. An exception to this are several data points belonging to MIS 4, which load together with data points representing MIS 5a most positive on PC2. These points reflect the samples that are also characterized by high diol indices, as shown in Figure 14C. Furthermore, the C_{32} 1,15-diol does not load similar to the other 1,13- and 1,15-diols. The C_{32} 1,15-diol loads positive, while the 1,13-diols and C30 1,15-diols load neutral and negative on PC2, respectively.

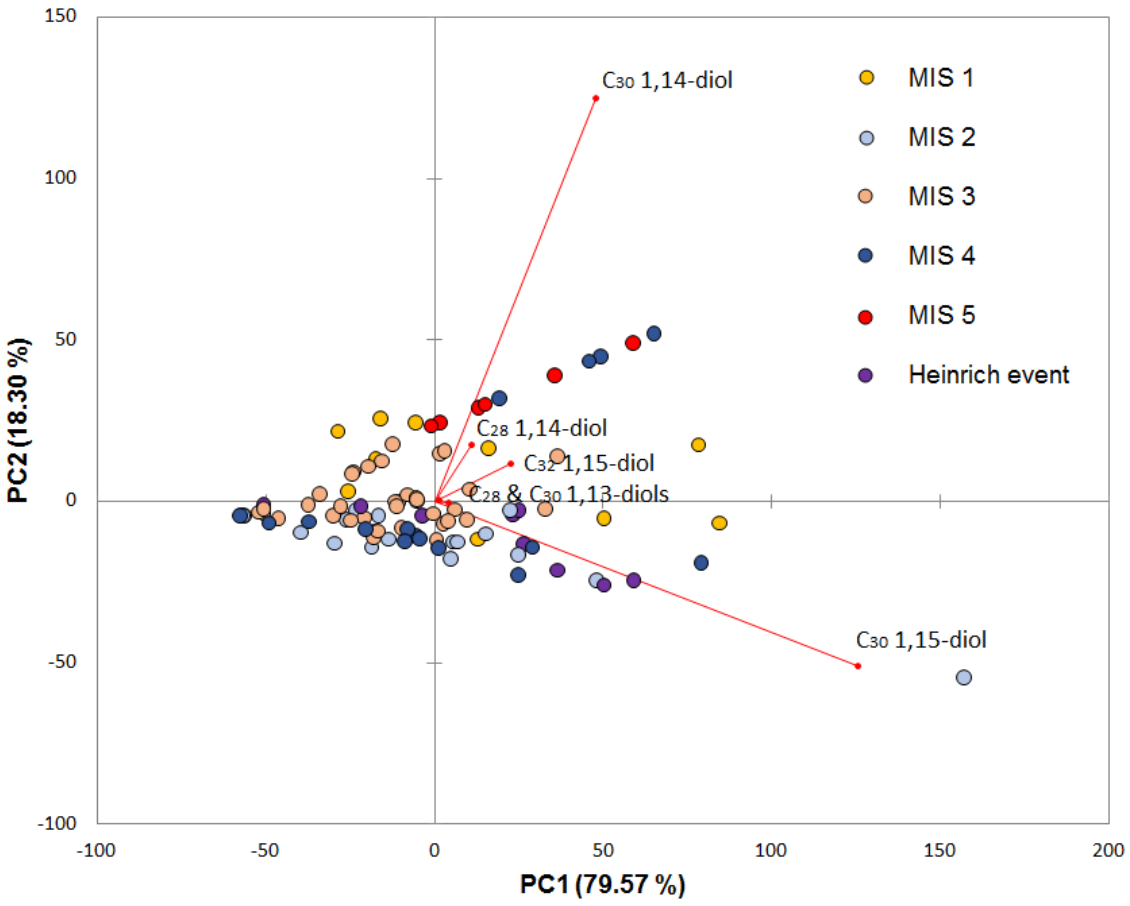

Figure 15: *PCA of PASOM 3 C_{28} 1,13-diol, C_{28} 1,14-diol, C_{30} 1,14-diol, C_{30} 1,15-diol and C_{32} 1,15-diol concentrations in µg/gC_{org}. Grouping of data within MIS 1 to 5a is based on Lisiecki and Raymo (2005) and timing of Heinrich events on Hemming (2004).*

The two principal components of the PCA including all biomarkers (concentrations of $C_{37:2}$ alkenone, sum of 1,13- and 1,15-diols, 1,14-diols, dinosterol, the sum of loliolide and isololiolide and crenarchaeol in ug/gCorg) explain 50.84% and 28.92% of the variance in biomarker distribution (Fig. 16A). Crenarchaeol loads negative on PC2, while the other biomarkers load positive. When crenarchaeol is excluded, the two principal components explain 63.66% and 25.43% of the variance in biomarker distribution (Fig. 16B). The sum of loliolide and isololiolide, 1,14-diols and dinosterol load in the same cluster, while the $C_{37:2}$ alkenone is the only biomarker loading negative on PC2.

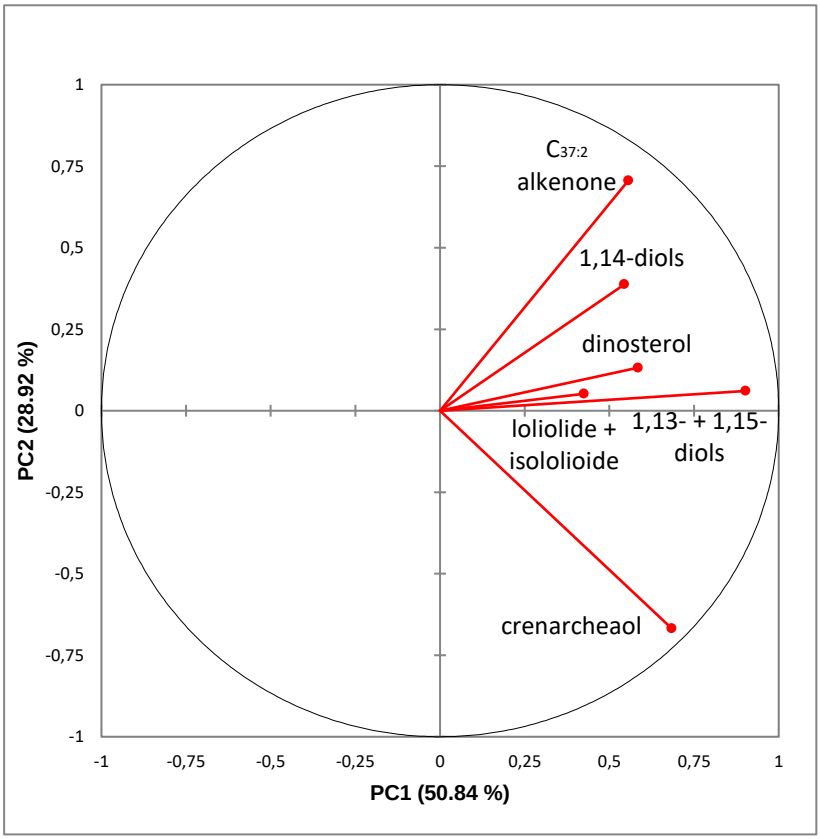

Figure 16A: *PCA of PASOM 3 biomarker concentrations in µg/gC$_{org}$, for the biomarkers $C_{37:2}$ alkenone, dinosterol, loliolide+isololiolide, 1,14-diols, 1,13- + 1,15-diols and crenarchaeol.*

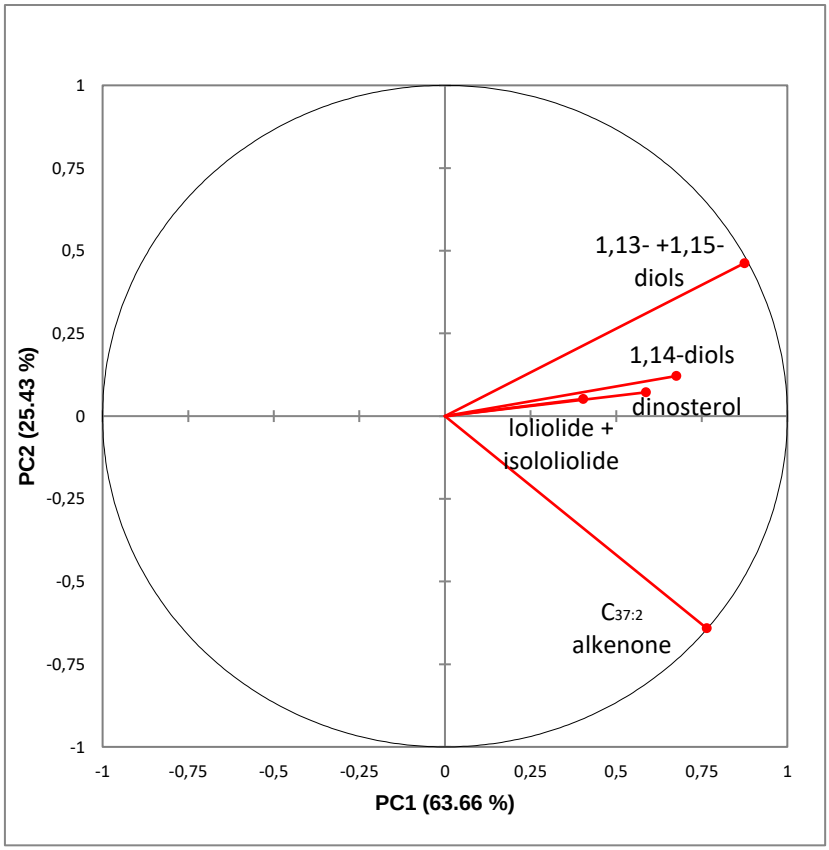

Figure 16B: *PCA of PASOM 3 biomarker concentrations in µg/gC_{org}, for the biomarkers $C_{37:2}$ alkenone, dinosterol, loliolide+isololiolide, 1,14-diols and 1,13- + 1,15-diols.*

5 DISCUSSION

5.1 Production and preservation of organic carbon and biomarkers

Accumulation of C_{org} and biomarkers within marine sediments is determined by primary productivity in the surface waters and the degree of degradation within the water column and sediments, also referred to as preservation. Preservation of OM is strongly affected by the O_2 exposure time, accounting for the C_{org} rain rate and the O_2 content of both bottom waters and surface sediments underlying O_2-containing bottom waters (Sinninghe Damsté et al., 2002b). An understanding of these factors is of importance for biomarker studies, but is complex within the Arabian Sea since the intensity of the OMZ and thus preservation is directly influenced by primary productivity (Reichart et al., 1998). Changes in productivity and preservation will influence biomarker accumulation and control the biomarker distribution within sediments, potentially influencing organic proxies.

OM production by primary producers within the Arabian Sea mainly occurs during the SWM with a second, smaller, production peak during the NEM (Haake et al., 1993; Honjo et al., 1999; Wakeham et al., 2002). Since characteristic $\delta^{13}C_{bulk}$ values for marine and

terrigenous OM are -20 ‰ and -26 ‰, respectively (Fontugne and Duplessy, 1986), input of terrigenous OM via the Indus River is insignificant (PASOM 3 $\delta^{13}C_{bulk}$ = -19.8 ± 0.3 ‰). Therefore, when surface productivity is the only factor governing OM accumulation, the C_{org} record is expected to vary synchronously with surface productivity. The Ba/Al ratio is often used as a measure for surface productivity, because Ba precipitates in sinking OM within the water column (e.g. Dehairs et al., 1980; Dymond et al., 1992) and Al is used to normalize for fluctuations in terrigenous content, which is minimum for PASOM 3. The element Al is susceptible for biases introduced by XRF core scanning, since its low elemental weight makes it susceptible to absorption issues, related to its relatively low fluorescence energy (Tjallingii et al., 2007). Formation of a water film between the plastic used to cover the core sections and the sediment surface results in an increase of the water content, reducing elemental counts for light elements. Differences between water contents within a sediment core can cause variation in the magnitude of the bias related to absorption (Hennekam and De Lange, 2012). But, since Ti is also terrestrially derived, it can replace Al within Ba normalization. Due to its relatively high elemental weight, Ti is not influenced by any property of the core section during XRF core scanning (Tjallingii et al., 2007). Comparison of the PASOM 3 Ba/Al and Ba/Ti XRF records (Fig. 9B, 9C and 9D) reveals that they vary more or less synchronously, although large differences within the magnitude of change exist during two periods: i.e. 75 - 63 ka BP and 6 - 3 ka BP. These periods are furthermore characterized by highest and lowest sedimentary water content, respectively (Fig. 9A). Although formation of a water film and thus bias within the Al record is not linearly related to sedimentary water content, these observations lead to the conclusion that the Ba/Al record might be biased. Therefore, Ba/Ti has been chosen to be used as a proxy for surface productivity within this study. When surface productivity would be the only factor determining OM accumulation, a close resemblance between the Ba/Ti and C_{org} records is expected. Despite the synchronous variation during most of the records, there exists no significant correlation. Consequently, other factors additional to surface productivity affect the C_{org} profile, and thus OM accumulation.

O_2 concentrations at the sediment-water interface and within the sediments are considered important factors in OM preservation. The degree of degradation of OM within the water column in the Arabian Sea is small compared to degradation within the sediments (Prahl et al., 2000; Wakeham et al., 2001; 2002). This can be explained by the longer time of exposure within sediments, as exposure to O_2 is an important factor governing OM accumulation (Hartnett et al., 1998; Hedges et al., 1999). Bottom water oxygenation during time of deposition can be assessed using the Sr/Ca record. Sr/Ca is a proxy for the aragonite compensation depth as aragonite makes up the Sr-rich fraction within the Arabian Sea (Reichart et al., 2004). Aragonite readily dissolves at the sediment-water interface within the OMZ (Berger, 1978) and Sr/Ca thus reflects O_2 content and OMZ intensity (Reichart et al., 2004; Singh, 2007). Sr is

related to biogenic carbonate and is therefore normalized to Ca. Since the Sr/Ca record is qualitative, high Sr/Ca values can only be interpreted as periods with higher O_2 contents and thus a less intense OMZ, with most Heinrich events and the period from the LGM to 14 ka BP being the most pronounced examples. Although arguments exist against an important role of preservation within OM accumulation (Reichart et al., 1998 and references therein), high PASOM 3 Sr/Ca values occur during most Heinrich events, which are characterized by decreases in C_{org} content. Since PASOM 3 surface productivity is not necessarily low during Heinrich events, high degradation during relatively oxic conditions exerts a control on OM accumulation, resulting in lower C_{org} values. This agrees with results of Koho et al. (2013), who found a relation between C_{org} content and bottom water O_2 concentrations for a set of Murray Ridge surface sediments.

It has been shown that biomarker distributions change in relation to varying O_2 exposure time, influencing paleoenvironmental reconstructions (Sinninghe Damsté et al., 2002b). Biomarkers are part of the total pool of OM and are thus included in the C_{org} record, but do not show the same variations regarding their accumulation as bulk OM. Considering the general lower relative preservation efficiencies of biomarkers compared to C_{org} (Sinninghe Damsté et al., 2002b), differences between variabilities within biomarker abundances and the C_{org} record reflect an influence of preservation. PASOM 3 biomarker accumulation is probably influenced by preservation since periods of high C_{org} and low Sr/Ca values, and thus high OMZ intensity, are not necessarily observed during periods of high biomarker abundances. The sum of concentrations of all individual biomarkers does thus not vary in accordance with the C_{org} content, which would be expected when solely primary productivity governs biomarker accumulation. Hence, biomarkers are preferentially degraded, a process which can occur even during relatively anoxic conditions. An example of this preferential degradation is visible between 18.5 and 14.5 ka BP, during which C_{org} content shows an increase, while the most labile biomarker dinosterol (Sinninghe Damsté et al., 2002b) is absent during this period. Synchronous high Sr/Ca values, and thus relatively oxic concentrations, serve as a support. The semiquantitative character of the XRF core scanning records of Ba/Ti and Sr/Ca ratios does not allow for quantification of neither surface productivity nor bottom water oxygenation, being one of the limitations of this study. Biomarker concentrations and mass accumulation rates show that both production and preservation play a role in biomarker accumulation within the Arabian Sea, potentially influencing the organic SST proxies, but since quantification of these processes is not possible, uncertainties regarding this influence remain.

Within the Arabian Sea, O_2 concentrations in the water column (i.e. intensity of the OMZ) are strongly influenced by the intensity of upwelling during the SWM. An increase in upwelling of nutrient-rich waters leads to enhanced surface production and results in high O_2 depletion and thus an intense OMZ. Although PASOM 3 was located outside the direct zone of upwelling

off Oman and Somalia, it could still be influenced by upwelling dynamics. Covarying patterns found in e.g. C_{org} records from the NIOP 464 core from the Murray Ridge and NIOP 497 from the upwelling cell in the Oman Margin (Reichart et al., 1998) show that upwelling dynamics can indeed be recorded at the Murray Ridge. Furthermore, the observed variation in DI 1 values of PASOM 3 (Fig. 14C) are comparable with the DI 1 record of NIOP 905 from the Somali continental slope (Rampen et al., 2008), part of a major upwelling system (Rampen et al., 2014a). Additionally, values of the diol indices are low during periods of low intensity of the OMZ (high Sr/Ca), i.e. MIS 2 and MIS 4. Since upwelling is expected to exert a major influence on oxygenation of intermediate waters via its control on surface productivity, synchronous high values of diol indices and Sr/Ca indicate that the diol indices are able to reconstruct upwelling and the comparability between PASOM 3 and NIOP 905 diol indices is thus related to upwelling processes, suggesting that PASOM 3 is susceptible to upwelling dynamics.

Rampen et al. (2014a) provided a comparison between DI 1 and DI 2 by assessing the influence of temperature, salinity, chlorophyll and nutrient concentrations on the behavior of the diol indices. They concluded that DI 1 is not suitable as a global indicator for upwelling, due to its negative correlation with temperature, although the index seems to work well within the Arabian Sea. The PASOM 3 DI 1 and DI 2 records, of which the last is unaffected by temperature (Rampen et al., 2014a), vary synchronously, in spite of the minor variations within the DI 2 record. Temperature, therefore, does not seem to have affected the variation within DI 1, although amplification of the magnitude of change related to the negative correlation between temperature and DI 1 cannot be ruled out. This supports the use of DI 1 as a measure for upwelling within the Arabian Sea. Since DI 2 has not been observed to be correlated with the parameters investigated by Rampen et al. (2014a) and is only insignificantly affected by changes in the residence time of the corresponding biomarkers within the oxic zone of the sediment (Rodrigo-Gámiz et al., 2016), it can be seen as a better applicable global indicator of upwelling. But, since the abundance of the 1,13-diols is low in the warm waters of the Arabian Sea, reflected in the high values of DI 2, DI 1 will be used in this study. It has been proposed that diol indices should be used as indicators for *Proboscia* productivity, linked to different parameters depending on the region on which they are applied (Rampen et al., 2014a). For the Arabian Sea, flux patterns of *Proboscia* valves and 1,14-diols have been observed to show similar trends and both are highest at the start of the SWM (Rampen et al., 2008), indicating that for PASOM 3, DI 1 values can be interpreted as a measure of SWM intensity and thus upwelling. Diol indices are qualitative measures, despite they can give valuable information on SWM intensity and therefore indirectly on O_2 conditions and OMZ intensity.

5.2 Variations in upwelling intensity and the LDI

The LDI is a recently established organic SST proxy and therefore not much is known about its behavior in upwelling areas. Rampen et al. (2012) demonstrated that the LDI correlates best with annual mean SST of 0 - 30 m water depth. The PASOM 3 LDI-SST (mean SST of 25.8 ± 0.5 ^{0}C) varies around the present-day annual mean SST of the Arabian Sea (27 ^{0}C; World ocean atlas 09 database; Locarnini et al., 2010), which is within the calibration error of the proxy (± 2 ^{0}C). The LDI-SST record does not vary synchronous with either the NH GRIP or the SH EPICA DOME C ice-core record (Fig 14A, 14B and 14D), indicating that the LDI does not record annual mean SST changes related to NH or SH climatic variability, i.e. low SST during the cold Heinrich events and occurrence of differences within MIS 1 to 5a. Also, glacial-interglacial SST differences within the Arabian Sea are at least 3 ^{0}C (Emeis et al., 1995), based on comparison of different $U^{K'}_{37}$ records. These records are from an area unaffected by upwelling (Rostek et al., 1993) and from ODP Site 723 close to the coast of Oman and thus within an upwelling cell. The comparable magnitude of the glacial-interglacial SST difference found for both sites, after correction for upwelling was conducted for ODP Site 723, led to the suggestion that the difference of 3 ^{0}C is a regional feature (Emeis et al., 1995) and would thus also be expected for PASOM 3. The absence of a SST difference of at least 3 ^{0}C between the present interglacial MIS 1 (Holocene) and MIS 2 to MIS 5a (part of the last glacial) within PASOM 3 sediments indicates that glacial-interglacial SST differences are not recorded by the LDI. Also, the warming between the LGM and present-day of 1.5 - 5 ^{0}C as reconstructed by both organic and inorganic SST proxies (Huguet et al., 2006 and references therein) is not reflected in the PASOM 3 LDI-SST record, the LDI even records a cooling of 1.5 ^{0}C. By combining $\delta^{18}O$ and $U^{K'}_{37}$ records from the northern Arabian Sea, Reichart et al. (2002) reconstructed annual mean SSTs for Heinrich events that varied between 21.5 and 23.5 ^{0}C, representing H1 and H3, respectively. These cold SSTs are not visible within the LDI-SST record. Therefore, the LDI does not record annual mean SST variations from the NH and SH as reflected by reference ice-core records and furthermore does not show the local SST variations reconstructed for the Arabian Sea.

Several explanations for the absence of the differences in annual mean SST between climatic states can be proposed. Since LCDs are affected by preferential degradation under oxic conditions (Rodrigo-Gámiz et al., 2016), changes in OMZ intensity and thus bottom water O_2 concentrations could have influenced the LCD distribution and thereby the LDI. Rodrigo-Gámiz et al. (2016) reported best preservation of the 1,13-diols, followed by the 1,14-diols and finally 1,15-diols, while there was no dependence on chain length. This different susceptibility towards degradation was attributed either to contrasting modes of physical protection of the LCDs or to the occurrence of LCDs as both free-lipids and in bound form. The

location of the PASOM 3 core at the bottom of the present-day OMZ leads to the hypothesis that O_2 concentrations strongly varied over time, as a result of extension and erosion of the OMZ (Reichart et al., 1998), thus potentially affecting the LDI. MIS 2 and MIS 4 are characterized by a less intense OMZ and thus higher O_2 concentrations of the bottom waters, reflected by high Sr/Ca values. A lower intensity of the OMZ results in an increase in the extent of oxic degradation, increased preferential degradation of the C_{30} 1,15-diol and would thus result in a lower LDI and LDI-SST. On the other hand, MIS 1, MIS 3 and MIS 5a are characterized by a high OMZ intensity (low Sr/Ca values) and oxic degradation, therefore, is expected to have less impact on the LDI-SST. Although these processes could have occurred within the PASOM 3 sediments, they cannot explain the absence of SST differences between MIS 2 and MIS 4 and MIS 1, MIS 3 and MIS 5a, since their influence on SST works in opposite direction, amplifying the SST differences. Relatively large influences of oxic degradation during the already colder MIS 2 and MIS 4 cause a decrease in recorded SSTs, while the minor influence of oxic degradation decreases SST of MIS 1, MIS 3 and MIS 5a to a lower extent, thereby increasing the SST difference between the two climatic states. The same holds for the differences between Heinrich events and interstadials, with cold Heinrich events being characterized by higher O_2 concentrations (higher Sr/Ca values) and thus a larger extent of oxic degradation than the warmer interstadials.

An alternative explanation for the absence of climate-related SST differences within the LDI-SST record is related to the effect of a shift in blooming season of the organisms producing the 1,13- and 1,15-diols and thereby of the season that is reflected within the LDI. This was reported to occur for other organic SST proxies, e.g. Rodrigo-Gámiz et al. (2014) observed the influence of a shift in the dominant production season of alkenones on the $U^{K'}_{37}$ within the Mediterranean Sea. The 1,13- and 1,15-diols included in the LDI are within the Arabian Sea related to the general productivity, with 50% of these LCDs being produced during the SWM and a lower production peak occurring during the NEM (Rampen et al., 2008). During periods of low upwelling and thus SWM intensity, a shift in LCD production away from the cold SWM towards increasing importance of the warmer intermonsoonal SI and FI would lead to a higher LDI-SST, assuming that present-day SST differences between seasons were similar in the past, with lowest SST during the NEM followed by the SWM (Levitus and Boyer, 1994). On the contrary, when upwelling is high, production is expected to be more concentrated within the cold SWM. High upwelling characterizes MIS 1, MIS 3 and MIS 5a within the Arabian Sea, as shown by relatively high DI 1 values and verified by the low O_2 concentrations resulting from high SWM intensity (low Sr/Ca values). This high upwelling is confirmed by PCA analysis, where MIS 1, MIS 3 and MIS 5a load closer to the 1,14-diols which are characteristic for upwelling than MIS 2 and MIS 4 (Fig. 15). High upwelling during the relatively warm MIS 1, MIS 3 and MIS 5a results in a concentration of 1,13- and 1,15-diol production during the

relatively cold SWM. MIS 2, MIS 4 and Heinrich events, on the contrary, generally load negative on PC2, with low upwelling confirmed by relatively low DI 1 values. Production of 1,13- and 1,15-diols during these relatively cold periods potentially shifted towards the warmer intermonsoonal periods, leading to an increase in LDI-SST. Differences between production patterns of 1,13- and 1,15-diols between MIS 1, MIS 3 and MIS 5a and MIS 2 and MIS 4 could thus cause a decrease within recorded SST differences of these warmer and colder stages, respectively. It still remains uncertain whether this dampening effect indeed has the potential to completely erase the SST differences. This will depend on the degree of the production shift and to SST differences between SWM and intermonsoon periods, which is expected to have varied over time.

A feature observed within the LDI-SST record that stands out both in the aspect of deviation from the general low variability within the record and the knowledge on temperature changes based on other SST proxies is the decrease in SST between 22 and 3 ka BP, comprising the LGM and Holocene. Several studies estimated a SST increase between the LGM and present-day of 1.5 - 5 ^{0}C within the Arabian Sea, comparable in magnitude to the PASOM 3 LDI-SST decrease of 1.5 ^{0}C between the LGM and 3 ka BP, despite this the LDI thus records an opposite trend. Although the decrease is still within the calibration error of the proxy (± 2 ^{0}C), the clear trend towards lower SST and the large magnitude of change compared to the rest of the record makes the recorded cooling remarkable. Furthermore, the decrease in LDI-SST is not as expected based on the δ^{18}O GRIP and the δD EPICA Dome C ice-core records. Therefore, a process other than SST differences related to climatic variability must be responsible for the observed decrease in LDI-SST between 22 and 3 ka BP.

Besides the gradual decrease in SST observed from 22 to 3 ka BP, two other periods are characterized by SST decreases with comparable magnitudes as the calibration error of the proxy (± 2 ^{0}C), i.e. 57 - 51 ka BP and 45 - 37 ka BP. Cooling of this degree is not expected based on the δ^{18}O record of *Neogloboquadrina dutertrei* of core NIOP 464 located on the Murray Ridge (Reichart et al., 1998). The period between 57 and 51 ka BP is known for an intensification of the OMZ around 52 ka BP, which caused an increase in preservation of OM (Sinninghe Damsté et al., 2002b). Indeed, PASOM 3 C_{org} values are high during this period, synchronous with a decrease in Sr/Ca. The presence of an intense OMZ is furthermore supported by high DI 1 values. Low LDI-SST between 45 and 37 ka BP occurs coeval with high upwelling intensities, which would indicate an intense OMZ. This is in contrast with the high Sr/Ca values from 38 to 40 ka BP (including H4), reflecting a less intense OMZ and thus low expected preservation. Rodrigo-Gámiz et al. (2016) attributed differences in LDI-SST of equal magnitude (2.0 - 3.5 ^{0}C) between stations with O_2 concentrations of < 3 and 77 µmol/L to preferential degradation of the C_{30} 1,15-diol. This process of oxic degradation causing an offset of the LDI to lower temperatures could potentially only explain the SST decrease during

the relatively oxic period from 40 to 38 ka BP, since during the major part of the periods 57 – 51 ka BP and 45 – 37 ka BP, the OMZ intensity was high and oxic degradation is therefore not expected to play an important role.

Other factors that can potentially explain the decreases in LDI-SST for the periods 57-51 ka BP, 45 - 37 ka BP and 22 - 3 ka BP include an increased input of LCDs by rivers. Lattaud et al. (2017) reported that LDI-SST underestimates in-situ SST close to the Berau River mouth and Gulf of Lions. An increased river input from the Indus River can thus potentially cause an offset of the LDI record towards lower SST. The C_{32} 1,15-diol which is proposed to be produced in-situ in rivers (De Bar et al., 2016; Lattaud et al., 2017) does indeed load opposite to the C_{30} 1,15-diol within PCA analysis (Fig. 15) and does furthermore not cluster with the 1,13-diols, indicating a different source and thereby supporting the terrestrial source hypothesis. River input is known to be higher during interstadials and the Holocene, and can thus potentially bias LDI-SST during these periods (Deplazes et al., 2014). In open marine environments, the C_{32} 1,15-diol rarely constitutes > 30% of the total LCD pool (Rampen et al. 2014b). With relative abundances of the C_{32} 1,15-diol of 16 ± 4 % normalized to the 1,13- and 1,15-diols and 10 ± 2 % relative to all LCDs, riverine LCD input is not expected to be important enough to significantly influence PASOM 3 LDI-SST. This is supported by low BIT values throughout the record (< 0.01), also indicating that river influence is minimal.

Potentially, a bias in the LDI index could have occurred when groups of organisms produce both the 1,14-diols and the 1,13- and 1,15-diols, leading to the observed decreases in SST for the periods 57 - 51 ka BP, 45 - 37 ka BP and 22 - 3 ka BP. The similar variability for all LCDs combined with the dominant abundance of 1,14-diols over 1,13- and 1,15-diols which Rodrigo-Gámiz et al. (2015) observed in the subpolar region around Iceland made them suggest that *Proboscia* diatoms are possibly able to produce besides 1,14-diols the 1,13- and 1,15-diols, and it was here examined whether this could also have occurred for PASOM 3 sediments. Rampen et al. (2008) reported maxima in 1,14-fluxes within the Arabian Sea during the early SWM, before intense upwelling. Up to 35% of the total lipid flux in the Arabian Sea is related to *Proboscia* diatoms during this period (Wakeham et al., 2002), with *Proboscia alata* and *Proboscia indica* as dominant producers (Smith, 2001; Koning et al., 2001). Maximum production of 1,14-diols during early upwelling is related to distinctive characteristics of *Proboscia* diatoms. The 1,13- and 1,15-diols used in the LDI are more related to general productivity than the 1,14-diols (Rampen et al., 2008). The observed different seasonality of the 1,14-diols compared to the 1,13- and 1,15-diols can be a sign of the occurrence of separate producers for these two groups of LCDs. LCD abundances also show these patterns for PASOM 3, with high concentrations of 1,14-diols during periods with an intense SWM as reflected by DI 1. Contrarily, 1,13- and 1,15-diols do not show this variation related to the SWM, suggesting a separate group of producers. PCA analysis supports the proposed production of

1,14-diols by *Proboscia* diatoms, since 1,14-diols, loliolide and its isomer isololiolide show a similar loading (Fig. 16B). Loliolide forms when the carotenoid fucoxantin, the most-abundant carotenoid of diatoms, is anoxically degraded (Klok et al., 1984; Repeta et al., 1989). Although fucoxanthin is also produced by dinoflagellates and haptophyte algae (Klok et al., 1984; Jeffrey and Vest, 1997), production of 1,14-diols has not been confirmed for these organisms and the similar loading of loliolide, isololiolide and 1,14-diols is thus probably related to production by diatoms. It can therefore be suggested that production of 1,14-diols by *Apedinella* does not occur within the northern Arabian Sea, or has at least an insignificant influence on 1,14-diol distribution. Furthermore, 1,14-diols load separately from 1,13- and 1,15-diols within PCA analysis solely accounting for LCDs (Fig 15). The C_{32} 1,15-diol should not be considered here, since an in-situ river source is proposed for this LCD. The 1,14-diols and 1,13- and 1,15-diols within PASOM 3 are thus produced by two distinct groups of organisms, i.e. *Proboscia* diatoms synthesizing the 1,14-diols, while 1,13- and 1,15-diols are produced by a second group, potentially eustigmatophyte algae. Although the general pattern of LCD production and abundance within the Arabian Sea and PASOM 3 core lead to the conclusion of two separate sources, high abundances of *Proboscia* diatoms that produce 1,13- and 1,15-diols along with 1,14-diols could distort the SST signal recorded by the LDI during certain intervals. Since the abundance of *Proboscia* diatoms is related to upwelling instead of temperature (Rampen et al., 2007; 2008), this potential distortion is expected to occur during periods of high upwelling. The three periods within PASOM 3 that show a clear decrease in SST are periods of high upwelling and during which, at least partly, 1,14-diol abundance and MARs are equal to or higher than 1,13- and 1,15-diol abundance and MARs. Although this observation is in line with the hypothesis of Rodrigo-Gámiz et al (2015), it should be mentioned that domination of the 1,14-diols only occurred between 6.5 and 3 ka BP (with fractional abundances increasing from 0.5 to 0.7; Appendix 2), and equal abundances were only observed for the intervals 53 - 52 ka BP and 41 - 40 ka BP. Domination of the 1,14-diol is not comparable in magnitude to that found by Rodrigo-Gámiz et al. (2015) and it can be questioned whether this process can cause offsets with equal magnitudes as those observed in the LDI-SST record.

A synchronous increase of DI 1 and decrease of SST for the periods 57 - 51 ka BP, 45 - 37 ka BP and 14 - 3 ka BP can refer to a direct relation between upwelling and LDI-SST, thereby explaining the deviations compared to the rest of the record during these periods. Stronger upwelling could cause a shift in the major production season of the 1,13- and 1,15-diols towards production concentrated around the NEM and SWM, a process which was also proposed for the absence of SST differences between different climatic states, e.g. MIS 1 to 5a. Furthermore, high upwelling intensity of relatively cold intermediate waters during these periods causes surface waters during the SWM to become even colder, and this lower SST is expected to be recorded within the LDI. This theory does not explain why LDI-SST

already starts to decrease from the LGM on. Upwelling and thus SWM intensity is low from the LGM towards 14 ka BP. It seems therefore contradictory that LDI-SSTs decrease. A potential explanation can be oxic degradation, since Sr/Ca values are extremely high during this period and although surface productivity increases, biomarker abundances remain low, indicating low preservation. The most labile biomarker dinosterol is even completely absent during part of the period 22 - 14 ka BP, supporting the low preservation related to low intensity of the OMZ. Although the combination of these two theories, namely upwelling of cold waters leading to a decrease in SST for the periods 57 - 51 ka BP, 45 - 37 ka BP and 14 - 3 ka BP and oxic degradation between 22 and 14 ka BP can explain the decreases in SST during these periods, it cannot explain why high upwelling at the end of MIS 4 and during MIS 5a does not lead to a decrease in SST. It can be suggested that conditions during this period are distinctive, which was also shown by the PCA analyses in which data points referring to the period of high upwelling conditions during MIS 4 and MIS 5a load separately from the other data points (Fig. 15). Probably some threshold must be exceeded before LDI records lower SST. Due to the uncertainty related to the source organisms of 1,13- and 1,15-diols in the marine environment, no conclusions can be made on its abundance within the Arabian Sea and therefore changes in species composition cannot be ruled out.

Overall, the LDI does not track climatic conditions in the northern Arabian Sea, since glacial-interglacial transitions, MIS 1 to MIS 5a and Heinrich events cannot be distinguished within the LDI-SST record. Monsoon dynamics can potentially dampen SST differences, while it cannot be ruled out that other factors than SST which are related to upwelling play a role in LCD distributions in this highly dynamic environment. Periods of relatively large decreases in SST are distinguishable, of which most are related to a high intensity of the SWM. Several hypotheses can be proposed, but a decrease in SST due to the influence of cold upwelling waters or a shift in the main season of 1,13- and 1,15-diol production seem the most probable explanations. Although this would explain a decrease in SST for the periods 57 - 51 ka BP, 45 - 37 ka BP and 14 - 3 ka BP, oxic degradation could be a possible explanation for the decrease in SST observed between the LGM and 14 ka BP. It can be concluded that the LDI in the northern Arabian Sea does not record annual mean SST, but is biased to represent the season of highest production and thus follows shifts in seasonal productivity and is furthermore influenced by upwelling dynamics.

5.3 TEX^{H}_{86}

Global calibration studies of Kim et al. (2008; 2012) revealed that TEX_{86} correlates with temperatures between 0 and 30 m water depth, but that the correlation could be equally significant for 0 - 200 m water depth. Also, several regional studies showed a dominant signal from subsurface waters (e.g. Huguet et al., 2007; Lopes dos Santos et al., 2010). Sediment

trap studies within the Arabian Sea revealed best correlations of TEX_{86} with annual mean SST (Wuchter et al., 2006b). Despite this, the absolute values of PASOM 3 TEX^{H}_{86}-SST (hereafter referred to as TEX_{86}) are much higher than annual mean SSTs. Arabian Sea annual mean SSTs during the LGM were between 21.5 and 24.5 ^{0}C, based on a combination of both organic and inorganic SST proxies (e.g. Mg/Ca ratios of planktonic foraminifera and the $U^{K'}_{37}$; Huguet et al., 2006 and references therein), while PASOM 3 TEX_{86}-SSTs during this period were as high as 30 ^{0}C. Furthermore, annual mean SSTs reconstructed for the northern Arabian Sea using a combination of $\delta^{18}O$ and $U^{K'}_{37}$ records (Reichart et al., 2002) are at least 4.5 ^{0}C lower than PASOM 3 TEX^{H}_{86}-SSTs during Heinrich events. Input of GDGTs transported by rivers, potentially carrying a high TEX_{86} signal, are not the cause for the high observed SSTs, since BIT values are below 0.1, within the range found for open marine settings by Hopmans et al. (2004). GDGTs are not transported by wind in significant amounts (Schouten et al., 2013), and for that reason the high dust input in the Arabian Sea (Rea, 1994) is thus not expected to bias the TEX_{86} signal.

The high absolute temperatures recorded by the TEX_{86} are comparable to or even above the maximum SSTs used within the calibration dataset (30 ^{0}C; Kim et al., 2010). While the maximum temperature that can be reconstructed equals 39 ^{0}C (Kim et al., 2010), SSTs in the top of the calibration range may potentially be biased. The calibration is based on globally distributed surface sediments and it can therefore not be excluded that a regional deviation occurs for the high-temperature Arabian Sea. PASOM 3 TEX^{H}_{86} values seem to be unrealistically high, but when converted to TEX_{86} appear to be comparable to other studies. PASOM 3 TEX_{86} values range between 0.68 and 0.78. Sediment trap studies conducted by Wuchter et al. (2006b) reported TEX_{86} values between 0.66 and 0.75 and surface sediments on the Murray Ridge record a TEX_{86} value of 0.78 for a core from comparable water depths and, thus, low bottom water O_2 concentrations as PASOM 3 (Lengger et al., 2012). Furthermore, paleotemperature reconstructions on core SO130-289KL from the northeastern Arabian Sea spanning the last 40 ka BP also show SSTs between 26 and 32 ^{0}C (J. Lattaud, personal communication), comparable to PASOM 3 reconstructed SSTs.

Regardless of the high absolute reconstructed SST values, NH climatic events are not visible within the TEX_{86}-SST record. Heinrich events cannot be distinguished as cold periods, additionally no SST differences exist between the warmer MIS 1, MIS 3 and MIS 5a and colder MIS 2 and MIS 4. Instead, the dominant trend for the TEX_{86}-SST is that of a gradual increase throughout the record, i.e. from 28.2 ^{0}C at 76 ka BP to 31.4 ^{0}C at 3 ka BP. A similar gradual increase, although with a larger magnitude, is visible within the SO130-289KL record (J. Lattaud, personal communication). The increase in TEX_{86}-SST may be related to a warming from the glacial towards the Holocene. Also, a shift in the dominant period of GDGT production can lead to the gradual increase in TEX_{86} values. Wuchter et al. (2006b) reported highest TEX_{86}

values during the onset of the SWM and a second peak in TEX_{86} during the FI within sediment traps. Gradual shifts of GDGT production towards one or both of these periods may lead to an increase in TEX_{86} values and thus reconstructed SST. This could only be an explanation when TEX_{86} does not reflect annual mean SST, but is instead biased to the SST during the dominant period of GDGT production. When the TEX_{86} is indeed biased to a certain season, the high TEX_{86} values within PASOM 3 could be explained by a predominant influence of the warmer SI and FI. Since no surface sediment or sediment trap data is available for PASOM 3, it is not possible to identify whether TEX_{86} reflects annual mean SST or is biased towards a certain season, and the hypothesis can thus not be verified.

One of the most pronounced increases in TEX_{86}-SST within the PASOM 3 record occurs from the LGM towards the Holocene, with a cooling observed during Termination I (around 14 ka BP), occurring synchronous with the Antarctic Cold Reversal, characteristic of the SH (Stenni et al., 2001). Comparison of the TEX_{86}-SST record with SH climate variability as reflected by the δD record of EPICA Dome C shows that variabilities are synchronous between 29 and 12 ka BP, leading to the suggestion that the TEX_{86} signal is influenced by SH climate dynamics during this period. SH influence within the TEX_{86} proxy is also observed by Huguet et al. (2006) within two cores from the western Arabian Sea. Huguet et al. (2006) concluded that the reason for the observed influence of the SH on TEX_{86} must be related to the SWM period, since their $U^{K'}_{37}$ record is forced by NH climate as also reported by other studies within the Arabian Sea (Schulte and Müller., 2001; Doose-Rolinski et al. 2001; Higginson et al., 2004). Based on the seasonal pattern of alkenone production, a decrease in SWM intensity leads to a shift of the alkenone production towards the NEM (Higginson et al., 2004), while the more year-round production of GDGTs will be less influenced. During these periods of low upwelling, the TEX_{86} is amongst others influenced by the SWM when SH dynamics are expected to affect the Arabian Sea, while the $U^{K'}_{37}$ is more influenced by NEM dynamics and would thus not record the SH influence. Indeed, most of the period for which the SH influence is observed within the PASOM 3 record (29 - 12 ka BP) is characterized by low DI 1 values and thus a relatively weak SWM. The fact that no SH influence is recorded within the PASOM 3 LDI signal is for the same reasons as for the $U^{K'}_{37}$ signal of Huguet et al. (2006). Production of the 1,13- and 1,15-diols will shift towards the NEM and intermonsoon periods when SWM intensity is low. SH influence during the SWM would thus be reflected within the TEX_{86}, while the LDI remains affected by NH climate dynamics.

SH influence could potentially be explained by the variability of inflow of intermediate water masses. Main intermediate water sources within the Arabian Sea are the RSW, PGW and from the south the ICW (Wyrtki, 1973; Swallow, 1984; You, 1998). The ICW is a mixture of aged Antarctic Intermediate Water (AAIW) and Banda Seawater (BSW) (Sharma, 1972; Sharma et al., 1978; You, 1998) and therefore could contain a SH signal. This water mass

enters the Arabian Sea during the SWM with the Somali current (You, 1998). During the last glacial, when the SH dynamics start to affect the TEX_{86} proxy, input of RSW and PGW decreases. Low sea levels during glacials lead to a desiccated Persian Gulf (Reichart et al., 2004) and furthermore prevents exchange between the Red Sea and Arabian Sea as a result of the sill that exist between both basins. It has been observed that inflow of RSW was reduced by 85% during the last glacial period (Rohling and Zachariasse, 1996). Since the circulation of RSW and PGW controls southern source water (ICW) inflow into the northern Arabian Sea, a decrease in inflow of these waters is expected to cause an increasing inflow of ICW during the SWM when sea-level is low. Combined with the low intensity of the SWM during the period of SH influence in the TEX_{86}, and thus a shift of the $C_{37:2}$ and $C_{37:3}$ alkenone and 1,13- and 1,15-diol producers towards the NEM and intermonsoonal periods, an increase of inflow of ICW waters during glacial sea-level lowstand can cause the TEX_{86} to be influenced by SH temperatures, while no such influence is recorded by the LDI. Since inflow of RSW is still very low at 10 ka BP (50% of present-day inflow) and only reached present-day intensity at 6 ka BP (Pichevin et al., 2007), the SH signal brought to the Arabian Sea by the ICW can also be recorded during the beginning of MIS 1. Questions remain, since no SH influence is recorded during MIS 3, MIS 4 and MIS 5a, also part of the last glacial and thus characterized by low sea-levels. Furthermore, MIS 4 is also typified by low SWM intensity, a prerequisite for the presence of SH influence within the TEX_{86} record. Probably a certain threshold related to the intensity of ICW inflow must be exceeded before it is recorded in the TEX_{86} signal. It can furthermore not be excluded that atmospheric processes play an important role, since this has also been shown to be of importance for the teleconnection between NH climate variability and the Arabian Sea (Deplazes et al., 2013).

The δD record of EPICA Dome C reaches a plateau at 6 ka BP, while TEX_{86}-SSTs keep increasing during the period 6 - 3 ka BP. This behavior of the PASOM 3 TEX_{86}-SST record contrasts with the studies of Huguet et al. (2006) and J. Lattaud (personal communication) in which a likewise plateau of TEX_{86} values is observed. The PASOM 3 SST record shows SST differences between the LGM and the core-top comparable to Huguet et al. (2006) and references therein, i.e. 1.5 - 5.0 ^{0}C, but the record is not corresponding to ice core records from both the Northern and Southern Hemisphere for the period 6 - 3 ka BP. There are two potential explanations for the increasing TEX_{86} values between 6 and 3 ka BP: either the TEX_{86} proxy records the actual increase in SST within the Arabian Sea, or some process causes a bias in reconstructed SST. Although the first option seems most likely, other suggestions can be made considering the processes causing a bias. Changes in species composition could occur, which can be supported by an observed lower relative decrease of crenarchaeol concentrations compared to the total isoprenoid GDGT pool. Isoprenoid GDGTs can furthermore be produced by Archaea other than Thaumarchaeota within the water column or

by sedimentary in-situ production (Schouten et al., 2013). These Archaea are expected to produce GDGT-0, GDGT-1 and/or GDGT-2 (Pancost et al., 2001; Blumenberg et al., 2004) and the ratio of these GDGTs to crenarchaeol (specific to Thaumarchaetoa) can therefore be used to assess potential production by non-Thaumarchaeotal Archaea (Blaga et al., 2009; Weijers et al., 2011). No significant increase is observed for both the GDGT-2 to crenarchaeol and GDGT-1 to crenarchaeol ratio, while the GDGT-0 to crenarchaeol ratio decreases throughout the Holocene (Appendix 3). Production of additional GDGT-0, GDGT-1 and/or GDGT-2 within the water column or sediments can thus be excluded. The influence of sedimentary GDGT production on the TEX_{86} index has also been excluded by Lengger et al. (2014) for other sediments from the Murray Ridge, who concluded that although GDGT-producing Archaea are present within the sediments, intact polar lipids that were produced by these Archaea did not cause any change in the pool of core lipids and thus cannot affect TEX_{86}. Furthermore, Lengger et al. (2014) reported that GDGTs produced within the water column did not make it to the core lipid pool.

The PASOM 3 TEX_{86} record is characterized by reconstructed SSTs consistently higher than for the LDI. Potentially the TEX_{86} and LDI proxies are biased towards a different dominant season of production of the corresponding biomarkers. The 1,13- and 1,15-diols are produced year-round, but peaks occur during the SWM and NEM. The GDGT-producing Thaumarchaeota are autotrophic ammonium oxidizers (Könneke et al., 2005) and thus depend on ammonium availability, which leads to a competition with algae. This competition explains the seasonal distribution of Thaumarchaeota in surface waters, i.e. being high during periods of low phytoplankton productivity (Murray et al., 1998; 1999; Wuchter et al., 2005). The different behavior of GDGTs compared to biomarkers included in the LDI and $U^{K'}_{37}$ proxies, i.e. LCDs and alkenones, is confirmed by PCA analysis (Fig. 16A). Crenarchaeol loads different to all LCDs as well as to the alkenones, indicating a different production pattern. GDGT production is less dependent on the SWM and NEM periods compared to production of LCDs. The relative increase of fluxes of GDGTs between the SI and SWM is lower than for the 1,13- and 1,15-diols and the relative abundance of Thaumarchaeota during upwelling is lower than during the SI and FI, opposite to the pattern observed for 1,13- and 1,15-diol producers (Wuchter et al., 2006b). Wuchter et al. (2006b) related the higher GDGT fluxes during the SWM not directly to higher abundances of Thaumarchaeotal cells, but highlight the importance of efficient transport mechanisms during this period. Thaumarchaetal cells are small and their settling through the water column is enhanced by incorporation into fecal pellets through grazing by zooplankton within the photic zone (Wakeham et al., 2003; Wuchter et al., 2006b). Large amounts of upwelling nutrients and resulting high surface productivity lead to an active food web within the surface waters during the SWM (Wakeham and Canuel, 1988; Wakeham et al., 2002). Thus, Wuchter et al. (2006b) record annual mean SSTs related to the year-round

production of GDGTs, while fluxes follow the pattern observed for C_{org} content and the 1,13- and 1,15-diols, due to variations in food-web efficiency. Since 1,13- and 1,15-diols and isoprenoid GDGT MARs vary synchronously throughout most of the record, the variation in food-web efficiency probably also influenced the GDGT flux within PASOM 3. The different seasonality of production for 1,13- and 1,15-diols and GDGTs could explain the observed lower SST for the LDI proxy, with 1,13- and 1,15-diol production more concentrated towards the colder SWM and NEM periods. Based on knowledge concerning the seasonality of production of GDGTs and 1,13- and 1,15-diols within the Arabian Sea, the higher TEX_{86}-SSTs compared to the reconstructed SSTs based on the LDI are thus as expected.

Differences between reconstructed SSTs by different proxies can furthermore be related to the depth habitat of the source organisms (e.g. Smith et al., 2013). Thaumarchaeota are chemoautotrophic nitrifiers (Könneke et al., 2005; Wuchter et al., 2006a; Park et al., 2010) and are therefore not restricted to the photic zone, explaining why their genetic markers are observed throughout the water column (e.g. Karner et al., 2001; Herndl et al., 2005). Sinninghe Damsté et al. (2002c) recorded higher Thaumarchaeotal cell concentrations below the photic zone within the Arabian Sea (e.g. Pearson et al., 2001; Ingalls et al., 2006). TEX_{86} signals from the Arabian Sea thus have the potential to contain a subsurface component. But, deep waters are expected to be colder, and a subsurface component within the TEX_{86} signal would cause an offset towards lower SST, opposite to the observed difference between the records. The difference between the TEX_{86}- and LDI-SSTs is thus most probably related to differences in the main season of production of the biomarkers, whereas difference in depth habitat does not play a significant role.

It can be concluded that the TEX_{86} index does not reflect NH climatic variability, but instead records SH climatic dynamics between 29 and 12 ka BP. This is probably related to SH influence induced by the ICW during the SWM when upwelling, SWM intensities and inflow of RSW and PGW are low. TEX_{86}-SSTs are consistently higher than present-day annual mean SSTs as recorded by different proxies throughout the Arabian Sea. Furthermore, TEX_{86}-SSTs are higher than those reconstructed using LDI, which may be related to differences within the production pattern for the corresponding biomarkers, i.e. 1,13- and 1,15-diols and GDGTs. These two observations might lead to the suggestion that the TEX_{86} does not reflect annual mean SST, but is instead biased towards the warmer intermonsoon periods, supported by the differences in TEX_{86}-SST and annual mean SST reconstructed for the Arabian Sea using other proxies. The gradual increase of TEX_{86}-SST throughout the record could be related to a shift in the seasonality of the GDGT production or a gradual warming towards the Holocene.

5.4 $U^{K'}_{37}$

The PASOM 3 $U^{K'}_{37}$-SST record does not vary synchronous with either the $\delta^{18}O$ record of the NH GRIP core or with the δD record of the SH EPICA Dome C core. Therefore, climatic events cannot be recognized, i.e. low SSTs during Heinrich events and MIS 2 and MIS 4, high SSTs during MIS 3 and MIS 5a or SST changes synchronous with the Antarctic Cold Reversal. Additionally, the low SST at 52 ka BP as identified within several $U^{K'}_{37}$ records around the Arabian Sea (Emeis et al., 1995; Rostek et al., 1997; Sinninghe Damsté et al., 2002b) is not visible within the PASOM 3 record. Although the SST reconstructed for the core-top (26.0 ^{0}C at 3 ka BP) is close to the present-day annual mean SST of the Arabian Sea of 27 ^{0}C, the variability within the record does not correspond with variabilities found in other records from the western and northeastern Arabian Sea (Budziak, 2001; Schulte and Müller, 2001). Within the Arabian Sea, alkenone fluxes are seasonal, yet sedimentary $U^{K'}_{37}$ records reflect annual mean SST (Doose-Rolinski et al., 2001; Rosell-Méle et al., 2004; Huguet et al., 2006). Indeed, surface sediments from the Murray Ridge were in good correspondence with present-day annual mean SST (Rodrigo-Gámiz et al., 2016). Although the reconstructed PASOM 3 core-top SST matches quite well with present-day annual mean SST, it cannot be excluded that seasonal signals were strong during certain periods, comparable to the study of Huguet et al. (2006) in which these were visible within the $U^{K'}_{37}$ record. Furthermore, the PASOM 3 record does not cover periods more recent than 3 ka BP and can therefore not be confidently compared with present-day SST.

Comparison of the core-top $U^{K'}_{37}$ values with $U^{K'}_{37}$ values from core GEOB3007-1 from the western (Budziak, 2001) and core SO90-136KL from the northeastern Arabian Sea (Schulte and Müller, 2001) at 3 ka BP reveals an offset towards lower SST for the PASOM 3 record (Fig. 17). Also, further confirmation of deviating behavior of the PASOM 3 $U^{K'}_{37}$ record came from a comparison of the variabilities reflected within the three $U^{K'}_{37}$ records. The range of SST covered by the PASOM 3 $U^{K'}_{37}$ record is extremely high (9.3 ^{0}C), while those from GEOB3007-1 and SO90-136KL show intercore differences of 4.5 ^{0}C. Apart from the large range of reconstructed SSTs, the PASOM 3 SST record is characterized by periods with low SST alternating with periods characterized by high SST on relatively short timescales (millennia), contrasting to the relatively stable records of GEOB3007-1 and SO0-136KL.

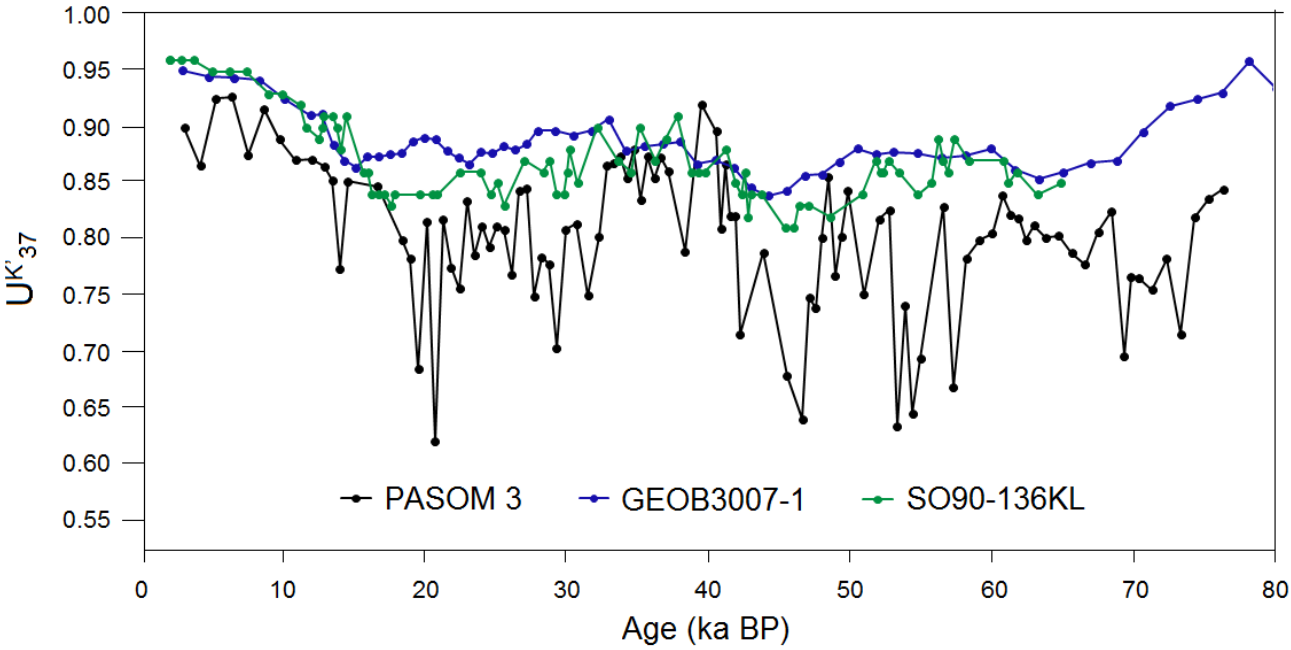

Figure 17: *Comparison of the PASOM 3 $U^{K'}_{37}$ record with $U^{K'}_{37}$ records of core GEOB3007-1 from Budziak (2001) and core SO90-136KL from Schulte and Müller (2001).*

Comparison between the PASOM 3 $U^{K'}_{37}$- and LDI-SST records shows differences in SST exceeding the calibration error of the LDI proxy (± 2 ^{0}C). Both proxies are based on biomarkers produced by organisms living in the photic zone and are thus expected to record similar annual mean SSTs, although much less is known about the eustigmatophyte algae which are proposed as the 1,13- and 1,15-diol producers compared to the alkenone-producing coccolitophorids (Volkman et al., 1992). Dos Santos et al. (2013) explained differences observed within SST records reconstructed using the $U^{K'}_{37}$ and LDI indices by differences in the growing season of the producing organisms. Sediment trap studies revealed a year-round production of alkenones within the Arabian Sea, although a peak in alkenone fluxes occurs in the middle of the SWM with moreover a minor peak during the NEM (Prahl and Dymond, 1996; Prahl et al., 2000). Since a similar seasonality of production was observed for the 1,13- and 1,15-diols forming the LDI index, differences in the dominant season of production cannot explain the observed SST differences between the $U^{K'}_{37}$- and LDI-SST records. Furthermore, related to the similar production pattern of the 1,13- and 1,15-diols and alkenones, the $U^{K'}_{37}$ is expected to react in the same way as the LDI on a potential shift in production and this can therefore not be an explanation for the large variability within the $U^{K'}_{37}$-SST record.

The large variability within the $U^{K'}_{37}$ record can thus not be explained by shifts in the dominant season of production or changes in depth habitat of the source organisms. Furthermore, it is not comparable to variability found in other cores within the Arabian Sea. It was therefore examined whether the followed analytical procedure could have introduced a bias. In the first place, co-elution between the $C_{37:3}$ alkenone and another compound has the potential to cause an offset towards lower $U^{K'}_{37}$ values and thereby a decrease in reconstructed

SST. GC-MS was used to measure a selection of ketone fractions in order to identify the eluting compounds within the peak that was before assumed to be composed of solely $C_{37:3}$ alkenones. Samples were selected based on their low SST values compared to surrounding samples, which make them the most probable candidates for co-elution and thus for an offset to lower reconstructed SST. Resulting chromatograms and corresponding mass spectra show that elution of different isomers of steryl alkyl ethers occurs at times comparable to that characteristic of the $C_{37:2}$ and $C_{37:3}$ alkenones, concluded based on mass spectra of the steryl alkyl ethers reported by Schouten et al. (2005). Steryl alkyl ethers were detected previously by Schouten et al. (2005) in Holocene sediments from the Arabian Sea and are proposed to be associated with diatoms (Schouten et al., 2000b). Although steryl alkyl ethers are present within the sample during the same interval, mass spectra of the peaks assigned to $C_{37:2}$ and $C_{37:3}$ alkenones do not show co-elution of steryl alkyl diols and it was therefore concluded that this could not be the cause of the variability within the $U^{K'}_{37}$ record. In the second place, incomplete fractionation during column chromatography could have occurred, leading to the presence of $C_{37:2}$ alkenones within the apolar fraction. This would result in an offset towards lower $U^{K'}_{37}$ values, since quantification of the $C_{37:2}$ alkenone by measuring the ketone fraction would underestimate the actual abundance of $C_{37:2}$ alkenones within the sample. Again, a selection of samples was measured using GC-MS, this time using the apolar fractions. The molecular ion characteristic of $C_{37:2}$ alkenones was not observed in significant amounts and a bias related to incomplete separation of the fractions could thus be ruled out. Therefore, problems within the analytical process could not explain the observed variability within the $U^{K'}_{37}$ record.

Müller et al. (1998) concluded that the growth rate of alkenone producing algae and nutrient availability do not significantly affect the $U^{K'}_{37}$. Since nutrient variability is connected to upwelling and is thus expected to vary synchronously with DI 1 and Sr/Ca, it will not lead to the shorter-term variation in the $U^{K'}_{37}$-SST record. The additional double bond of the $C_{37:3}$ alkenone led to the suggestion that it has a higher reactivity than its $C_{37:2}$ counterpart (Hoefs et al., 1998), causing preferential degradation and changes in $U^{K'}_{37}$-SST (Prahl et al., 1998). Since the degree of preferential degradation is related to O_2 availability (Prahl et al., 1988), changes in OMZ intensity could have influenced reconstructed SST values. Preferential degradation of the $C_{37:3}$ alkenone leads to an increase in SST and thus higher SST values are expected for the relative oxic Heinrich events and LGM. By reason of an absence of high reconstructed SST during these periods, preferential degradation probably did not significantly influence the $U^{K'}_{37}$ proxy. This is in line with Sinninghe Damsté et al. (2002b) and Rodrigo-Gámiz et al. (2016), who did not find evidence for preferential degradation within other sediments from the Murray Ridge.

Mollenhauer et al. (2008) reported selective preservation of alkenones over crenarchaeol during lateral transport and related this to either the differing chemical structure or the mode of association of the biomarkers within mineral particles. Lateral transport of re-suspended material can cause input of alkenones with a different distribution and thus carrying a different $U^{K'}_{37}$ signal, resulting in an offset of sedimentary $U^{K'}_{37}$ from in-situ SST. The process of lateral transport is well-known for alkenones and is observed previously within various environments (e.g. Benthien and Müller, 2000; Kim et al., 2009b). The monsoon-related processes within the Arabian Sea make it a highly dynamic region in which eddies and filaments are produced that move resuspended sediment (Smith et al., 1998). This, in combination with the location of PASOM 3 on the slopes of the Murray Ridge, makes lateral transport a likely process influencing PASOM 3 sediments. The apparent greater resistance towards degradation of alkenones compared to isoprenoid GDGTs, represented by crenarchaeol, during lateral transport can explain why this process can be visible within the $U^{K'}_{37}$ record, while it has no influence on the TEX_{86} record. Similar findings were made by the study of Kim et al. (2009b), in which the $U^{K'}_{37}$ proxy was affected by the transport of alkenones from other regions, while this effect was not observed within the TEX_{86}. Within the Arabian Sea, lateral advection of re-suspended sediment from the Oman Shelf and Arabian Shelf have been observed (Siegel and Deuser, 1997; Honjo et al., 1999; Witte and Pfannkuche, 2000; Wakeham et al., 2002) and lateral transport from these areas could have influenced PASOM 3. Regardless of their exact origin, lateral advected alkenones most probably come from relatively cold areas, since comparison of the PASOM 3 $U^{K'}_{37}$ record with that of GEOB3007-1 and SO90-136KL and comparison between PASOM 3 $U^{K'}_{37}$-SST and LDI-SST records indicate that the offset mainly occurs towards lower SST. The many processes influencing lateral transport (e.g. re-suspension, current directions) make it a variable process, potentially able to explain the PASOM 3 $U^{K'}_{37}$-SST record. This is supported by the alkenone MAR pattern, for which no correlation can be found with variations in MARs of the 1,13- and 1,15-diols, although this could be expected based on the similar seasonality of production. For an extra confirmation, alkenone MARs were compared with isoprenoid GDGT MARs. Again, no correlation was found, in line with the conclusion that lateral transport affects the $U^{K'}_{37}$ record, while it has no influence on that of the TEX_{86}.

The absence of climatic events and the high variability observed, both in magnitude of SST changes and in the time interval over which these changes occur, cannot be related to the analytical procedure and is furthermore contrasting to other $U^{K'}_{37}$ records within the Arabian Sea. The PASOM 3 $U^{K'}_{37}$ record does thus most probably not reflect annual mean SST. Lateral transport might exert a major influence on $U^{K'}_{37}$ values, causing an offset from the in-situ SST by input of pre-aged alkenones from locations characterized by different alkenone distributions

and thus a different $U^{K'}_{37}$ signal.

6 CONCLUSIONS

The ability of organic SST proxies to reconstruct climatic conditions within the upwelling-influenced northern Arabian Sea was evaluated. Comparison of the obtained LDI, TEX^{H}_{86} and $U^{K'}_{37}$ PASOM 3 records with $\delta^{18}O$ and δD of the NH GRIP and SH EPICA Dome C ice-core records and more local records from the Arabian Sea revealed that only the TEX^{H}_{86} recorded climatic variation, i.e. a SH influence on the TEX^{H}_{86}-SST was observed between 29 and 12 ka BP. On the contrary, the LDI is suggested to be particularly influenced by upwelling dynamics. Shifts in the seasonality of 1,13- and 1,15-diol production related to changes in SWM intensity probably led to the absence of differences between MIS 1 to 5a, the same holds for the inability of the LDI to record Heinrich events as cold events. Furthermore, increased upwelling of cold subsurface waters during periods of an intense SWM could distort the LDI signal, leading to decreases in reconstructed SST. Oxic degradation during periods of low upwelling intensity and thus a less intense OMZ could as well lead to a decrease in LDI-SSTs. Monsoon dynamics within the Arabian Sea thus cause the LDI to not record the expected annual mean SST, but rather shifts in production patterns related to the intensity of the SWM. Additionally, the LDI proxy might be influenced by OMZ intensity and thereby preferential degradation.

The TEX^{H}_{86} SST proxy does not record NH climatic variability, but is instead influenced by SH dynamics between 29 and 12 ka BP. Since the LDI does not show any SH influence, it is likely that the influence took place during the SWM when upwelling intensity was low. Low upwelling intensities may cause a shift in 1,13- and 1,15-diol production away from the SWM, while the more year-round GDGT production was less affected. SH influence could be the result of increased inflow of SH sourced ICW waters during glacial sea-level lowstand. The observed gradual increase of TEX^{H}_{86}-SST throughout the record may be related to a shift in production towards the SWM and/or FI or a gradual warming towards the Holocene. TEX^{H}_{86}-SSTs are higher than the annual mean SST they are expected to represent within the Arabian Sea. Furthermore, TEX_{86}-SSTs are typically higher than LDI-SSTs, which can be explained by a difference in production pattern between the corresponding biomarkers. TEX^{H}_{86} does thus probably not reflect annual mean SST, but is biased towards the warmer intermonsoon periods. The observed higher TEX^{H}_{86} also led to the suggestion that the TEX^{H}_{86} index does not contain a significant subsurface signal. The $U^{K'}_{37}$ SST proxy does not show NH or SH climatic dynamics and furthermore records more variability and a higher SST range than other $U^{K'}_{37}$ records within the Arabian Sea. Additionally, the $U^{K'}_{37}$-SST does not vary synchronous with either the TEX^{H}_{86}-SST or LDI-SST. Clearly, an offset of the $U^{K'}_{37}$ index has occurred, which is not due to biases within the analytical procedure. Probably the input of re-suspended

alkenones via lateral transport distorted the sedimentary $U^{K'}_{37}$ signal, as supported by alkenone MAR patterns. The less efficient degradation of alkenones compared to the isoprenoidal GDGT crenarchaeol during lateral transport may explain why this process did not influence the TEX^{H}_{86} record.

Clearly, a multi-proxy approach using several organic SST proxies supported by data on upwelling intensity, oxygenation and surface production is needed to constrain the SST dynamics within upwelling areas like the Arabian Sea. Organic SST proxies can be influenced by e.g. shifts in the production pattern of the corresponding biomarkers or processes as lateral transport and oxic degradation, thereby preventing them to show similarities to ice-core records and thus complicating paleoclimatic SST reconstructions. Combination of the proxies is a necessity to identify what signal is reflected by each SST proxy and thereby has the potential to be a useful approach to understand the studied region.

7 ACKNOWLEDGEMENTS

First of all, I want to thank my supervisors, Jaap Sinninghe Damsté and Julie Lattaud, for their help, advice and reviews. In addition, thanks to both Gert-Jan Reichart for providing the sediment core and the help concerning the age model and Stefan Schouten for advice and letting me use the facilities of the long chain diol project. Then I want to thank Jort Ossebaar, Anchelique Mets and Ronald van Bommel for the support with the biomarker and C_{org} measurements and Rineke Gieles-Witte and Rick Hennekam for operating the XRF core scanner. And last, but not least, I want to thank everyone from the MMB department for their nice company. I really enjoyed my time at the NIOZ and on the island of Texel.

8 REFERENCES

Anderson, D.M. and Prell, W.L. (1993). A 300 kyr record of upwelling off Oman during the late Quaternary: Evidence of the Asian southwest monsoon, Paleoceanography 8(2), p. 193-208.

Alley, R.B., Meese, D.A., Shuman, A.J., Gow, K.C., Taylor, P.M., Grootes, J.W.C., Ram, M., Wadington, E.D., Mayewski, P.A. and Zielinski, G.A. (1993). Abrupt increase in Greenland snow accumulation at the end of the Younger Dryas event. Nature 362, p. 527-529

Altabet, M.A., Francois, R., Murray, D.W. and Prell, W.L. (1995). Climate-related variations in denitrification in the Arabian Sea from sediment 15N/14N ratios. Nature 373(6514), p. 506-509.

Altabet, M.A., Higginson, M.J. and Murray, D.W. (2002). The effect of millennial-scale changes in Arabian Sea denitrification on atmospheric CO2. Nature 415(6868), p. 159-162.

Andruliet, H.A., Von Rad, U., Brans, A. and Ittekkot, V. (2000). Coccolithophore fluxes from sediment traps in the northeastern Arabian Sea off Pakistan. Marine Micropaleontology 38(3), p. 285-308.

Behl, R.J. and Kennett, J.P. (1996). Brief interstadial events in the Santa Barbara basin, NE Pacific, during the past 60 kyr. Nature 379(6562), p. 243-246.

Benthien, A. and Müller, P. (2000). Anomalously low alkenone temperatures caused by lateral particle and sediment transport in the Malvinas Current region, western Argentine Basin. Deep-Sea Research Part I: Oceanographic Research Papers 47(12), p. 2369-2393.

Berger, W.H. (1978). Deep-sea carbonate: pteropod distribution and the aragonite compensation depth. Deep-Sea Research 25(5), p. 447-452.

Blaga, C.I., Reichart, G.-J., Heiri, O. and Sinninghe Damsté, J.S. (2009). Tetraether membrane lipid distributions in water-column particulate matter and sediments: a study of 47 European lakes along a north-south transect. Journal of Paleolimnology 41(3), p. 523-540.

Blumenberg, M., Seifert, R., Reitner, J., Pape, T. and Michaelis, W. (2004). Membrane lipid patterns typify distinct anaerobic methanotrophic consortia. Proceedings of the National Academy of Sciences of the United States of America 101(30), p. 11111-11116.

Boos, W.R. and Kuang, Z. (2010). Dominant control of the South Asian monsoon by orographic insulation versus plateau heating. Nature 463(7278), p. 218-222.

Boyd, E.S., Pearson, A., Pi, Y., Li, W.-J., Zhang, Y.G., He, L., Zhang, C.L. and Geesey, G.G. (2011). Temperature and pH controls on glycerol dibiphytanyl tetraether lipid compostion in the hyperthermophilic crenarchaeon Acidilobus sulfurireducens. Extremophiles 15(1), p. 59-65.

Brassell, S.C. (1993). Applications of biomarkers for delineating marine paleoclimatic fluctuations during the Pleistocene. In: Organic Geochemistry: Principles and Applications. Engel, M.H.a nd Macko, S.A. (eds.) New York: Plenum Press, p. 699-738.

Brassell, S.C., Eglinton, G., Marlowe, I.T., Pflaumann, U. and Sarnthein, M. (1986). Molecular stratigraphy: a new tool for climatic assessment. Nature 320(6058), p. 129-133.

Budziak, D (2001): Alkenone analyses of sediment cores from the western Arabian Sea. doi:10.1594/PANGAEA.804466

Chiang, J.C.H. and Bitz, C.M. (2005). Influence of high latitude ice cover on the marine Intertropical Convergence Zone. Climate Dynamics 25(5), p. 477-496.

Clemens, S.C. and Prell, W.L. (2003). A 350,000 year summer-monsoon multi-proxy stack from the Owen ridge, Northern Arabian sea. Marine Geology 201(1), p. 35-51.

Conte, M.H., Volkman, J.K. and Eglinton, G. (1994). Lipid biomarkers of the Haptophyta. In: The Haptophyte Algae. Green, J.C. and Leadbeater, B.S.C. (eds.) Oxford: Clarendon Press, p. 351-377

Dansgaard, W., Johnsen, S.J., Clausen, H.B., Hvidberg, C.S. and Steffensen, J.P. (1993). Evidence for general instability of past climate from a 250-kyr. Nature 364, p. 218-220.

De Bar, M.W., Dorhout, D.J.C., Hopmans, E.C., Rampen, S.W., Sinninghe Damsté, J.S. and Schouten, S. (2016). Constraints on the application of long chain diol proxies in the Iberian Atlantic margin. Organic Geochemistry 101, p. 184-195.

De la Torre, J.R., Walker, C.B., Ingalls, A.E., Könneke, M. and Stahl, D.A. (2008). Cultivation of a thermophilic ammonia oxidizing archaeon synthesizing crenarchaeol. Environmental Microbiology 10(3), p. 810-818.

De Leeuw, J.W., Van der Meer, F.W., Rijpstra, W.I.C. and Schenck, P.A. (1980). On the occurrence and structural identification of long chain unsaturated ketones and hydrocarbons in sediments. Physics and Chemistry of the Eart 12, p. 211-217.

De Leeuw, J.W., Rijpstra, W.I.C. and Schenck, P.A. (1981). The occurence and identificaton of C30, C31 and C32 alkan-1,15-diols and alkan-15-one-1-ols in Unit I and Unit II Black Sea sediments. Geochimica et Cosmochimica Acta 45(11), p.2281-2285.

De Rosa, M. and Gambacorta, A. (1988). The lipids of archaebacteria. Progress in lipid research, 27(3), p, 153-175.

De Rosa, M., Esposito, E., Gambacorta, A., Nicolaus, B. and Bu'Lock, J.D. (1980). Effects of temperature on ether lipid composition of Calderiella acidophila. Phytochemistry 19(5), p. 827-831.

Dehairs, F., Chesselet, R. and Jedwab, J. (1980). Discrete suspended particles of barite and the barium cycle in the open ocean. Earth and Planetary Science Letters 49(2), p. 528-550.

Deplazes, G., Lückge, A., Peterson, L.C., Timmermann, A., Hamann, Y., Hughen, K.A., Röhl, U., Laj, C., Cane, M.A., Sigman, D.M. and Haug, G.H. (2013). Links between tropical rainfall and North Atlantic climate during the last glacial period. Nature Geoscience 6(3), p. 213-217.

Deplazes, G., Lückge, A., Stuut, J.-B. W., Pätzold, J., Kuhlmann, H., Husson, D., Fant, M. and Haug, G.H. (2014). Weakening and strengthening of the Indian monsoon during Heinrich events and Dansgaard-Oeschger oscillations. Paleoceanography 29(2), p. 99-114.

Doose-Rolinski, H., Rogalla, U., Scheeder, G., Lückge, A. and Von Rad, U. (2001). High-resolution temperature and evaporation changes during the late Holocene in the northeastern Arabian Sea. Paleoceanography 16(4), p. 358-367.

Dymond, J., Suess, E. and Lyle, M. (1992). Barium in deep-sea sediment: A geochemical proxy for paleoproductivity. Paleoceanography 7(2), p. 163-181.

Eglinton, T.I. and Eglinton, G. (2008). Molecular proxies for paleoclimatology. Earth and Plantary Science Letters 275(1), p. 1-16.

Emeis, K.-C., Anderson, D.M., Doose, H., Kroon, D. and Schulz-Bull, D. (1995). Sea-surface temperatures and the history of monsoon upwelling in the northwest Arabian Sea during the last 500,000 years. Quaternary Research 43(3), p. 355-361.

Fontugne, M.R. and Duplessy, J.C. (1986). Variations of the monsoon regime during the upper Quaternary: Evidence from carbon isotopic record of organic matter in North Indian Ocean sediment cores. Palaeogeography, Palaeoclimatology, Palaeoecology 56(1-2), p. 69-88.

Freeman, K.H. and Wakeham, S.G. (1992). Variations in the distributions and isotopic composition of alkenones in Black Sea particles and sediments. Organic Geochemistry 19(1-3), p. 277-285.

Gliozzi, A., Paoli, G., De Rosa, M and Gambacorta, A. (1983). Effect of isoprenoid cyclization on the transition temperature of lipids in thermophilic archaebacteria. Biochimica et Biophysica Acta (BBA)-Biomembranes 735(2), p. 234-242.

Gong, C. and Hollander, D.J. (1999). Evidence for differential degradation of alkenones under contrasting bottom water oxygen conditions: Implication for paleotemperature reconstruction. Geochimica et Cosmochimica Acta 63(3), p. 405-411.

Haake, B., Ittekkot, V., Rixen, T., Ramaswamy, V., Nair, R.R. and Curry, W.B. (1993). Seasonality and interannual variability of particle fluxes to the deep Arabian Sea. Deep-Sea Research Part I: Oceanograophic Research Papers 40(7), p. 1323-1344.

Hammer, Ø., Harper, D.A.T., Ryan, P.D. (2001). PAST: Paleontological statistics software package for education and data analysis. Palaeontologia Electronica 4(1), p 1-9.

Hartnett, H.E., Keil, R.G., Hedges, J.I. and Devol, A.H. (1998). Influence of oxygen exposure time on organic carbon preservation in continental margin sediments. Nature 391(6667), p. 572-575.

Hatzenpichler, R., Lebedeva, E.V., Spieck, E., Stoecker, K., Richter, A., Daims, H. and Wagner, M. (2008). A moderately thermophilic ammonia-oxidizing crenarchaeote from a hot spring. Proceedings of the National Academy of Sciences of the United States of America 105(6), p. 2134-2139.

Hedges, J.I., Hu, F.S., Devol, A.H., Hartnett, H.E., Tsamakis, E. and Keil, R.G. (1999). Sedimentary organic matter preservation: A test for selective degradation under oxic conditions. American Journal of Science 299(7-9), p. 529-555.

Hennekam, R. and De Lange, G. (2012). X-ray fluorescence core scanning of wet marine sediments: methods to improve quality and reproducibility of high-resolution paleoenvironmental records. Limnology and Oceanography: Methods 10(12), p. 991-1003.

Herbert, T.D. (2003). Alkenone paleotemperature determinations. In: Treatise on Geochemistry, Volume 6: The Ocean and Marine Geochemistry. Holland, H.D. and Turekian, K.K., (eds) New York: Elsevier, p. 391-432.

Hernández-Becerril, D.U. (1995). Planktonic diatoms from the Gulf of California and coasts off Baja California: The genera Rhizosolenia, Proboscia, Pseudosolenia, and former Rhizosolenia species. Diatom Research 10(2), p. 251-267.

Herndl, G.J., Reinthaler, T., Teira, E., Van Aken, H., Veth, C., Pernthaler, A. and Pernthaler, J. (2005). Contribution of Archaea to total prokaryotic production in the deep Atlantic Ocean. Applied and Environmental Microbiology 71(5), p. 2303-2309.

Higginson, M.J., Altabet, M.A., Wincze, L., Herbert, T.D. and Murray, D.W. (2004). A solar (irradiance) trigger for millennial-scale abrupt changes in the southwest monsoon? Paleoceanography 19(3), PA3015, doi:10.1029/2004PA001031.

Hoefs, M.J.L., Versteegh, G.J.M., Rijpstra, W.I.C., De Leeuw, J.W. and Sinninghe Damsté, J.S. (1998). Postdepositional oxic degradation of alkenones: Implications for the measurement of palaeo sea surface temperatures. Paleoceanography 13(1), p. 42-49.

Hoefs, M.J.L., Rijpstra, W.I.C. and Sinninghe Damsté, J.S. (2002). The influence of oxic degradation on the sedimentary biomarker record I: Evidence from Madeira Abyssal Plain turbidites. Geochimica et Cosmochimica Acta 66(15), p. 2719-2735.

Honjo, S., Dymond, J., Prell, W. and Ittekkot, V. (1999). Monsoon-controlled export fluxes to the interior of the Arabian Sea. Deep-Sea Research Part II: Topical Studies in Oceanography 46(8), p. 1859-1902.

Hopmans, E.C., Schouten, S., Pancost, R.D., Van der Meer, M.T.J. and Sinninghe Damsté, J.S. (2000). Analysis of intact tetraether lipids in archaeal cell material and sediments by high performance liquid chromatography/atmospheric pressure chemical ionization mass spectrometry. Rapid Communications in Mass Spectrometry 14(7), p. 585-589.

Hopmans, E.C., Weijers, J.W.H., Schefuß, E., Herfort, L., Sinninghe Damsté, J.S. and Schouten, S. (2004). A novel proxy for terrestrial organic matter in sediments based on branched and isoprenoid tetraether lipids. Earth and Planetary Science Letters 224(1), p. 107-116.

Huguet, C., Kim, J.-H., Sinninghe Damsté, J.S. and Schouten, S. (2006). Reconstruction of sea surface temperature variations in the Arabian Sea over the last 23 kyr using organic proxies (TEX_{86} and $U^{K'}_{37}$). Paleoceanography 21(3), PA3003, doi: 10.1029/2005PA001215.

Huguet, C., Schimmelmann, A., Thunell, R., Lourens, L.J., Sinninghe Damsté, J.S. and Schouten, S. (2007). A study of the TEX_{86} paleothermometer in the water column and sediments of the Santa Barbara Basin, California. Paleoceanography 22(3), PA3203, doi: 10.1029/2006PA001310.

Imbrie, J., Hays, J.D., Martinson, D.G., McIntyre, A., Mix, A.C., Morley, J.J., Pisias, N.G., Prell, W.L. and Shackleton, N.J. (1984). The orbital theory of Pleistocene climate: Support from a revised chronology of the marine δ18O record. In: Milankovitch and Climate. Berger, A., Imbrie, J., Hays, J., Kukla, G. and Saltzman (eds.) Dordrecht: D. Reidel Publ. Comp., p. 269-305.

Ingalls, A.E., Shah, S.R., Hansman, R.I., Aluwihare, L.I., Santos, G.M., Druffel, E.R.M. and Pearson, A. (2006). Quantifying archaeal community autotrophy in the mesopelagic ocean using natural radiocarbon. Proceedings of the National Academy of Sciences of the United States of America 103(7), p. 6442-6447.

Ivanochko, T.S., Ganeshram, R.S., Brummer, G.J.A., Ganssen, G., Jung, S.J.A., Moreton, S.G. and Kroon, D. (2005). Variations in tropical convection as an amplifier of global climate change at the millennial scale. Earth and Planetary Science Letters 235(1-2), p. 302-314.

Jeffrey, S.W. and Vest, M. (1997). Introduction to marine phytoplankton and their pigment signatures. In: Phytoplankton pigments in oceanography: guidelines to modern methods. Jeffrey, S.W., Mantoura, R.F.C. and Wright, S.W (eds) Paris: UNESCO, p. 407-428.

Jouzel, J., Vimeux, F., Caillon, N., Delaygue, G., Hoffmann, G., Masson-Delmotte, V. and Parrenin, F. (2003). Magnitude of isotope/temperature scaling for interpretation of central Antarctic ice cores. Journal of Geophysical Research: Atmospheres 108(D12), 4361, doi:10.1029/2002JD002677.
Kabanova, Y.G. (1968). Primary production in the northern part of the Indian Ocean. Oceanology 8(2), p. 214-225.

Karner, M.B., DeLong, E.F. and Karl, D.M. (2001). Archaeal dominance in the mesopelagic zone of the Pacific Ocean. Nature 409(6819), p. 507-510.

Kim, J.-H., Schouten, S., Hopmans, E.C., Donner, B. and Sinninghe Damsté, J.S. (2008). Global sediment core-top calibration of the TEX_{86} paleothermometer in the ocean. Geochimica et Cosmochimica Acta 72(4), p. 1154-1173.

Kim, J.-H., Huguet, C., Zonneveld, K.A.F., Versteegh, G.J.M., Roeder, W., Sinninghe Damsté, J.S. and Schouten, S. (2009a). An experimental field study to test the stability of lipids used for the TEX_{86} and $U^{K'}_{37}$ palaeothermometers. Geochimica et Cosmochimica Acta 73(10), p. 2888-2898.

Kim, J.-H., Crosta, X., Michel, E., Schouten, S., Duprat, J. and Sinninghe Damsté, J.S. (2009b). Impact of lateral transport on organic proxies in the Southern Ocean. Quaternary Research 71(2), p. 246-250.

Kim, J.-H., Van der Meer, J., Schouten, S., Helmke, P., Willmott, V., Sangiorgi, F., Koç, N., Hopmans, E.C. and Sinninghe Damsté, J.S. (2010). New indices and calibrations derived from the distribution of crenarchaeal isoprenoid tetraether lipids: Implications for past sea surface temperature reconstructions. Geochimica et Cosmochimica Acta 74(16), p. 4639-4654.

Kim, J.-H., Romero, O.E., Lohmann, G., Donner, B., Laepple, T., Haam, E. and Sinninghe Damsté, J.S. (2012). Pronounced subsurface cooling of North Atlantic waters off Northwest Africa during Dansgaard-Oeschger interstadials. Earth and Planetary Science Letters 339-340, p. 95-102.

Klöcker, R. and Henrich, R. (2006). Recent and late Quaternary pteropod preservation on the Pakistan shelf and continental slope. Marine Geology 231(1-4), p. 103-111.

Klok, J., Baas, M., Cox, H.C., De Leeuw, J.W. and Schenk, P.A. (1984). Loliolides and dihydroactinidiolide in a recent marine sediment probably indicate a major transformation pathway of carotenoids. Tetrahedron Letters 25, p. 5577-5580.

Koho, K.A., Nierop, K.G.J., Moodley, L., Middelburg, J.J., Pozzato, L., Soetaert, K., Van der Plicht, J. and Reichart, G.-J. (2013). Microbial bioavailability regulates organic matter preservation in marine sediments. Biogeosciences 10, p. 1131-1141.

Koning, E., Van Iperen J.M., Van Raaphorst, W., Helder, W., Brummer, G.-J.A. and Van Weering, T.C.E. (2001). Selective preservation of upwelling-indicating diatoms in sediments off Somalia, NW Indian Ocean. Deep-Sea Research Part I: Oceanographic Research Papers 48(11), p. 2473-2495.

Kornprobst, J.-M. (2014). Encyclopedia of marine natural products. 2180 pp. Wiley-Blackwell: New Jersey.

Könneke, M., Bernhard, A.E., De la Torr, J.R., Walker, C.B., Waterbury, J.B. and Stahl, D.A. (2005). Isolation of an autotrophic ammonia-oxidizing marine archaeon. Nature 437, p. 543-546.

Lai, D., Springstead, J.R. and Monbouquette, H.G. (2008). Effect of growth temperature on ether lipid biochemistry in Archaeoglobus fulgidus. Extremophiles 12(2), p. 271-278.

Lattaud, J., Kim, J.-H., De Jonge, C., Zell, C., Sinninghe Damsté, J.S. and Schouten, S. (2017). The C32 alkane-1,15-diol as a tracer for riverine input in coastal seas. Geochimica et Cosmochimica Acta 202, p. 146-158.

Lea, D.W. (2003). Elemental and isotopic proxies of past ocean temperatures. In: The Oceans and Marine Geochemistry, Volume 6. Elderfield, H. (eds.) Oxford, Amsterdam: Elsevier, p.365-390.

Lengger, S.K., Hopmans, E.C., Reichart, G.-J., Nierop, K.G.J., Sinninghe Damsté, J.S. and Schouten, S. (2012). Intact polar and core glycerol dibiphytanyl glycerol tetraether lipids in the Arabian Sea oxygen minimum zone. Part II: Selective preservation and degradation in sediments and consequences for the TEX_{86}. Geochimica et Cosmochimica Acta 98, p. 244-258.

Lengger, S.K., Hopmans, E.C., Sinninghe Damsté, J.S. and Schouten, S. (2014). Impact of sedimentary degradation and deep water column production on GDGT abundance and distribution in surface sediments in the Arabian Sea: Implications for the TEX_{86} paleothermometer. Geochimica et Cosmochimica Acta 142, p. 386-399.

Levitus, S. and Boyer, T.P. (1994). World Ocean Atlas 1994, Volume 4: Temperature. NOAA Atlas NESDIS, Volume 4, Washington DC: US Government Printing Office, 117 p.

Lindell, S.R. and Reddy, C.M. (2012). Use of marine algae for producing polymers. [WWW] at https://www.google.com/patents/US20120165490, 2017-04-23.

Lipp, J.S. and Hinrichs, K.-U. (2009). Structural diversity and fate of intact-polar lipids in marine sediments. Geochimica et Cosmochimica Acta 73(22), p. 6816-6833.

Lisiecki, L.A. and Raymo, M.E. (2005). A Pliocene-Pleistocene stack of 57 globally distributed benthic δ18O records. Paleoceanography 20(1), PA1003, doi:10.1029/2004PA001071

Locarnini, R.A., Mishonov, A.V., Antonov, J.I., Boyer, T.P., Garcia, H.E., Baranova, O.K., Zweng, M.M. and Johnson, D.R. (2010). In: World Ocean Atlas 2009, Volume 1: Temperature. NOAA Atlas NESDIS 68. Levitus, S. (eds.) Washington DC: US Government Printing Office, 184 p.

Lopes dos Santos, R.A., Prange, M., Castañeda, I.S, Schefuß, E., Mulitza, S., Schulz, M., Niedermeyer, E.M., Sinninghe Damsté, J.S. and Schouten, S. (2010). Glacial-interglacial variability in Atlantic meridional overturning circulation and thermocline adjustments in the tropical North Atlantic. Earth and Planetary Science Letters 300(3-4), p. 407-414.

Madhupratap, M., Kumar, S.P., Bhattathiri, P.M.A., Kumar, M.D., Raghukumar, S., Nair, K.K.C. and Ramaiah, N. (1996). Mechanism of the biological response to winter cooling in the northeastern Arabian Sea. Nature 384(6609), p. 549-552.

Marlowe, I.T., Green, J.C., Neal, A.C., Brassell, S.C., Eglinton, G. and Course, P.A. (1984). Long chain (n-C37-C39) alkenones in the Prymnesiophyceae. Distribution of alkenones and other lipids and their taxonomic significance. British Phycological Journal 19(3), p. 203-216.

McManus, J.F., Oppo, D.W. and Cullen, J.L. (1999). A 0.5-million-year record of millennial-scale climate variability in the North Atlantic. Science, 283(5404), p. 971-975.

McManus, J.F., Francois, R., Gherardi, J.-M., Keigwin, L.D. and Brown-Leger, S. (2004). Collapse and rapid resumption of Atlantic meridional circulation linked to deglacial climate changes. Nature 428(6985), p. 834-837.

Merbt, S.N., Stahl, D.A., Casamayor, E.O., Marti, E., Nicol, G.W. and Prosser, J.I. (2012). Differential photoinhibition of bacterial and archaeal ammonia oxidation. FEMS Microbiology Letters 327(1), p. 41-46.

Mollenhauer, G., MCManus, J.F., Benthien, A., Müller, P.J. and Eglinton, T.I. (2006). Rapid lateral particle transport in the Argentine Basin: molecular 14C and 230Thxs evidence. Deep-Sea Research Part I: Oceanographic Research Papers 53(7), p. 1224-1243.

Mollenhauer, G., Inthorn, M., Vogt, T., Zabel, M., Sinninghe Damsté, J.S. and Eglinton, T.I. (2007). Aging of marine organic matter during cross-shelf lateral transport in the Benguella upwelling system revealed by compound-specific radiocarbon dating. Geochemistry, Geophysics, Geosystems 8(9), Q09004, doi:10.1029/2007GC001603.

Mollenhauer, G., Eglinton, T.I., Hopmans, E.C. and Sinninghe Damsté, J.S. (2008). A radiocarbon-based assessment of the preservation characteristics of crenarchaeol and alkenones from continental margin sediments. Organic Geochemistry 39(8), p. 1039-1045.

Müller, P.J., Kirst, G., Ruhland, G., Von Storch, I. and Rossell-Melé, A. (1998). Calibration of the alkenone paleotemperature index $U^{K'}_{37}$ based on core-tops from the eastern South Atlantic and the global ocean (60ºN-60ºS). Geochimica et Cosmochimica Acta 62(10), p. 1757-1772.

Murray, A.E., Preston, C.M., Massana, R., Taylor, L.T., Blakis, A., Wu, K. and DeLong, E.F. (1998). Seasonal and spatial variability of bacterial and archaeal assemblages in the coastal waters near Anvers Island, Antarctica. Applied and Environmental Microbiology 64(7), p. 2585-2595.

Murray, A.E., Blakis, A., Massana, R., Strawzewski, S., Passow, U., Alldredge, A. and DeLong, E.F. (1999). A time series assessment of planktonic archaeal variability in the Santa Barbara Channel. Aquatic Microbial Ecology 20, p. 129-145.

Olson, D.B., Hitchcock, G.L., Fine, R.A. and Warren, B.A. (1993). Maintenance of the low-oxygen layer in the Arabian Sea. Deep-Sea Research Part II: Topical Studies in Oceanography 40(3), p. 673-685.

Paillard, D., Labeyrie, L. and Yiou, P. (1996). AnalySeries 1.0: a Macintosh software for the analysis of geophysical time-series. EOS Transactions of the American Geophysical Union 77, p. 379.

Pancost, R.D., Hopmans, E.C., Sinninghe Damsté, J.S. and the MEDINAUT Schipboard Scientific Party (2001). Archaeal lipids in Mediterranean cold seeps: Molecular proxies for anaerobic methane oxidation. Geochemica et Cosmochimica Acta 65(10), p. 1611-1627.

Park, B.-J., Park, S.-J., Yoon, D.-N., Schouten, S. Sinninghe Damsté, J.S. and Rhee, S.-K. (2010). Cultivation of autotrophic ammonia-oxidizing archaea from marine sediments in coculture with sulfur-oxidizing bacteria. Applied and Environmental Microbiology 76(22), p. 7575-7587.

Paulmier, A. and Ruiz-Pino, D. (2009). Oxygen minimum zones (OMZs) in the modern ocean. Progress in Oceanography 80(3), p. 113-128.

Peterson, L.C., Haug, G.H., Hughen, K.A. and Röhl, U. (2000). Rapid changes in the hydrologic cycle of the tropical Atlantic during the last glacial. Science 290(5498), p. 1947-1951.

Pearson, A., McNichol, A.P., Benitez-Nelson, B.C., Hayes, J.M. and Eglinton, T.I. (2001). Origins of lipid biomarkers in Santa Monica Basin surface sediment: A case study using compound-specific Δ14C analysis. Geochimica et Cosmochimica Acta 65(18), p. 3123-3127.

Pichevin, L., Bard, E., Martinez, P. and Billy, I. (2007). Evidence of ventilation changes in the Arabian Sea during the late Quaternary: Implication for denitrification and nitrous oxide emission. Global Biogeochemical Cycles 21(4), GB4008, doi:10.1029/2006GB002852.

Prahl, F.G. and Wakeham, S.G. (1987). Calibration of unsaturation patterns in long-chain ketone compositions for palaeotemperature assessment. Nature 330(6146), p. 367-369.

Prahl, F.G. and Dymond, J. (1996). Semi-annual sediment trap time series for alkenones at an open ocean site (15º59'N, 61º30'E) in the Arabian Sea. American Geophysical Union Ocean Sciences meeting, San Diege, California. Poster. http://www1.whoi.edu/mzweb/prahl/poster.htm

Prahl, F., Muehlhausen, L.A. and Zahnle, D.L. (1988). Further evaluation of long-chain alkenones as indicators of paleoceanographic conditions. Geochimica et Cosmochimica Acta 52(9), p. 2303-2310.

Prahl, F.G., De Lange, G.J., Lyle, M. and Sparrow, M.A. (1989). Post-depositional stability of long-chain alkenones under contrasting redox conditions. Nature 341(6241), p. 434-437.

Prahl, F.G., Pisias, N., Sparrow, M.A. and Sabin, A. (1995). Assessment of sea-surface temperature at 42ºN in the California Current over the last 30,000 years. Paleoceanography 10(4), p. 763-773.

Prahl, F.G., Dymond, J. and Sparrow, M.A. (2000). Annual biomarker record for export production in the central Arabian Sea. Deep-Sea Research Part II: Topical Studies in Oceanography 47(7), p. 1581-1604.

Prahl, F.G., Sparrow, M.A. and Wolfe, G.V (2003). Physiological impacts on alkenone paleothermometry. Paleoceanography 18(2), 1025, doi:10.1029/2002PA000803.

Prahl, F.G., Mix, A.C. and Sparrow, M.A. (2006). Alkenone paleothermometry: Biological lessons from marine sediment records off western South America. Geochimica et Cosmochimica Acta 70(1), p. 101-117.

Qasim, S.Z. (1982). Oceanography of the northern Arabian Sea. Deep-Sea Research Part A: Oceanographic Research Papers 29(9), p. 1041-1068.

Rampen, S.W., Schouten, S., Wakeham, S.G. and Sinninghe Damsté, J.S. (2007). Seasonal and spatial variation in the sources and fluxes of long chain diols and mid-chain hydroxyl methyl alkanoates in the Arabian Sea. Organic Geochemistry 38(2), p. 165-179.

Rampen, S.W., Schouten, S., Koning, E., Brummer, G.-J. A. and Sinninghe Damsté, J.S. (2008). A 90 kyr upwelling record from the northwestern Indian Ocean using a novel long-chain diol index. Earth and Planetary Science Letters 276(1), p. 207-213.

Rampen, S.W., Schouten, S. and Sinninghe Damsté, J.S. (2011). Occurrence of long chain 1,14-diols in Apedinella radians. Organic Geochemistry 42(5), p. 572-574.

Rampen, S.W., Willmott, V., Kim, J.-H., Uliana, E., Mollenhauer, G., Schefuß, E., Sinninghe Damsté, J.S. and Schouten, S. (2012). Long chain 1,13- and 1,15-diols as a potential proxy for palaeotemperature reconstruction. Geochimica et Cosmochimica Acta 84, p. 204-216.

Rampen, S.W., Willmott, V., Kim, J.-H., Rodrigo-Gámiz, M., Uliana, E., Mollenhauer, G., Schefuß, E., Sinninghe Damsté, J.S. and Schouten, S. (2014a). Evaluation of long chain 1,14-alkyl diols in marine sediments as indicators for upwelling and temperature. Organic Geochemistry 76, p. 39-47.

Rampen, S.W., Datema, M., Rodrigo-Gámiz, M., Schouten, S., Reichart, G.-J. and Sinninghe Damsté, J.S. (2014b). Sources and proxy potential of long chain alkyl diols in lacustrine environments. Geochimica et Cosmochimica Acta 144, p. 59-71.

Rea, D.K. (1994). The paleoclimate record provided by eolian deposition in the deep sea: The geologic history of wind. Reviews of Geophysics 32(2), p. 159-195.

Reichart, G.-J. (2009). Cruise report 64PE301, PASOM, Muscat-Muscat, January 8th – January 24th. UU: Utrecht, NIOZ: Texel and NIOO: Wageningen. 107 pp.

Reichart, G.-J., Den Dulk, M., Visser, H.J., Van der Weijden, C.H. and Zachariasse, W.J. (1997). A 225 kyr record of dust supply, paleoproductivity and the oxygen minimum zone from the Murray Ridge (northern Arabian Sea). Palaeogeography, Palaeoclimatology, Palaeoecology 134(1-4), p. 149-169.

Reichart, G.-J., Lourens, L.J. and Zachariasse, W.J. (1998). Temporal variability in the northern Arabian Sea Oxygen Minimum Zone (OMZ) during the last 225,000 years. Paleoceanography 13(6), p. 607-621.

Reichart, G.-J., Nortier, J., Versteegh, G. and Zachariasse, W.J. (2002). Periodical breakdown of the Arabian Sea oxygen minimum zone caused by deep convective mixing. Geological Society, London, Special Publication 195(1), p. 407-419.

Reichart, G.-J., Brinkhuis, H., Huiskamp, F. and Zachariasse, W.J. (2004). Hyperstratification following glacial overturning events in the northern Arabian Sea. Paleoceanography 19(2), PA2013, doi:10.1029/2003PA0009000.

Reimer, P.J., Bard, E., Bayliss, A., Beck, J.W., Blackwell, P.G., Ramsey, C.B., Buck, C.E., Cheng, H., Edwards, R.L., Friedrich, M. and Grootes, P.M. (2013). IntCal13 and Marine13 radiocarbon age calibration curves 0-50,000 years cal BP. Radiocarbon 55(4), p. 1869-1887.

Repeta, D.J. (1989). Carotenoid diagenesis in recent marine sediment: II. Degradation of fucoxanthin to loliolide. Geochmica et Cosmochimica Acta 53, p. 699-707.

Richter, T.O., Van der Gaast, S., Koster, B., Vaars, A., Gieles, R., De Stigter, H.C., De Haas, H. and Van Weering, T.C.E. (2006). The Avaatech XRF Core Scanner: technical description and applications to NE Atlantic sediments. Geological Society, London, Special Publications 267(1), p. 39-50.

Rixen, T., Haake, B. and Ittekkot, V. (2000). Sedimentation in the western Arabian Sea the role of coastal and open-ocean upwelling. Deep-Sea Research Part II: Topical Studies in Oceanography 47(9), p. 2155-2178.

Rodrigo-Gámiz, M., Martínez-Ruiz, F., Rampen, S.W., Schouten, S. and Sinninghe Damsté, J.S. (2014). Sea surface temperature variations in the western Mediterranean Sea over the last 20 kyr: A dual-organic proxy ($U^{K'}_{37}$ and LDI) approach. Paleoceanography 29(2), p. 87-98.

Rodrigo-Gámiz, M., Rampen, S.W., De Haas, H., Baas, M., Schouten, S. and Sinninghe Damsté, J.S. (2015). Constraints on the applicatbility of the organic temperature proxies $U^{K'}_{37}$, TEX_{86} and LDI in the subpolar region around Iceland. Biogeosciences 12, p. 6573-6590.

Rodrigo-Gámiz, M., Rampen, S.W., Schouten, S. and Sinninghe Damsté, J.S. (2016). The impact of oxic degradation on long chain alkyl diol distributions in Arabian Sea surface sediments. Organic Geochemistry 100, p. 1-9.

Rohling, E.J. and Zachariasse, J.W. (1996). Red Sea outflow during the last glacial maximum. Quaternary International 31, p. 77-83.

Rosell-Melé, A. (1998). Interhemispheric appraisal of the value of alkenone indices as temperature and salinity proxies in high-latitude locations. Paleoceanogrphy 13(6), p. 694-703.

Rosell-Melé, A., Bard, E., Emeis, K.C., Grieger, B., Hewitt, C., Müller, P.J. and Schneider, R.R. (2004). Sea surface temperature anomalies in the oceans at the LGM estimated from the alkenone- $U^{K'}_{37}$ index: comparison with GCMs. Geophysical Research Letters 31(3), L03208, doi:10.1029-2003GL018151.

Rostek, F., Ruhlandt, G., Bassinot, F.C., Müller, P.J., Labeyrie, L.D., Lancelot, Y. and Bard, E. (1993). Reconstructing sea surface temperature and salinity using δ18O and alkenone recods. Nature 364(6435), p. 319-321.

Rostek, F., Bard, E., Beaufort, L., Sonzogni, C. and Ganssen, G. (1997). Sea surface temperature and productivity records for the past 240 kyr in the Arabian Sea. Deep-Sea Research Part II: Topical Studies in Oceanography 44(6), p. 1461-1480.

Sachs, J.P. and Anderson, R.F. (2003). Fidelity of alkenone paleotemperatures in southern Cape Basin sediment drifts. Paleoceanogrphy 18(4), 1082, doi:10.1029/2002PA000862.

Sawada, K., Handa, N., Shiraiwa, Y., Danbara, A. and Montani, S. (1996). Long-chain alkenones and alkyl alkenoates in the coastal and pelagic sediments of the northwest North Pacific, with special reference to the reconstruction of Emiliania huxleyi and Gephyrocapsa oceanica ratios. Organic Geochemistry 24(8), p. 751-764.

Schefuß, E., Versteegh, G.J.M., Jansen, J.H.F. and Sinninghe Damsté, J.S. (2001). Marine and terrigenous lipids in southeast Atlantic sediments (Leg 175) as paleoenvironmental indicators: In: Proceedings of the Ocean Drilling Program, Scientific Results, Volume 175. Wefer, G., Berger, W.H. and Richter, C. (eds.) Texas: A&M University, p. 1-34.

Schouten, S., Hopmans, E.C., Pancost, R.D. and Sinninghe Damsté, J.S. (2000a). Widespread occurrence of structurally diverse tetraether membrane lipids: evidence for the ubiquitous presence of low-temperature relatives of hyperthermophiles. Proceeding of the National Acadamy of Sciences of the United States of America 97(26), p. 14421-14426.

Schouten, S., Hoefs, M.J.L. and Sinninghe Damsté, J.S. (2000b). A molecular and stable carbon isotopic study of lipids in late Quarternary sedimentary sediments from the Arabian Sea. Organic Geochemistry 316), p. 509-521.

Schouten, S., Hopmans, E.C., Schefuß, E. and Sinninghe Damsté, J.S. (2002). Distributional variations in marine crenarchaeotal membrane lipids: A new tool for reconstructing ancient sea water temperatures? Earth Planetary Science Letters 204(1-2), p. 265-274.

Schouten, S., Hopmans, E.C. and Sinninghe Damsté, J.S. (2004). The effect of maturity and depositional redox conditions on archaeal tetraether lipid palaeothermometry. Organic Geochemistry 35(5), p. 567-571.

Schouten, S., Rampen, S.W., Geenevasen, J.A.J., Sinninghe Damsté, J.S. (2005). Structural identification of steryl alkyl ethers in marine sediments. Organic Geochemistry 36(9), p. 1323-1333.

Schouten, S., Huguet, C., Hopmans, E.C., Kienhuis, M.V.M. and Sinninghe Damsté, J.S. (2007). Analytical methodology for TEX_{86} paleothermometry by high-performance liquid chromatography/atmospheric pressure chemical ionization-mass spectrometry. Analytical Chemistry 79(7), p. 2940-2944.

Schouten, S., Hopmans, E.C. and Sinninghe Damsté, J.S. (2013). The organic geochemistry of glycerol dialkyl glycerol tetraether lipids: A review. Organic Geochemistry 54, p. 19-61.

Schulte, S. and Müller, P.J. (2001). Variations of sea surface temperature and primary productivity during Heinrich and Dansgaard-Oescher events in the northeastern Arabian Sea. Geo-Marine Letters 21(3), p. 168-175.

Schulz, H., Von Rad, U. and Von Stackelberg, U. (1996). Laminated sediments from the oxygen-minimum zone of the northeastern Arabian Sea. Geological Society, Londen, Special Publications 116(1), p. 185-207.

Schulz, H., Von Rad, U. and Erlenkeuser, H. (1998). Correlation between Arabian Sea and Greenland climate oscillations of the past 110,000 years, Nature 393(6680), p. 54-57.

Shah, S.R., Mollenhauer, G., Ohkouchi, N., Eglinton, T.I. and Pearson, A. (2008). Origins of archaeal tetraether lipids in sediments: Insights from radiocarbon analysis. Geochimica et Cosmochimica Acta 72(18), p. 4577-4594.

Sharma, G.S. (1972). Water characteristics at 200 Cl/T in intertropical Indian Ocean during Southwest Monsoon. Journal of Marine Research 30(1), p. 102-111.

Sharma, G.S., Gouveia, A.D. and Satyendranath, S. (1978). Incursion of the Pacific Ocean Water into Indian Ocean. Journal of Earth System Science 87(3), p. 29-45.

Sicre, M.A., Labeyrie, L., Ezat, U., Duprat, J., Turon, J.L., Schmidt, S., Michel, E. and Mazaud, A. (2005). Mid-latitude Southern Indian Ocean response to northern hemisphere Heinrich events. Earth and Planetary Science Letters 240(3), p. 724-731.

Siegel, D.A. and Deuser, 1997. Deep ocean time-series particle trapping in the Sargasso Sea: The modelling of “statistical funnels”. Deep-Sea Research Part I: Oceanographic Research Papers 44, p. 1519-1541.

Sikes, E.L., O’Leary, T., Nodder, S.D. and Volkman, J.K. (2005). Alkenone temperature records and biomarker flux at the subtropical front on the Chatham Rise, SW Pacific Ocean. Deep-Sea Research Part I: Oceanographic Research Papers 52(5), p. 721-748.

Singh, A.D. (2007). Episodic preservation of pteropods in the eastern Arabian Sea: Monsoonal change, oxygen minimum zond intensity and aragonite compensation depth. Indian Journal of Marine Sciences 36, p. 378-383.

Sinninghe Damsté, J.S., Hopmans, E.C., Schouten, S., Van Duin, A.C.T., Geenevasen, J.A.J. (2002a). Crenarchaeol: The characteristic core glycerol dibiphytanyl glycerol tetraether membrane lipid of cosmopolitan pelagic crenarchaeota. Journal of Lipid Research 43(10), p. 1641-1651.

Sinninghe Damsté, J.S., Rijpstra, W.I.C. and Reichart, G.-J. (2002b). The influence of oxic degradation on the sedimentary biomarker record II. Evidence from Arabian Sea sediments. Geochimica et Cosmochimica Acta, 66(15), p. 2737-2754.

Sinninghe Damsté, J.S., Rijpstra, W.I.C., Hopmans, E.C., Prahl, F.G, Wakeham, S.G. and Schouten, S. (2002c). Distribution of membrane lipids of planktonic Crenarchaeota in the Arabian Sea. Applied and Environmental Microbiology 68(6), p. 2997-3002.

Sinninghe Damsté, J.S., Rampen, S.W., Rijpstra, W.I.C., Abbas, B., Muyzer, G. and Schouten, S. (2003). A diatomaceous origin for long-chain diols and mid-chain hydroxy methyl alkanoates widely occurring in Quaternary marine sediments: indicators for high-nutrient conditions. Geochimica et Cosmochimica Acta 67(7), p. 1339-1348.

Sinninghe Damsté, J.S., Van Bentum, E.C., Reichart, G.-J., Pross, J. and Schouten, S. (2010). A CO2 decrease-driven cooling and increased latitudinal temperature gradient during the mid-Cretaceous Oceanic Anoxic Event 2. Earth and Planetary Science Letters 293(1), p. 97-103.

Smith, M., De Deckker, P., Rogers, J., Brocks, J., Hope, J., Schmidt, S., Lopes dos Santos, R. and Schouten, S. (2013). Comparison of $U^{K'}_{37}$, TEX^{H}_{86} and LDI temperature proxies for reconstruction of south-east Australian ocean temperatures. Organic Geochemistry 64, p. 94-104.

Smith, S.L. (2001). Understanding the Arabian Sea: Reflections on the 1994-1996 Arabian Sea Expedition. Deep-Sea Research Part II: Topical Studies in Oceanogrphy 48(6-7), p. 1385-1402

Spero, H.J., Bijma, J., Lea, D.W. and Bemis, B.E. (1997). Effect of seawater carbonate concentration on foraminiferal carbon and oxygen isotopes. Nature 390(6659), p. 497-500.

Stenni, B., Masson-Delmotte, V., Johnsen, S., Jouzel, J., Longinelli, A., Monnin, E., Röthilsberger, R. and Selmo, E. (2001). An oceanic cold reversal during the last deglaciation. Science 293(5537), p. 2074-2077.

Stuiver, M., Reimer, P.J. and Reimer, R.W. (2017). CALIB 7.1 [WWW program] at http://calib.org, 2017-3-13.

Swallow, J.C. (1984). Some aspects of the physical oceanography of the Indian Ocean. Deep-Sea Research Part I: Oceanographic Research Papers 31(6-8), p. 639-650.

Tjallingii, R., Röhl, U., Kölling, M. and Bickert, T. (2007). Influence of the water content on X-ray fluorescence core-scanning measurements in soft marine sediments. Geochemistry, Geophysics, Geosystems 8(2), Q02004, doi:10.1029/2006GC001393.

Uda, I., Sugai, A., Itoh, Y.H. and Itoh, T. (2001). Variation in molecular species of polar lipids from Thermoplasma acidophilum depends on growth temperature. Lipids 36(1), p. 103-105.

Uda, I., Sugai, A., Itoh, Y.H. and Itoh, T. (2004). Variation in molecular species of core lipids from the order Thermoplasmales strains depends on growth temperature. Journal of Oleo Science 53(8), p. 399-404.

Van Bennekom, A.J. and Hiehle, M.A. (1994). CTD operations and calibrations during legs D1, D2, D3 of the Netherlands Indian Ocean Programme. In: Geological study of the Arabian Sea. Van der Linden, W.J.M., Van der Weijden, C.H. (eds.) The Hague: Netherlands Geosciences Foundation, p. 37-66.

Van Bennekom, A.J., Hiehle, M.A., Van Ooyen, J., Van Weerlee, E. and Van Koutrik, M. (1995). CTD and hydrography. In: Tracing a Seasonal Upwelling. Van Hinte, E., Van Weering, T.J.C.E. and Troelstra, S.R. (eds.) The Hague: Netherlands Geosciences Foundation, p. 41-54.

Van der Weijden, C. H., Reichart, G.-J. and Visser, H.J. (1999). Enhanced preservation of organic matter in sediments deposited within the oxygen minimum zone in the northeastern Arabian Sea. Deep-Sea Research Part I: oceanographic Research Papers 46(5), p. 807-830.

Versteegh, G.J.M., Bosch, H.-J. and De Leeuw, J. W. (1997). Potential palaeoenvironmental information of C24 to C36 mid-chain diols, keto-ols and mid-chain hydroxy fatty acids; a critical review. Organic Geochemistry 27(1-2), p. 1-13.

Volkman, J.K., Barrerr, S.M., Blackburn, S.I. and Sikes, E.L. (1995). Alkenones in Gephyrocapsa oceanica: Implications for studies of paleoclimate. Geochimica et Cosmochimica Acta 59(3), p. 513-520.

Volkman, J.K., Barrett, S.M. and Blackburn., S.I. (1999). Eustigmatophyte microalgae are potential sources of C29 sterols, C22-C28 n-alcohols and C28-C32 n-alkyl diols in freshwater environments. Organic Geochemistry 30(5), p. 307-318.

Volkman, J.K., Barrett, S.M., Dunstan, G.A. and Jeffrey, S.W. (1992). C30-C32 alkyl diols and unsaturated alcohols in microalgae of the class Eustigmatophyceae. Organic Geochemistry 18(1), p. 131-138.

Volkman, J.K., Eglinton, G., Corner, E.D.S., Forsberg, T.E.V. (1980a). Long-chain alkenes and alkenones in the marine coccolithophorid Emiliania huxleyi. Phytochemistry 19, p. 2619-2622.

Volkman, J.K., Eglinton, G., Corner, E.D.S. and Sergent, J.R. (1980b). Novel unsaturated straight-chain C37-C39 methyl and ethyl ketones in marine sediments and coccolithophore Emiliana huxleyi. Physics and Chemistry of the Earth 12, p. 219-227.

Von Rad, U., Schulz, H., Riech, V., Den Dulk, M., Berner, U. and Sirocko, F. (1999a). Multiple monsoon-controlled breakdown of oxygen-minimum conditions during the past 30,000 years documented in laminated sediments off Pakistan. Palaeogeography, Palaeoclimatology, Palaeoecology 152(1-2), p. 129-161.

Von Rad, U., Schaaf, M., Michels, K.H., Schulz, H., Berger, W.H. and Sirocko, F. (1999b). A 5000-yr record of climate change in varved sediments from the oxygen minimum zone off Pakistan, Northeastern Arabian Sea. Quaternary Research 51(1), p. 39-53.

Wakeham, S.G. and Canuel, E.A. (1988). Organic geochemistry of particulate matter in the eastern tropical North Pacific Ocean: Implications for particle dynamics. Journal of Marine Research 46(1), p. 183-213.

Wakeham, S.G., Hedges, J.I., Lee, C. and Peterson, M.L. (2001). Organic matter degradation in surface sediments: Water column fluxes vs. sediment accumulation. Abstract Book, Volume 2, 20th International Meeting on Organic Geochemistry, Nancy, France, p.333-334.

Wakeham, S.G., Peterson, M.L., Hedges, J.I. and Lee, C. (2002). Lipid biomarker fluxes in the Arabian Sea, with a comparison to the equatorial Pacific Ocean. Deep-Sea Research Part II: Topical Studies in Oceanography 49(12), p. 2265-2301.

Wakeham, S.G., Lewis, C.M., Hopmans, E.C., Schouten, S. and Sinninghe Damsté, J.S. (2003). Archaea mediate anaerobic oxidation of methane in deep euxinic waters of the Black Sea. Geochimica et Cosmochimica Acta 67(7), p. 1359-1374.

Wang, Y.J., Cheng, H., Edwards, R.L., An, Z.S., Wu, J.Y., Shen, C.-C. and Dorale, J.A. (2001). A high-resolution absolute-dated late Pleistocene monsoon record from Hulu Cave, China. Science 294(5550), p. 2345-2348.

Webster, P.J. (1987). The elementary monsoon. In: Monsoons. Fein, J.S. and Stephens, P.L. (eds.) New York: John Wiley, p. 3-32.

Webster, P.J., Magana, V.O., Palmer, T.N., Shukla, J., Tomas, R.A., Yanai, M.U. and Yasunari, T. (1998). Monsoons: Processes, predictability, and the prospects for prediction. Journal of Geophysical Research: Oceans 103(C7), p. 14451-14510.

Wefer, G., Berger, W.H., Bijma, J. and Fisher, G. (1999). Clues to ocean history: A brief overview of proxies. In: Use of proxies in paleoceanography: Examples from the South Atlantic. Fisher, G. and Wefer, G. (eds.) Berlin, Heidelberg: Springer, p. 1-68.

Weijers, J.W.H., Schouten, S., Spaargaren, O.C. and Sinninghe Damsté, J.S. (2006). Occurrence and distribution of tetraether membrane lipids in soils: Implications for the use of the TEX_{86} SST proxy and the BIT index. Organic Geochemistry 37(12), p. 1680-1693.

Weijers, J.W.H., Lim, K.L.H., Aquilina, A., Sinninghe Damsté, J.S. and Pancost, R.D. (2011). Biogeochemical controls on glycerol dialkyl glycerol tetraether lipid distributions in sediments characterized by diffusive methane flux. Geochemistry Geophysics, Geosystems 12(10), Q10010, doi:10.1029/2011GC003724.

Weltje, G.J. and Tjallingii, R. (2008). Calibration of XRF core scanners for quantitative geochemical logging of cores: Theory and application. Earth and Planetary Science Letters 2743), p. 423-438.

Willmott, V., Rampen, S.W., Domack, E., Canals, M., Sinninghe Damsté, J.S. and Schouten, S. (2010). Holocene changes in Proboscia diatom productivity in shelf waters of the north-western Antarctic Peninsula. Antarctic Science 22(1), p. 3-10.

Witte, U. and Pfannkuche, O. (2000). High rates of benthic remineralization in the abyssal Arabian Sea. Deep-Sea Research Part II: Topical Studies in Oceanography 47, p. 2785-2804.
Wu, G., Liu, Y., He, B., Bao, Q., Duan, A. and Jin, F.F. (2012). Thermal controls on the Asian summer monsoon. Scientific Reports 2(404), doi:10.1023/srep00404.

Wuchter, C., Schouten, S., Coolen, M.J.L. and Sinninghe Damsté, J.S. (2004). Temperature-dependent variation in the distribution of tetraether membrane lipids of marine Crenarchaeota: Implications for TEX_{86} paleothermometry. Paleoceanography 19(4), PA4028, doi:10.1029/2004PA001041.

Wuchter, C., Schouten, S., Wakeham, S.G. and Sinninghe Damsté, J.S. (2005). Temporal and spatial variation in tetraether membrane lipids of marine Crenarchaeota in particulate organic matter:

Implications for TEX_{86} paleothermometry. Paleoceanography 20(3), PA3013, doi:10.1029/2004PA001110.

Wuchter, C., Abbas, B., Coolen, M.J.L., Herfort, L., Timmers, P., Strous, M., Van Bleijswijk, J., Teira, E., Herndl, G.J., Middelburg, J.J., Schouten, S. and Sinninghe Damsté, J.S. (2006a). Archaeal nitrification in the ocean. Proceedings of the National Academy of Sciences of the United States of America 103(33), p. 12317-12322.

Wuchter, C., Schouten, S., Wakeham, S.G. and Sinninghe Damsté, J.S. (2006b). Archaeal tetraether membrane lipid fluxes in the northeastern Pacific and the Arabian Sea: Implications for TEX_{86} paleothermometry. Paleoceanography 21(4), PA4208, doi:10.1029/2006PA001279.

Wyrtki, K. (1973). Physical oceanography of the Indian Ocean. In: The biologogy of the Indian Ocean. Zeirzscker, B. (eds.) New York: Springer, p. 18-36.

You, Y. (1998). Intermediate water circulation and ventilation of the Indian Ocean derived from water-mass contributions. Journal of Marine Research 56, p. 1029-1067.

You, Y. and Tomczak, M. (1993). Thermocline circulation and ventilation in the Indian Ocean derived from water mass analysis. Deep-Sea Reseach Part I: Oceanographic Research Papers 40(1), p. 13-56.

Zahn, R. and Pederson, T.F. (1991). Late Pleistocene evolution of surface and mid-depth hydrography at the Oman Margin: Planktonic and benthic isotope records at site 724. Proceeding of the Ocean Drilling Program Scientific Results 117, p. 291-308.

Zhang, R. and Delworth, T.L. (2005). Simulated tropical response to a substantial weakening of the Atlantic thermohaline circulation. Journal of Climate 18(12), p. 1853-1860.

Ziegler, M., Jilbert, T., De Lange, G. J., Lourens, L. J., Reichart, G.-J. (2008). Bromine counts from XRF scanning as an estimate of the marine organic carbon content of sediment cores. Geochemistry, Geophysics, Geosystems 9(5), Q05009, doi:10.1029/2007GC001932.

Ziegler, M., Lourens, L.J., Tuenter, E., Hilgen, F., Reichart, G.-J., Weber, N. (2010). Precession phasing offset between Indian summer monsoon and Arabian Sea productivity linked to changes in Atlantic overturning circulation. Paleoceanography 25(3), PA3213, doi:10.1029/2009PA001884

APPENDIX 1: STRUCTURES OF COMPOUNDS INCLUDED IN THE $U^{K'}_{37}$, TEX^{H}_{86}, LDI, BIT INDEX, DI 1 AND DI 2, WITH ADDITIONALLY GDGT-0, DINOSTEROL, LOLIOLIDE AND ISOLOLIOLIDE.

The structures are those of compounds used within the organic SST proxies (A, B, D), BIT index (B, C), DI 1 (D), DI 2 (D) and furthermore structures of GDGT-0 (B), loliolide and dinosterol (E) are shown. Structures of $C_{37:2}$ and $C_{37:3}$ alkenones are taken from Lindell and Reddy (2012), isoprenoid and branched GDGT structures are from Schouten et al. (2013) and LCD structures are based on Kornprobst (2014). Structures of loliolide and isololiolide (isomer of loliolide, therefore not shown) and dinosterol are taken from Schefuß et al. (2001).

A. Alkenones

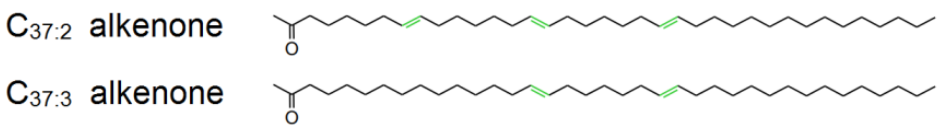

B. Isoprenoid GDGTs

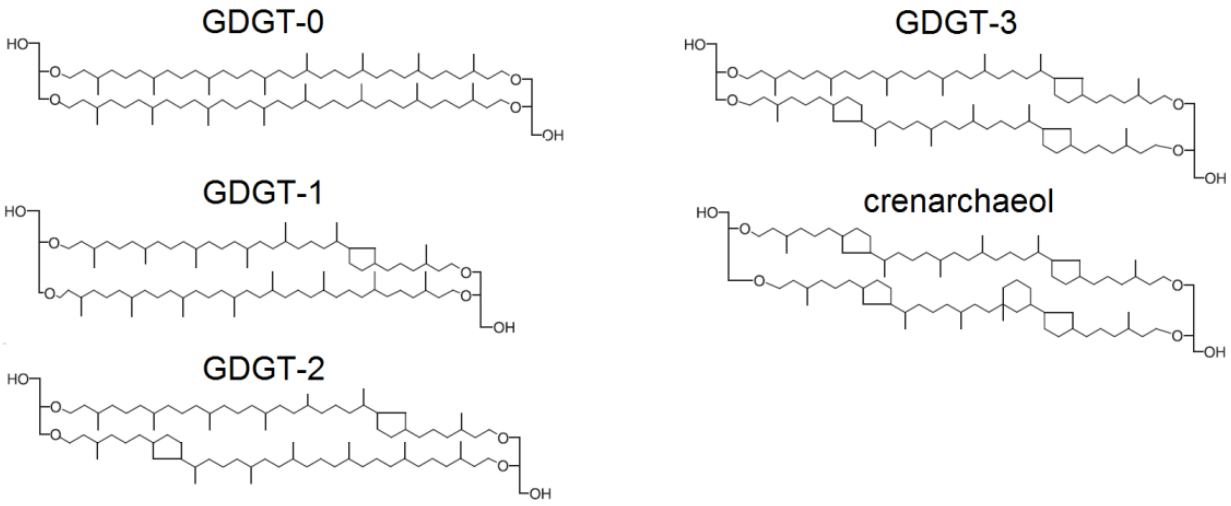

C. Branched GDGTs

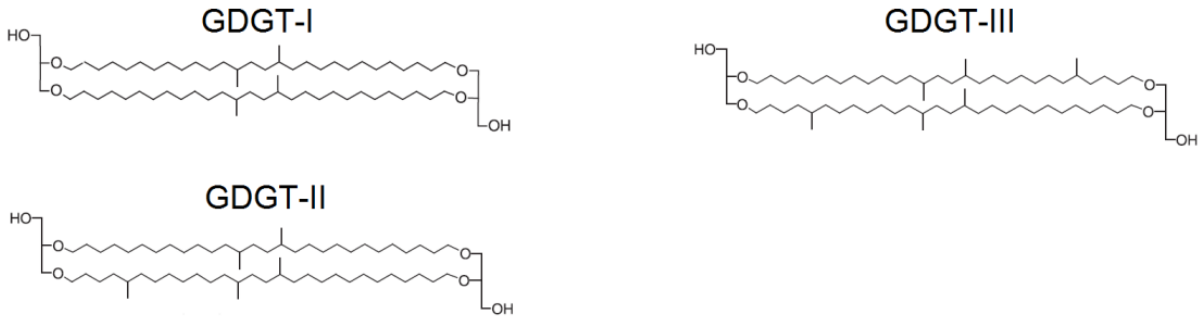

D. LCDs

C_{30} 1,13-diol 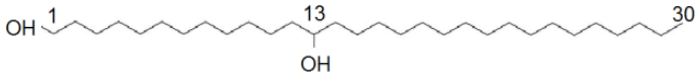

C_{28} 1,14-diol 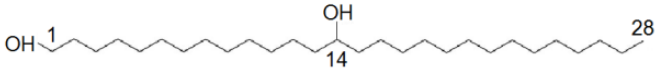

C_{30} 1,14-diol 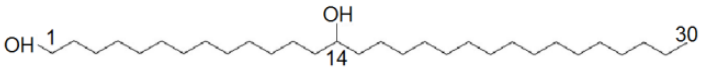

C_{30} 1,15-diol 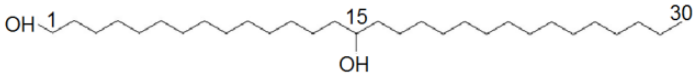

C_{32} 1,15-diol 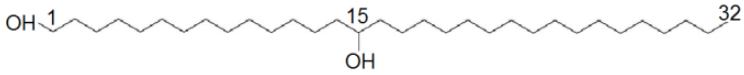

E. Dinosterol and loliolide

Loliolide 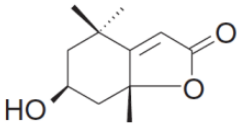

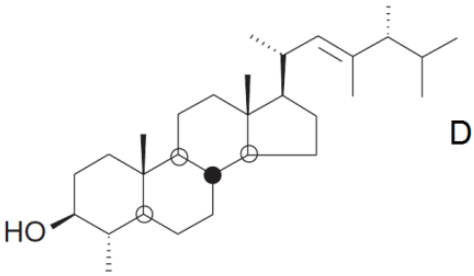

Dinosterol

APPENDIX 2: FRACTIONAL ABUNDANCES OF THE LCDs, THE BIT INDEX AND STABLE CARBON ISOTOPIC COMPOSITION

Fractional abundances are normalized to the total pool of LCDs (1,13-diols, 1,14-diols and 1,15-diols). C_{32} 1,15-diol fractional abundances highlighted with * are normalized to the total abundance of 1,13- and 1,15-diols. $\delta^{13}C$ reflects $\delta^{13}C_{bulk}$.

Age (ka BP)	Fractional abundance							BIT	$\delta^{13}C$ (‰)
	C_{28} 1,13-diol	C_{30} 1,13-diol	C_{28} 1,14-diol	C_{30} 1,14-diol	C_{30} 1,15-diol	C_{32} 1,15-diol	C_{32} 1,15-diol*		
3,11	0,01	0,01	0,31	0,38	0,25	0,04	0,13	0,009	-20,49
4,23	0,01	0,02	0,23	0,39	0,29	0,06	0,16	0,009	-20,41
5,35	0,01	0,02	0,20	0,36	0,34	0,07	0,15	0,009	-20,23
6,47	0,01	0,03	0,18	0,33	0,38	0,07	0,14	0,009	-20,22
7,59	0,01	0,02	0,14	0,29	0,47	0,07	0,12	0,008	-20,11
8,71	0,01	0,03	0,19	0,28	0,42	0,08	0,15	0,008	-20,13
9,83	0,01	0,02	0,14	0,26	0,48	0,09	0,16	0,008	-20,20
10,96	0,01	0,02	0,09	0,20	0,57	0,11	0,16	0,008	-20,19
12,08	0,01	0,03	0,07	0,22	0,60	0,08	0,12	0,008	-20,12
12,97	0,01	0,03	0,06	0,19	0,62	0,08	0,11	0,007	-20,04
13,52	0,01	0,03	0,05	0,17	0,64	0,10	0,13	0,009	-20,01
14,06	0,00	0,03	0,03	0,13	0,71	0,10	0,12	0,007	-20,09
14,61	0,01	0,03	0,07	0,15	0,64	0,10	0,13	0,007	-20,21
16,70	0,01	0,03	0,09	0,16	0,62	0,09	0,12	0,007	-20,03
18,46	0,01	0,02	0,07	0,11	0,69	0,09	0,11	0,009	-19,94
19,03	0,01	0,02	0,11	0,15	0,63	0,08	0,11	0,008	-19,91
19,61	0,01	0,02	0,05	0,10	0,74	0,07	0,09	0,008	-19,63
20,18	0,01	0,02	0,07	0,14	0,69	0,07	0,09	0,007	-19,78
20,76	0,01	0,03	0,06	0,11	0,71	0,09	0,11	0,007	-19,72
21,33	0,01	0,02	0,05	0,08	0,78	0,06	0,07	0,006	-19,54
21,91	0,01	0,03	0,04	0,09	0,77	0,06	0,07	0,006	-19,57
22,48	0,00	0,02	0,02	0,11	0,76	0,08	0,09	0,007	-19,47
23,01								0,007	-19,51
23,53	0,01	0,02	0,06	0,15	0,67	0,09	0,12	0,006	-19,63
24,06	0,01	0,02	0,10	0,20	0,56	0,11	0,16	0,009	-19,49
24,59	0,01	0,02	0,12	0,20	0,54	0,11	0,16	0,007	-19,61
25,12	0,01	0,02	0,14	0,19	0,55	0,09	0,13	0,006	-19,70
25,64	0,01	0,03	0,15	0,16	0,55	0,10	0,14	0,007	-19,56
26,17	0,01	0,02	0,09	0,16	0,58	0,14	0,19	0,008	-19,66
26,70	0,01	0,02	0,07	0,16	0,59	0,15	0,19	0,005	-19,42
27,22	0,01	0,02	0,12	0,17	0,56	0,12	0,17	0,008	-19,31
27,75	0,01	0,02	0,14	0,18	0,51	0,13	0,20	0,009	-19,45
28,28	0,01	0,03	0,16	0,20	0,48	0,12	0,19	0,009	-19,45
28,81	0,01	0,02	0,14	0,20	0,51	0,12	0,19	0,008	-19,37
29,33	0,01	0,02	0,15	0,22	0,49	0,11	0,18	0,009	-19,28
29,95	0,01	0,02	0,13	0,20	0,54	0,10	0,14	0,006	-19,31
30,74	0,01	0,03	0,09	0,16	0,64	0,08	0,11	0,008	-19,45
31,53	0,01	0,02	0,11	0,20	0,57	0,08	0,12	0,007	-19,76
32,31	0,01	0,03	0,13	0,19	0,55	0,08	0,12	0,007	-19,38
32,85	0,01	0,02	0,06	0,13	0,67	0,11	0,13	0,008	-19,47
33,33	0,01	0,02	0,06	0,20	0,63	0,08	0,11	0,009	-19,67
33,81	0,01	0,02	0,09	0,22	0,56	0,10	0,15	0,010	-19,69
34,29	0,01	0,02	0,06	0,19	0,63	0,09	0,12	0,008	-19,54
34,77	0,01	0,02	0,06	0,15	0,63	0,13	0,16	0,008	-19,45
35,24	0,01	0,02	0,05	0,25	0,56	0,11	0,16	0,006	-19,59
35,72	0,01	0,02	0,08	0,30	0,50	0,10	0,16	0,006	-19,53
36,20	0,01	0,02	0,07	0,20	0,59	0,11	0,15	0,007	-19,65
36,68	0,01	0,02	0,08	0,19	0,60	0,10	0,14	0,006	-19,82
37,20	0,01	0,03	0,14	0,30	0,40	0,12	0,21	0,007	-20,10
38,37	0,01	0,03	0,12	0,29	0,44	0,11	0,19	0,006	-20,08
39,54	0,01	0,03	0,19	0,31	0,38	0,09	0,17	0,007	-19,86
40,57	0,01	0,02	0,18	0,31	0,39	0,10	0,19	0,007	-19,77
40,90	0,01	0,02	0,15	0,30	0,40	0,12	0,22	0,006	-19,75
41,23	0,01	0,03	0,11	0,26	0,49	0,11	0,17	0,006	-19,74
41,57	0,01	0,02	0,13	0,23	0,47	0,13	0,20	0,006	-20,00
41,90	0,01	0,02	0,12	0,24	0,49	0,12	0,19	0,007	-19,92

Age (ka BP)	Fractional abundance							BIT	δ ^{13}C (‰)
	C_{28} 1,13-diol	C_{30} 1,13-diol	C_{28} 1,14-diol	C_{30} 1,14-diol	C_{30} 1,15-diol	C_{32} 1,15-diol	C_{32} 1,15-diol*		
42,25	0,01	0,02	0,11	0,24	0,51	0,11	0,17	0,006	-19,81
43,89	0,01	0,02	0,09	0,21	0,55	0,12	0,18	0,005	-19,90
45,53	0,01	0,02	0,10	0,23	0,53	0,12	0,18	0,005	-19,96
46,65	0,01	0,02	0,08	0,27	0,52	0,10	0,15	0,005	-19,81
47,10	0,01	0,02	0,09	0,24	0,52	0,12	0,18	0,005	-19,97
47,56	0,01	0,02	0,08	0,23	0,52	0,14	0,20	0,006	-19,85
48,01	0,01	0,02	0,08	0,21	0,56	0,13	0,18	0,006	-19,89
48,47	0,01	0,02	0,10	0,22	0,53	0,12	0,17	0,005	-19,72
48,92	0,01	0,02	0,11	0,26	0,49	0,12	0,19	0,006	
49,38	0,01	0,02	0,09	0,18	0,57	0,13	0,18	0,005	-19,70
49,83	0,01	0,02	0,07	0,16	0,60	0,14	0,18	0,006	-19,72
50,94	0,01	0,02	0,09	0,19	0,57	0,12	0,17	0,005	-19,54
52,07	0,01	0,03	0,16	0,32	0,40	0,09	0,17	0,005	-20,30
52,77	0,01	0,03	0,13	0,37	0,38	0,09	0,18	0,005	-19,82
53,31	0,01	0,03	0,11	0,34	0,41	0,11	0,20	0,005	-19,95
53,85	0,01	0,02	0,12	0,29	0,46	0,10	0,17	0,005	-20,17
54,39	0,01	0,02	0,10	0,24	0,52	0,10	0,16	0,005	-19,95
54,93	0,01	0,02	0,10	0,19	0,58	0,11	0,15	0,005	-19,94
55,47								0,002	-19,85
56,01								0,002	-19,76
56,56	0,01	0,02	0,07	0,15	0,65	0,11	0,14	0,005	-19,61
57,25	0,00	0,02	0,04	0,11	0,71	0,12	0,14	0,004	-19,67
58,17	0,00	0,02	0,06	0,17	0,63	0,12	0,15	0,005	-19,63
59,09	0,01	0,02	0,07	0,15	0,62	0,13	0,17	0,005	-19,76
60,02	0,01	0,02	0,08	0,14	0,61	0,15	0,19	0,005	-19,73
60,74	0,01	0,02	0,08	0,15	0,63	0,11	0,15	0,004	-19,85
61,29	0,01	0,02	0,08	0,14	0,63	0,13	0,16	0,004	-19,80
61,84	0,01	0,02	0,10	0,14	0,60	0,14	0,18	0,004	-19,83
62,40	0,01	0,02	0,09	0,15	0,60	0,13	0,17	0,005	-19,97
62,95	0,01	0,02	0,07	0,13	0,68	0,09	0,11	0,006	-20,22
63,74	0,01	0,02	0,05	0,14	0,71	0,08	0,10	0,007	-20,11
64,67	0,01	0,02	0,08	0,17	0,62	0,09	0,12	0,004	-20,06
65,60	0,01	0,02	0,06	0,14	0,68	0,10	0,13	0,007	-20,10
66,52	0,01	0,02	0,05	0,14	0,68	0,09	0,12	0,007	-20,02
67,45	0,01	0,02	0,05	0,10	0,71	0,11	0,13	0,007	-19,99
68,38	0,01	0,01	0,05	0,42	0,42	0,10	0,18	0,006	-19,84
69,28	0,01	0,01	0,06	0,41	0,41	0,11	0,20	0,005	-19,90
69,78	0,00	0,01	0,05	0,40	0,40	0,13	0,23	0,006	-20,01
70,28	0,01	0,01	0,05	0,41	0,41	0,11	0,21	0,007	-19,94
71,27	0,01	0,01	0,05	0,41	0,41	0,10	0,19	0,006	-19,97
72,27	0,00	0,02	0,04	0,41	0,41	0,13	0,23	0,005	-19,99
73,27	0,01	0,01	0,06	0,41	0,41	0,11	0,20	0,006	-19,92
74,27	0,00	0,01	0,07	0,40	0,40	0,11	0,21	0,005	-19,95
75,26	0,01	0,01	0,09	0,40	0,40	0,08	0,16	0,005	-20,07
76,26	0,00	0,01	0,07	0,42	0,42	0,07	0,14	0,005	-20,26

APPENDIX 3: CONCENTRATIONS OF GDGT-0, GDGT-1, GDGT-2 AND CRENARCHAEOL AND CORRESPONDING RATIOS

Age (ka BP)	Concentration (µg/gCorg)				GDGT-0/	GDGT-1/	GDGT-2/
	GDGT-0	GDGT-1	GDGT-2	crenarchaeol	crenarchaeol	crenarchaeol	crenarchaeol
3.11	15.32	6.14	8.89	68.83	0.22	0.09	0.13
4.23	18.62	7.88	11.40	71.11	0.26	0.11	0.16
5.35	27.58	11.56	16.99	96.85	0.28	0.12	0.18
6.47	24.81	10.45	15.84	87.09	0.28	0.12	0.18
7.59	27.22	10.19	13.94	92.06	0.30	0.11	0.15
8.71	29.99	11.41	16.63	104.93	0.29	0.11	0.16
9.83	41.89	15.72	21.48	140.77	0.30	0.11	0.15
10.96	44.36	16.11	21.60	137.11	0.32	0.12	0.16
12.08	45.06	16.22	21.24	135.79	0.33	0.12	0.16
12.97	12.77	4.09	5.42	43.71	0.29	0.09	0.12
13.52	38.85	14.40	18.27	107.62	0.36	0.13	0.17
14.06	56.99	21.18	26.64	189.60	0.30	0.11	0.14
14.61	42.91	16.81	21.55	140.45	0.31	0.12	0.15
16.70	51.63	19.35	25.59	154.63	0.33	0.13	0.17
18.46	48.30	16.70	21.34	124.52	0.39	0.13	0.17
19.03	35.65	12.11	15.83	97.95	0.36	0.12	0.16
19.61	34.49	12.16	15.39	91.07	0.38	0.13	0.17
20.18	34.60	12.21	15.31	99.69	0.35	0.12	0.15
20.76	33.59	11.73	14.49	92.50	0.36	0.13	0.16
21.33	29.84	9.54	11.27	87.61	0.34	0.11	0.13
21.91	21.33	6.60	7.81	65.21	0.33	0.10	0.12
22.48	34.76	11.38	13.55	103.14	0.34	0.11	0.13
23.01	31.38	10.40	12.35	96.17	0.33	0.11	0.13
23.53	45.23	14.46	17.25	136.62	0.33	0.11	0.13
24.06	42.62	15.82	19.22	112.41	0.38	0.14	0.17
24.59	58.57	20.59	24.31	160.65	0.36	0.13	0.15
25.12	32.88	10.60	12.13	97.39	0.34	0.11	0.12
25.64	67.12	24.29	29.29	189.35	0.35	0.13	0.15
26.17	47.71	16.77	20.92	125.52	0.38	0.13	0.17
26.70	7.05	2.03	2.51	25.34	0.28	0.08	0.10
27.22	30.20	10.65	13.59	82.82	0.36	0.13	0.16
27.75	48.50	16.86	20.66	129.69	0.37	0.13	0.16
28.28	27.07	9.30	11.18	71.96	0.38	0.13	0.16
28.81	24.48	7.91	9.21	69.05	0.35	0.11	0.13
29.33	25.25	8.54	10.03	70.40	0.36	0.12	0.14
29.95	12.45	3.82	4.43	40.88	0.30	0.09	0.11
30.74	21.52	7.66	9.40	67.60	0.32	0.11	0.14
31.53	31.55	9.21	11.99	143.39	0.22	0.06	0.08
32.31	21.18	7.30	8.30	57.36	0.37	0.13	0.14
32.85	44.26	15.30	20.84	123.76	0.36	0.12	0.17

Age (ka BP)	Concentration (µg/gCorg)				GDGT-0/	GDGT-1/	GDGT-2/
	GDGT-0	GDGT-1	GDGT-2	crenarchaeol	crenarchaeol	crenarchaeol	crenarchaeol
33.33	17.40	5.06	6.30	48.62	0.36	0.10	0.13
33.81	59.81	20.55	25.90	148.37	0.40	0.14	0.17
34.29	22.04	7.07	8.93	59.66	0.37	0.12	0.15
34.77	35.80	12.36	15.48	95.41	0.38	0.13	0.16
35.24	13.46	4.08	5.01	40.95	0.33	0.10	0.12
35.72	22.63	6.21	6.98	76.35	0.30	0.08	0.09
36.20	10.76	3.22	4.00	32.87	0.33	0.10	0.12
36.68	9.82	2.81	3.48	30.04	0.33	0.09	0.12
37.20	14.40	3.96	4.86	44.16	0.33	0.09	0.11
38.37	6.08	1.71	2.25	19.11	0.32	0.09	0.12
39.54	6.35	1.76	1.97	20.98	0.30	0.08	0.09
40.57	7.40	2.02	2.25	24.17	0.31	0.08	0.09
40.90	20.70	5.68	6.62	61.92	0.33	0.09	0.11
41.23	4.45	1.17	1.34	15.21	0.29	0.08	0.09
41.57	22.42	6.14	7.64	70.75	0.32	0.09	0.11
41.90	19.82	5.53	6.74	58.77	0.34	0.09	0.11
42.25	16.14	4.56	5.66	52.03	0.31	0.09	0.11
43.89	23.59	6.83	9.04	80.64	0.29	0.08	0.11
45.53	7.66	2.14	2.30	30.86	0.25	0.07	0.07
46.65	5.30	1.38	1.48	19.73	0.27	0.07	0.08
47.10	10.33	2.86	3.19	35.14	0.29	0.08	0.09
47.56	14.58	4.03	4.68	44.58	0.33	0.09	0.11
48.01	17.68	4.99	6.09	52.79	0.33	0.09	0.12
48.47	19.79	5.50	6.59	68.36	0.29	0.08	0.10
49.38	19.13	5.25	6.23	61.74	0.31	0.09	0.10
49.83	19.66	5.51	6.87	58.38	0.34	0.09	0.12
50.94	24.03	7.02	8.11	77.73	0.31	0.09	0.10
52.07	9.67	2.49	2.63	30.70	0.31	0.08	0.09
52.77	14.42	3.80	4.17	50.36	0.29	0.08	0.08
53.31	13.40	3.76	4.88	42.11	0.32	0.09	0.12
53.85	17.33	5.09	6.37	54.74	0.32	0.09	0.12
54.39	15.78	4.41	5.06	53.08	0.30	0.08	0.10
54.93	25.17	7.12	8.16	83.73	0.30	0.09	0.10
55.47	0.29	0.08	0.09	0.86	0.34	0.09	0.10
56.01	0.34	0.09	0.10	0.90	0.38	0.10	0.11
56.56	23.32	6.68	7.92	74.80	0.31	0.09	0.11
57.25	10.37	2.81	3.15	35.59	0.29	0.08	0.09
58.17	10.86	2.91	3.15	38.06	0.29	0.08	0.08
59.09	11.54	3.07	3.27	38.33	0.30	0.08	0.09
60.02	16.04	4.34	4.57	57.23	0.28	0.08	0.08

Age (ka BP)	Concentration (µg/gCorg)				GDGT-0/	GDGT-1/	GDGT-2/
	GDGT-0	GDGT-1	GDGT-2	crenarchaeol	crenarchaeol	crenarchaeol	crenarchaeol
60.74	1.55	0.42	0.44	6.57	0.24	0.06	0.07
61.29	16.69	5.00	6.04	60.00	0.28	0.08	0.10
61.84	27.51	7.94	9.07	105.49	0.26	0.08	0.09
62.40	29.46	8.47	9.94	105.28	0.28	0.08	0.09
62.95	25.94	7.10	9.34	77.41	0.34	0.09	0.12
63.74	27.23	7.37	9.56	76.96	0.35	0.10	0.12
64.67	17.85	4.97	5.77	52.47	0.34	0.09	0.11
65.60	15.05	3.93	4.72	40.85	0.37	0.10	0.12
66.52	24.58	6.30	7.59	69.21	0.36	0.09	0.11
67.45	19.66	5.06	6.02	48.75	0.40	0.10	0.12
68.38	20.54	5.44	6.21	55.56	0.37	0.10	0.11
69.28	18.55	4.94	5.45	49.85	0.37	0.10	0.11
69.78	18.17	5.02	5.52	52.26	0.35	0.10	0.11
70.28	22.16	5.66	6.56	56.97	0.39	0.10	0.12
71.27	21.30	5.60	6.51	58.53	0.36	0.10	0.11
72.27	16.80	4.50	5.15	47.18	0.36	0.10	0.11
73.27	12.90	3.48	4.03	37.44	0.34	0.09	0.11
74.27	8.43	2.27	2.38	28.08	0.30	0.08	0.08
75.26	5.39	1.42	1.48	17.81	0.30	0.08	0.08
76.26	5.76	1.58	1.64	22.63	0.25	0.07	0.07